Master's thesis

NTNU
Norwegian University of Science and Technology
Faculty of Engineering
Department of Civil and Environmental Engineering

Jean-Gabriel Dorval

Using local Svalbard rocks as a construction material

Master's thesis in Cold Climate Engineering

Supervisor: Arne Aalberg (UNIS), Inge Hoff (NTNU) & Thomas Guldborg Petersen (DTU)

December 2020

NTNU
Kunnskap for ei betre verd

UNIS
The University Centre in Svalbard

DTU

Jean-Gabriel Dorval

Using local Svalbard rocks as a construction material

Master's thesis in Cold Climate Engineering
Supervisor: Arne Aalberg (UNIS), Inge Hoff (NTNU) & Thomas Guldborg Petersen (DTU)
December 2020

Norwegian University of Science and Technology
Faculty of Engineering
Department of Civil and Environmental Engineering

NTNU
Norwegian University of
Science and Technology

Abstract

The archipelago of Svalbard has a diversified geology that witnesses its migration across various temperature zones before reaching the polar region. The bedrock surrounding Longyearbyen is composed of sedimentary rocks which are believed to be unsuitable for construction. The current practice in town is to import good quality granular material from mainland Norway. This study aimed at determining properties of locally available rock masses for further use by the construction industry in road or infrastructure projects on the archipelago. These properties were compared to standards to validate potential use by local stakeholders. A large sample of natural rocks was imported from Longyearbyen and crushed before undergoing numerous laboratory tests. The Los Angeles and Micro-Deval coefficients were found after a series of abrasion tests. The particle shape, the freeze-thaw resistance, the thermal conductivity and grain specific density were also determined. The mineral composition of five sub-samples was assessed by X-Ray diffraction. Additionally, a repeated load triaxial test was done on four samples to evaluate their behavior in a road structure. The crushed granular material from Longyearbyen were found to be resistant to fragmentation to some extent, but very susceptible to wear. The shape and freeze-thaw resistance results were excellent according to the standards. The quartz content is high in the samples analyzed and this has an influence on the thermal conductivity. The repeated load triaxial tests gave good quality data which led to usable road design parameters. The aggregates from Longyearbyen do not have the same mechanical behavior and resistance as those originating from mainland Norway. However, the option to use that material should not simply be discarded without further analysis. Multiple parameters are brought forward to take those differences into account during the design process. This study shows that the crushed local granular material can be used for specific purposes in road structure and for some infrastructure work.

Abstract (in Norwegian)

Øygruppen Svalbard har en diversifisert geologi som er vitne til at den vandrer over forskjellige temperatursoner før den når polarområdet. Berggrunnen rundt Longyearbyen består av sedimentære bergarter som antas å være uegnet som konstruksjonsmateriale. Dagens praksis i byen er å importere granulatmateriale av god kvalitet fra fastlands-Norge. Denne studien tok sikte på å bestemme egenskapene til lokalt tilgjengelige bergmasser for videre bruk av byggenæringen i vei- eller infrastrukturprosjekter på øygruppen. Disse egenskapene ble sammenlignet med standarder for å validere potensiell bruk av lokale interessenter. En stor prøve av naturlige bergarter ble importert fra Longyearbyen og knust før de gjennomgikk en serie med laboratorietester. Los Angeles- og Micro-Deval-koeffisientene ble funnet etter en serie slitetester. Partikkelform, fryse-tine-motstand, varmeledningsevne og kornspesifikk tetthet ble også bestemt. Mineralsammensetningen av fem delprøver ble vurdert ved røntgendiffraksjon. I tillegg ble det utført en triaksial test med gjentatt belastning på fire prøver for å evaluere deres atferd i en veistruktur. Det knuste granulære materialet fra Longyearbyen ble funnet å være motstandsdyktig mot fragmentering til en viss grad, men veldig sensitiv for slitasje. Formene og fryse-tine motstandsresultatene var gode i henhold til standardene. Kvartsinnholdet er høyt i de analyserte prøvene, og dette har innflytelse på varmeledningsevnen. De triaksiale testene med gjentatt belastning ga data av god kvalitet som førte til brukbare veidesignparametere. Aggregatene fra Longyearbyen har ikke samme mekaniske oppførsel og motstand som de som kommer fra fastlands-Norge. Imidlertid bør muligheten til å bruke dette materialet ikke bare kastes uten nærmere analyse. Flere parametere blir frembrakt for å ta hensyn til forskjellene under designprosessen. Denne studien viser at det knuste lokale granulære materialet kan brukes til spesifikke formål i veistruktur og til noe infrastrukturarbeid.

Acknowledgements

This MSc thesis is the culminating point of my arctic journey with the Nordic Master in Cold Climate Engineering – Land Track. This research project was under the supervision and management of NTNU and UNIS with the participation of DTU. I would like to greatly acknowledge the Nordic Road Association (NVF), for their research grant to support the implementation of this study and Longyearbyen Lokalstyre for their support regarding the shipping of the samples to the laboratory in Trondheim.

Firstly, I would like to express my gratitude to my thesis supervisors: Dr. Arne Aalberg (UNIS), Dr. Inge Hoff (NTNU) and Dr. Thomas Guldborg Petersen (DTU). Their continued collaboration, guidance and insights were very useful and greatly contributed to the completion of this research project. I would like to extend my thanks to the laboratory personnel who took the necessary time to coach me through many tests: Steinar Seehus and Bent Lervik; and the two post-doctoral researchers that supervised me through the more specific tasks: Diego Maria Barbieri and Karlis Rieksts. Many individuals from the industry and the public road agencies contributed to shape my understanding of the standards and specifications. I would like to mention the following persons for their patience in answering my requests for information: Kjersti Olsen Ingerø (Longyearbyen Lokalstyre), Kjell Arne Skoglund (Norwegian Public Roads Administration), Asmus Skar (DTU), Thomas Ingeman-Nielsen (DTU), Matteo Pettinari (Danish Road Directorate), Benoît Loranger (NTNU) and Michaël Gagné Pomerleau (Quebec Ministry of Transportation). For their guidance and interesting discussions during part of this project, many thanks to Aleksey Shestov (UNIS), Anatoly Sinitsyn (SINTEF) and Lars Olav Grande (Norconsult). The local knowledge and past construction experiences are important in Longyearbyen and this study would not have been an accurate depiction without the participation of local stakeholders that kindly accepted to be interviewed during my thesis.

Table of content

List of tables

List of figures

Nomenclature

a = apparent attraction (kPa)
C_c = Coefficient of Curvature (-)
C_u = Coefficient of Uniformity (-)
D_{XX} = grain diameter at XX percent passing (mm)
g = the gravitational acceleration (m/s^2)
k_1 and k_2 = Hicks & Monismith regression parameters
M_R = resilient modulus (MPa)
m_1 = sample mass in the air (g)
m_2 = sample mass in the water (g)
V = volume of the sample (cm^3)
ΔT_c = critical temperature difference (°C)
Δz = vertical elastic settlement at the ground surface (mm)
ε_p = permanent or residual deformation (%)
ε_r = elastic or resilient deformation (%)
$\varepsilon_{r,v}$ = axial resilient vertical strain (%)
$\dot{\varepsilon}_{v,p}$ = permanent strain rate, vertical (%)
λ_s = thermal conductivity of solid particle (W/m°C)
$\lambda_{sat,u}$ = unfrozen saturated thermal conductivity of sample (W/m°C)
$\lambda_{sat,f}$ = frozen saturated thermal conductivity of sample (W/m°C)
ρ = mobilized angle of friction (°)
ρ_s = specific density of solid particle (g/cm^3)
ρ_w = the water density at the temperature during measurement (g/cm^3)
ρ_{sample} = the sample's density (g/cm^3)
φ = angle of friction at incremental failure (°)
σ_a = a reference pressure in the Hicks & Monismith model (kPa)
σ_d = deviatoric stress (kPa)
σ_t = triaxial stress (kPa)
σ_1 = major principal stress (kPa)
σ_2 & σ_3 = minor principal stresses (kPa)
θ = bulk-stress (kPa)

1 Introduction

Rock masses are used for several applications in the development of transport and civil infrastructure in Longyearbyen, Svalbard. This includes crushed material for asphalt and unbound road material, rock boulders for coastal protection, aggregates for concrete, sand for icy roads and to make up protective barriers against debris flow. In the light of sustainable development, there is a need to investigate in more detail for a utilization of local rock resources. Currently, the local granular material is used to some extent. The experience with using local rock is variable, and the common practice now is to import a large amount of rock masses from mainland Norway. That material is transported by trucks and then by freight ship to Longyearbyen.

This study is motivated by a desire to reduce the negative impacts of the construction sector in Svalbard. The use of transported rock material has several significant drawbacks such as a large environmental footprint due to maritime shipping, a cost increase due to the transportation from mainland and a more demanding planning for the execution of projects (the materials are transported in «on demand», hence the available stocks in Longyearbyen are limited).

1.1 Purpose and objectives of this study

The main goal of this study is to assess whether the local rock can be useful for construction purposes. This study is targeted on a few pertinent engineering parameters that can be compared to construction standards and guidelines. The approach will combine experimental results with simple modelling via an established road design software (i3c-me) and desktop geotechnical calculations. The main objectives of this study are defined as follows:

- To identify gaps in Longyearbyen's applied engineering knowledge
- To quantify and detail the current use of rock masses in Svalbard by the various actors
- To determine the properties of the locally available rock by a variety of laboratory experiments
- To classify that material according to multiple cold regions standards (Norway, Svalbard, Quebec, Denmark and Greenland)
- To give recommendations for the use of local crushed rock material for civil infrastructure and transport application

This study is limited to unbound crushed granular material originating from Longyearbyen as a geomaterial. The use of this material in concrete or other bound material was not investigated other than in a literature review. The samples tested in laboratory were originating only from the Bolterelva stockpile.

1.2 Outline of sections

The outline of the study is organized as follows:

- **Section 2: Background**
  General information regarding the geological history, the study area and the human history of Svalbard.
- **Section 3: Theory**
  Information regarding road structure and unbound granular material, introduction to the triaxial test apparatus and permafrost engineering considerations.
- **Section 4: State of the art**
  Previous scientific work related to the local granular masses and the common construction practises in Longyearbyen.
- **Section 5: Methodology**
  Laboratory techniques used during the experimental portion of this study.
- **Section 6: Results and discussion**
  Presentation of the findings of the laboratory experiments followed by a critical discussion of the results, reliability of the methods used and comparison to the technical literature.
- **Section 7: Recommendations**
  Based on the results, the discussion and modelling, recommendations regarding the usage of the local rocks for construction in Longyearbyen.

2 Background

2.1 Geological history of Svalbard

The Svalbard archipelago is located in the high north (above 76°N) and its landscape is composed of rugged mountains with steep flanks, coastal lowlands, mountain plateaus and multiples fjord systems. Svalbard's area is 60% covered by glacier. It is located in the continuous permafrost zone with thicknesses ranging from 10m to around 500m depending on the landscape. The oldest parts of what became Svalbard were moved over large distances and across various climate zones. The archipelago has a very rich and unique geological history that witnesses that displacement. During extensive periods, the archipelago was submerged. Hence, large amount of material was deposited, and it progressively turned into bedrock. Large portion of rocks are now exposed due to the sparse vegetation cover and the absence of forest. This study will focus on Isfjorden because Longyearbyen is established on its shore, as marked by the red circle on Figure 1. (Elvevold, Dallmann and Blomeier, 2007; Ingólfsson, 2008; Piepjohn *et al.*, 2012)

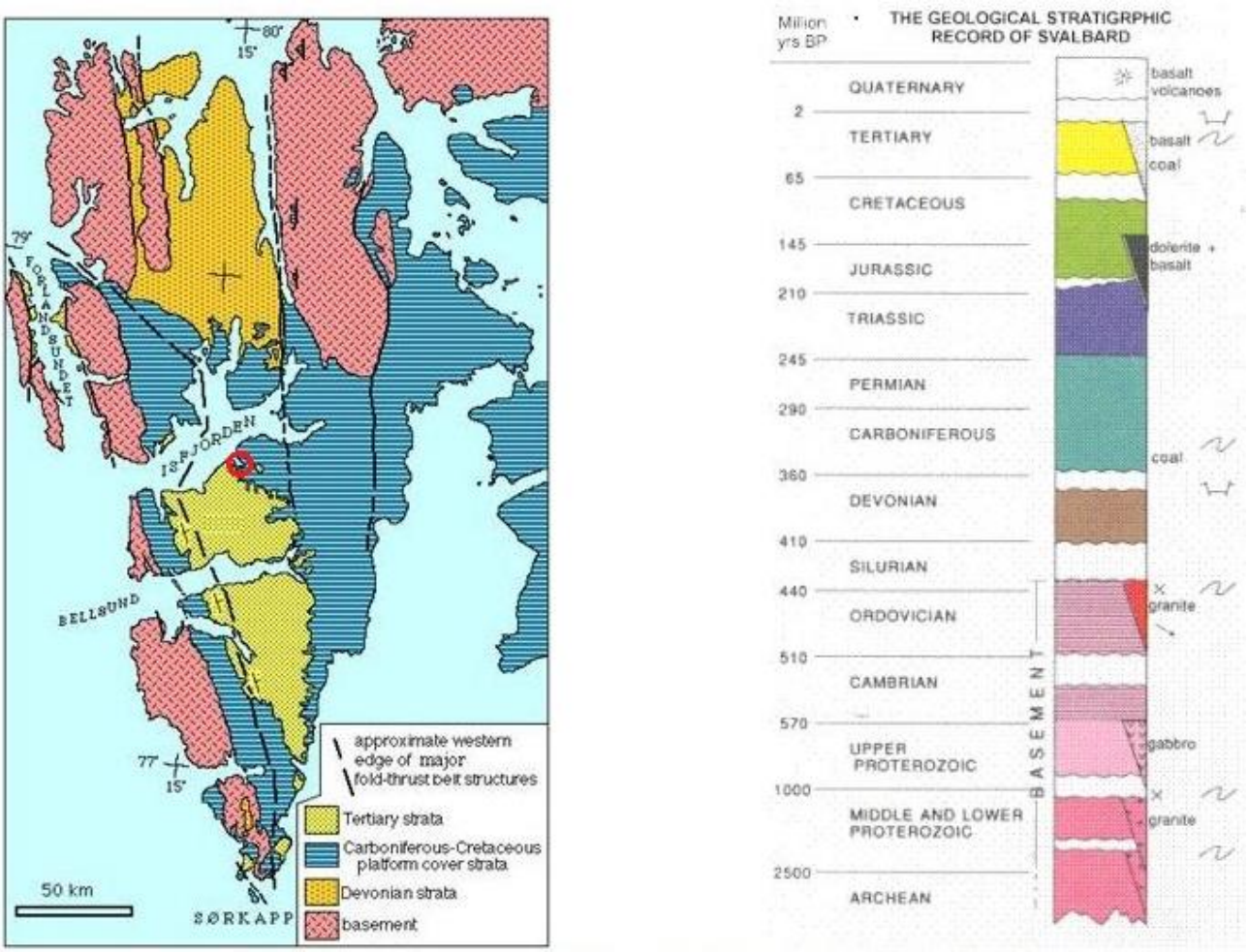

Figure 1: Simplified geological map and stratigraphical column for Svalbard modified from (Hjelle, 1993)

The geological strata around Svalbard can be divided into three main categories: the basement, the sedimentary cover rocks (platform cover strata) and the unconsolidated deposits.

The basement is represented by the oldest rocks on Svalbard and it suffered folding and alterations. It is made of igneous and metamorphic rocks that once were the inner parts of ancient mountains. Some of them were buried within the crust (under high temperature and pressure) so they recrystallized and became metamorphic (e.g. gneiss, crystalline schist, quartzite, marble). (Dallmann, 2009) These rocks are more than 570 million years (MY) old. The oldest deposits were likely deposited when its landmass was south of the Equator more than 600 MY ago. During the Devonian Period, northern Svalbard began sinking and the mountains were eroded by water and weather. It was located near the Equator during these events (360-400 MY ago). Today the areas with outcropping basement rocks can identified as mountainous landscapes with high, sharp, tooth-edged mountains.The global path followed by Svalbard is shown on Figure 2, it shows the climatic zones it crossed toward its current position. (Elvevold, Dallmann and Blomeier, 2007; Dallmann, 2009; Piepjohn *et al.*, 2012)

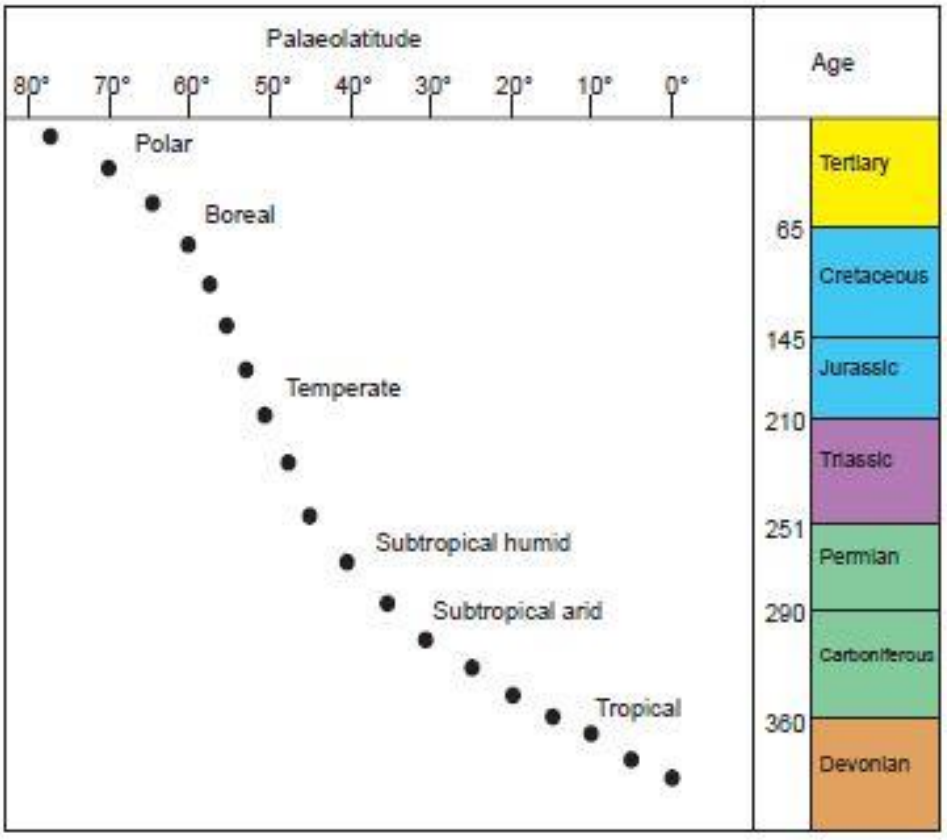

Figure 2: Paleo latitude of Svalbard through Ages (Elvevold, Dallmann and Blomeier, 2007)

The sedimentary cover rocks originate from the time when Svalbard had a relatively flat topography, was covered by those deposits and subsequently submerged by the sea. The erosion of the basement mountains led to the deposition of enormous masses of gravel, sand and mud on the newly created flat areas and in the sea. Short intervals of land uplift subjected the archipelago to alternating deposition on land and in shallow marine seas. Limestone breccias and dolostone was created during that period. (Elvevold, Dallmann and Blomeier, 2007) At that time, Svalbard was under the influence of a more tropical climate, and sometimes the shallow water bodies would dry up completely resulting in layers of gypsum, anhydrate and dolomite. (Ingólfsson, 2008) Those sedimentary successions are still observable to these days in Isfjorden. Later, new deposition episodes formed limestone successions during the Carboniferous and Permian. Sedimentary rocks from the Carboniferous contains coal seams. During the Mesozoic and part of the Cenozoic (up to 40 MY ago), sandstone and shale successions were formed as well as siltstone and limestone. From the Triassic to the Cretaceous Period, Svalbard drifted toward the north (approximately from 45° N to 65° N) and the climate shifted to temperate humid. Sedimentary rocks from those periods would be shale (either marine or terrestrial depending on the deposition period), siltstone, limestone and sandstone. (Elvevold, Dallmann and Blomeier, 2007) At the beginning of the Cenozoic (65-60 MY ago), Greenland and Svalbard collided which caused extensive folding of the west-coast strata and a depression basin (trough-shaped) to the east. That basin accumulated eroded material which became sandstone and shale (visible around Longyearbyen). It has the particularity of having the oldest beds on the perimeter and the youngest in the core. Vegetation was abundant during that period and consequently coal deposits were formed afterward. The climate got cooler at the end of the Tertiary period of the Cenozoic. (Elvevold, Dallmann and Blomeier, 2007; Ingólfsson, 2008; Dallmann, 2009)

Svalbard sustained repeated glaciations during the Quaternary which carved its fjords, valleys and other landscape features as we see them today. Sediments from that period were mostly removed by each following glaciation. The heavy ice (1000m thick) pressed down the Earth's crust (isostatic subsidence). (Piepjohn *et al.*, 2012) At the disappearance of the ice, the landmass reacted elastically and slowly rose again (isostatic rebound). This phenomenon brings the shoreline 40m to 80m lower than at the end of the last major glaciation that occurred around 10 000 years ago. (Dallmann, 2009) It left marine terraces and raised beaches all around Svalbard. The unconsolidated deposits from the Quaternary are still present in the form of moraines, talus, river or coastal deposits, scree fields and rock falls. (Elvevold, Dallmann and Blomeier, 2007; Ingólfsson, 2008)

2.2 Study area

Longyearbyen is located in Adventdalen, a U-shaped valley that leads to Isfjorden. In that area the upper marine limit reached 70m above the actual sea level. In front of the town, the Adventelva River is fed by many smaller streams originating in connecting valleys (see Figure 3). Weathered rock material (from frost shatter), traces of previous rockfalls or snow avalanches as well as debris flow tracks can be observed in the lower parts of the slopes surrounding the settlement. The bedrock around Longyearbyen is mainly mudstone and sandstone (from Cretaceous and Cenozoic) in horizontal layers. (Piepjohn *et al.*, 2012) The active layer thickness is approximately 1m in the valley bottom. Permafrost around Longyearbyen contains massive ice structures (i.e. pingos, ice wedges), some ice-rich areas near the surface and ice formation of various size (i.e. lenses). There is both saline and non-saline permafrost in the region. Consequently, the freezing point of water in the ground may not be 0°C which directly impacts its phase change. (Elvevold, Dallmann and Blomeier, 2007; Cable, Elberling and Kroon, 2018)

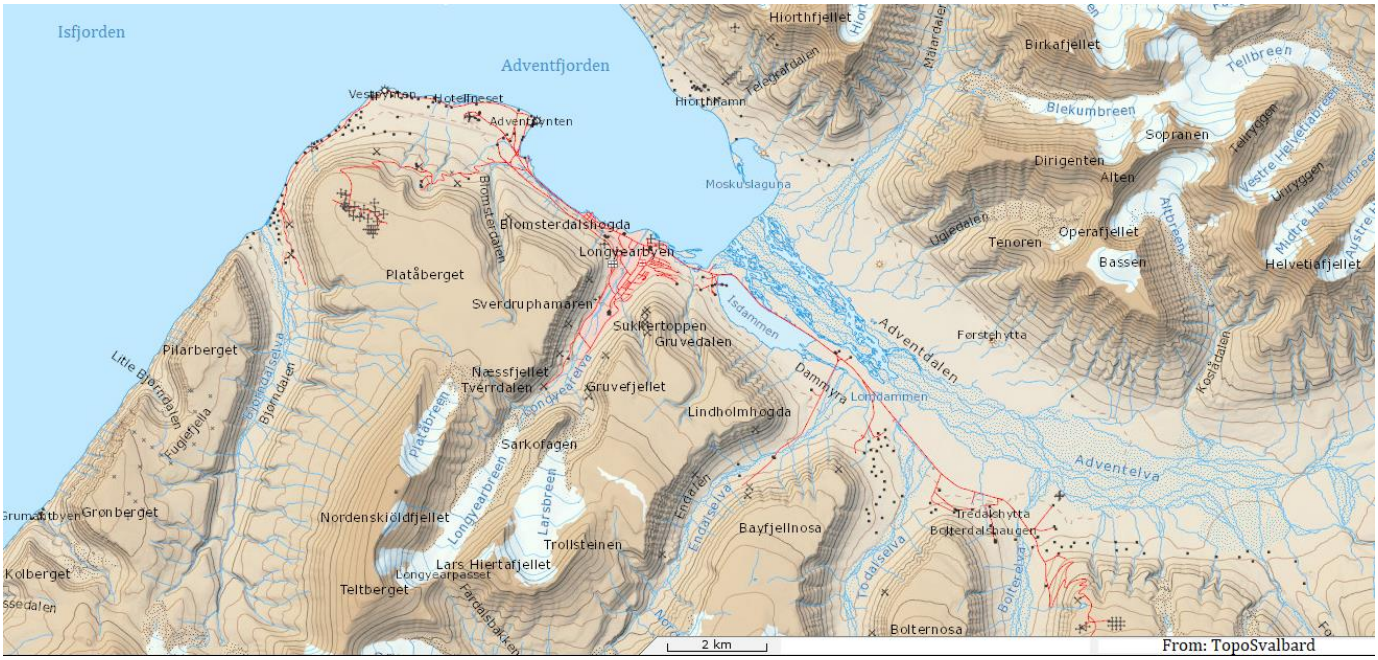

Figure 3: Longyearbyen area map

The town is separated in two by the Longyearelva river which is fed by two glaciers (Longyearbreen and Larsbreen). As can be seen on Figure 4, the river is braided and carries a large amount of sediments in suspension and bedload (note that the banks have been reworked by heavy equipment to limit flooding). According to the Geomorphological and Quaternary Geological map of Svalbard (see Appendix 2), the banks and the stream bed of the river are made of fluvial and glaciofluvial deposits. Due to the transport by water, the granular material from the river has been rounded and ranges from sand to pebbles. The corresponding glacial deposition landform is similar

to a valley sandar. (Dallmann, W; Kjaenet, T; Nottvedt, 2001; Benn, Douglas I.; Evans, 2010; Institute, 2020)

Figure 4: Satellite view of Longyearelva (left) and granular material deposited in one the braided channels (right; orange key ring is 4cm long)

2.3 History of human presence on Svalbard

In 1596, the archipelago was discovered by Willem Barentsz, a Dutch navigator. He was searching for a sea route to the Asian continent. Scientists have found no trace of human activity on Svalbard before its discovery. More than a decade later, the whaling industry started around the islands with ships from a few European nations. The end of the 18th century marked the end of the whaling industry due to an intensive hunt that nearly caused the extinction of the whale species in the area. Russian trappers established camps and started using the archipelago to gather profitable products from approximately 1700's to 1852. They overwintered to collect high quality furs (Arctic fox and polar bears) and other animals during summer. The Norwegians also started to overwinter around the 1800's to collect similar products as their Russian counterparts. The 19th century brought new explorers to Svalbard: the scientists. Many scientific expeditions were organized by European countries to gather data necessary for breakthrough in the fields of geology, ocean currents, shape of the Earth, global climate, glaciers, etc. Nowadays Svalbard is still a famous scientific destination and it has a university centre. (Prestvold, 2015)

Early in the 20th century, industrialized countries required large amount of raw material for their factories. Svalbard was then explored for mineral resources such as coal, gypsum, iron, copper and zinc. Based on promising surveys, an American businessman (John Munro Longyear) founded Longyearbyen as a coal mining town in 1906. The mining activities went well, and in 1916 all the facilities were sold to Norwegian interests (Store Norske Spitsbergen Kulkompani AS; SNSK). Many mines were operated in the valleys around Longyearbyen, but only one location is still active today. (Reymert, 2013; Prestvold, 2015)

Since its discovery, most of the human activities on Svalbard were concentrated on natural resources extraction. Longyearbyen shifted from a mining company town to a more open society in 1989 when SNSK divided its operations into mining, municipal services and tourism. The two latter were completely dissociated from SNSK. Longyearbyen is the largest settlement on Svalbard and the Norwegian administrative centre. The population has grown from around 1800 to more than 2400 in the last thirteen years. (Reymert, 2013; Statistics Norway, 2020)

3 Theory

3.1 Basics of road structure and properties of unbound granular material

A road is composed of multiple layers that each plays a role in the overall structure. Figure 5 shows a typical pavement system for cold regions. The pavement structure distributes the load, through each layer, toward the soil. It also attenuates the geotechnical effects on the surface of the road (i.e. frost-heave or thaw settlements occurring below the surfacing layer). (Hoff, 2008; Doré and Zubeck, 2009)

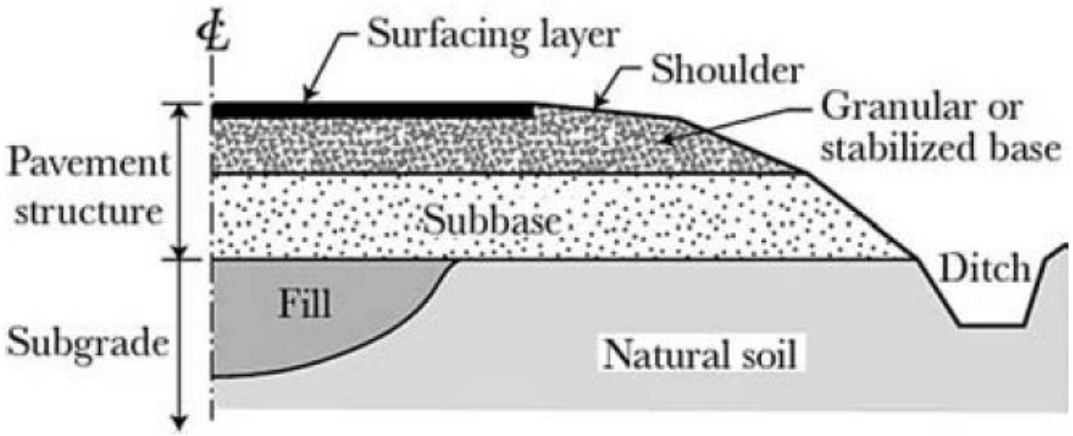

Figure 5: Typical pavement system (from Doré and Zubeck, 2009)

The surfacing layer used for the main roads in Lonyearbyen is hot mix asphalt imported from mainland Norway. This layer is stiff and effective to distribute load to the granular base (also referred to as base layer or base course). Hot mix asphalt seals the underlying granular material and effectively keeps it relatively dry. Additionally, it provides adherence for vehicles and a good drive quality (although this is influenced by all layers). A good drive quality can be defined as safe and comfortable for the users. (Hoff, 2008; Doré and Zubeck, 2009)

The base and subbase layers form a platform for the stabilized asphalt layers. The base layer is made of unbound granular material and mainly has a structural purpose. The density of the material, the moisture content, the gradation, the roughness and the shape of the particle are factors impacting the stiffness and the ability to distribute traffic loads. The main role of the subbase is to dampen the environmental effects from three fronts. First, it acts as a drainage layer that helps regulate the moisture content of the base course. Secondly, the subbase intercepts the fine particles that could migrate from the subgrade soil toward the base layer during periods of high hydraulic pressure (e.g. spring thaw). Thirdly, it provides a frost protection layer for frost-sensitive subgrade soils. To a lesser extent, it also plays a structural role since it is usually stiffer than the underlying soil. (Dawson, 1999; Hoff, 2008; Doré and Zubeck, 2009)

The stiffness of unbound granular material is an important property for road design and analysis. It can be improved by using material that have a good quality of grain contacts (interlocking of the grains) and a high density. Particle shape have an influence on the achievable density of a pavement material and on the quality of grain contacts. Flat and elongated particles are prone to fragmentation and tend to reduce the density and stiffness of aggregates. On the contrary, crushed particles increases the internal friction of granular material. This results in an increased stiffness and strength of the layer. However, it makes the material resist compaction and tends to reduce density for similar compaction energy. Table 1 presents a summary of the granular material properties and their impacts on elements of their behavior. It is important to note that changing one aggregate property independently from the others is rarely possible. (Dawson, 1999; Hoff, 2008; Doré and Zubeck, 2009)

Table 1: Influences of properties of aggregates on behavior of granular material in pavement layers (from Dawson, 1999)

Property	Stiffness	Susceptibility to Permanent Deformation	Strength	Permeability	Durability
Type - Gravel instead of Crushed Rock	↑	↑	↑	none	usually ↑
Grading - Well graded instead of Single-sized	minor ↑	↓	↑	major ↓	↓
Fines content	↓?	↑	varies	major ↓	↓
Maximum Size - Large instead of Small	↑	↓?	minor ↑	↑	↓?
Shape - Angular/Rough instead of Rounded/Smooth	↑	↓	↑	minor	minor
Density	↑	↓	↑	↓	minor
Moisture Content	major ↓	major ↑	major ↓	major ↑	varies
Stress History	↑?	major ↓	minor ↓	none	?
Mean Stress Level	↑	↓	↑	minor ↓	↓

3.2 Unified Soil Classification System (USCS)

The USCS is a classification system which aims to identify soils according to their textural and plasticity qualities and to group them by their behavior. The system is based on past engineering experiences and the characteristics of a soil that indicates how it will behave as a construction material. These characteristics can be determined by simple tests such as:

- Sieving to determine the percentage of gravel, sand and fines.
- Determining the coefficient of uniformity and curvature which indicates the shape of the grain size distribution curve.
- Determining the plastic limit (PL), liquid limit (LL) and plasticity index (PI) which will influence the final classification of the soil.

The sieve differencing gravel and sand is the 4.76mm (No. 4). To differentiate sand and fines, the No. 200 sieve is used (0.074mm). The Coefficient of Uniformity (C_u) and Coefficient of Curvature (C_c) are indicating how the soil is graded. A soil with identical particles (uniformly graded) will have a value close to 1. High values of C_u indicate that there are large variations within the soil mass particle sizes. A well-graded soil will have a C_c between 1 and 3 which indicates a concave curvature of the grading curve. Those coefficients can be calculated with the help of a grading curve and the following formulas:

$$C_u = \frac{D_{60}}{D_{10}} \qquad \text{Eq. (1)}$$

$$C_c = \frac{{D_{30}}^2}{D_{10} * D_{60}} \qquad \text{Eq. (2)}$$

Where:

D_{10} is the grain diameter at 10 percent passing
D_{30} is the grain diameter at 30 percent passing
D_{60} is the grain diameter at 60 percent passing

This study focussed on granular material with few fines and the third tests are not relevant for such soils in the classification (Army, 2001). Classifying the studied granular material within the USCS allowed comparison with literature from the United States of America.

3.3 Cyclic triaxial test and resilient modulus theory

This test is also referred to as a Repeated Load Triaxial Test (RLTT) in the literature. The resilient modulus and and the resistance against permanent deformation of a granular material can be determined with this test. During a RLTT, the apparatus applies a confining pressure in all directions (the triaxial stress, σ_t) and a supplementary vertical dynamic stress (the deviatoric stress, σ_d). This vertical stress will increase for the different levels of the cyclic triaxial test, as described in Section 5.5. Figure 6 shows a specimen and the stresses applied in relation to the regular triaxial principal stresses.

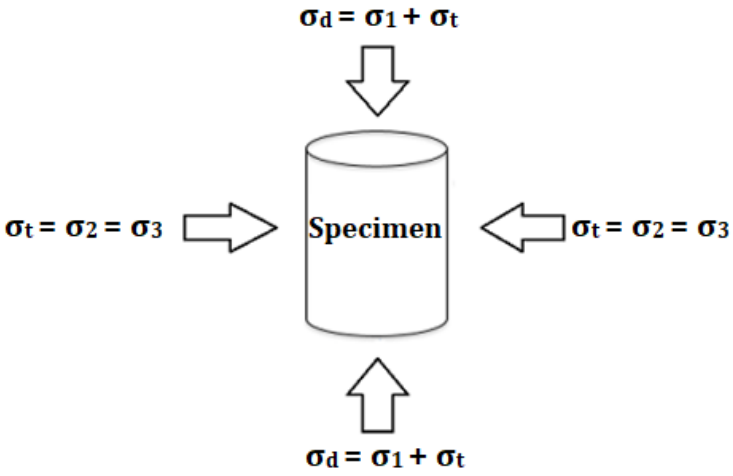

Figure 6: Cyclic triaxial stresses

The deformation response of a granular material under a loading can be divided into two types: one resilient (elastic, recoverable; ε_r) and one permanent (residual, not recoverable; ε_p). For a known variation of the dynamic deviatoric stress and a constant confining pressure, the resilient modulus (M_R) is calculated according to this equation:

$$M_R = \frac{\Delta\sigma_{d,dyn}}{\varepsilon_{r,v}} \qquad \text{Eq. (3)}$$

Where:

$\varepsilon_{r,v}$ is the axial resilient vertical strain

M_R characterizes the mechanical properties of the material and it is used to calculate the mechanical response (stresses, strains, and displacements) of the pavement under traffic loading (Doré and Zubeck, 2009; Barbieri, 2019)

There are multiple non-linear relationships to describe M_R with different parameters, but this study uses the Hicks and Monismith regression model (Eq. 4). This relationship is easily plottable as a M_R - θ graph. The bulk stress (θ) is defined as the sum of stresses applied to the specimen ($\theta = \sigma_d + 3\sigma_t$).

$$M_R = k_1\sigma_a\left(\frac{\theta}{\sigma_a}\right)^{k_2} \qquad \text{Eq. (4)}$$

Where:

θ is the bulk-stress

k_1 and k_2 are regression parameters

σ_a is a reference pressure (here 100 kPa)

The resistance against permanent deformation is another result of the RLTT. The permanent axial strain is plotted for each load cycle of the test. Figure 7 presents a typical plot for five load sequences. The fifth sequence reaches the 0.5% axial strain limit (mentioned in Section 5.5).

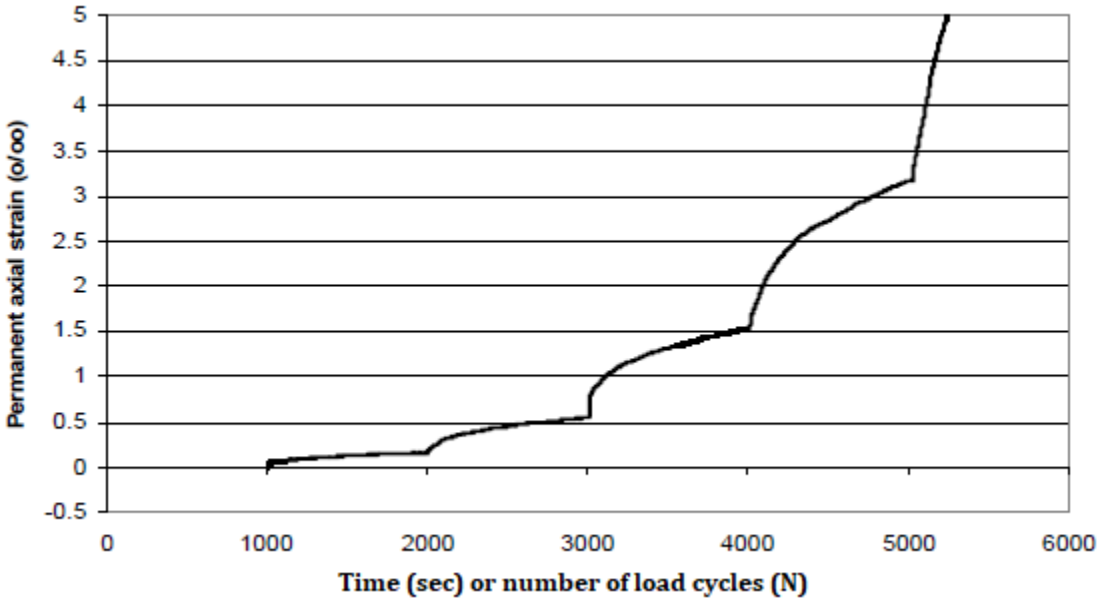

Figure 7: Example of a RLTT's permanent axial strain vs number of load cycles plot (modified from Hoff & al., 2003)

It can be observed that the permanent deformation develops faster in the beginning of a load cycle than at its end. Each load step is analyzed to determine in which stage the material belongs according to Table 2: The average strain rate for the last 5 000 cycles in each step has been used to limit the different stages as explained in (Hoff, Bakklok and Aurstad, 2003).

Table 2: Permanent strain rates and the stages of material behaviour

Permanent strain rate $\dot{\varepsilon}_{v,p}$	Stage
$\leq 2.5 * 10^{-8}$	Elastic zone
$2.5 * 10^{-8} < \dot{\varepsilon}_{v,p} \leq 1.0 * 10^{-7}$	Elastoplastic zone
$> 1.0 * 10^{-7}$	Plastic (failure) zone

After the classification of each load step, the best fit lines between the boundary of the stages can be found using the Coulomb approach. It defines the mobilized angle of friction «ρ» and the angle of friction at incremental failure «φ» as shown on Figure 8. To simplify the comparison, the apparent attraction «a» was fixed at a value of 20 kPa for all samples of this study.

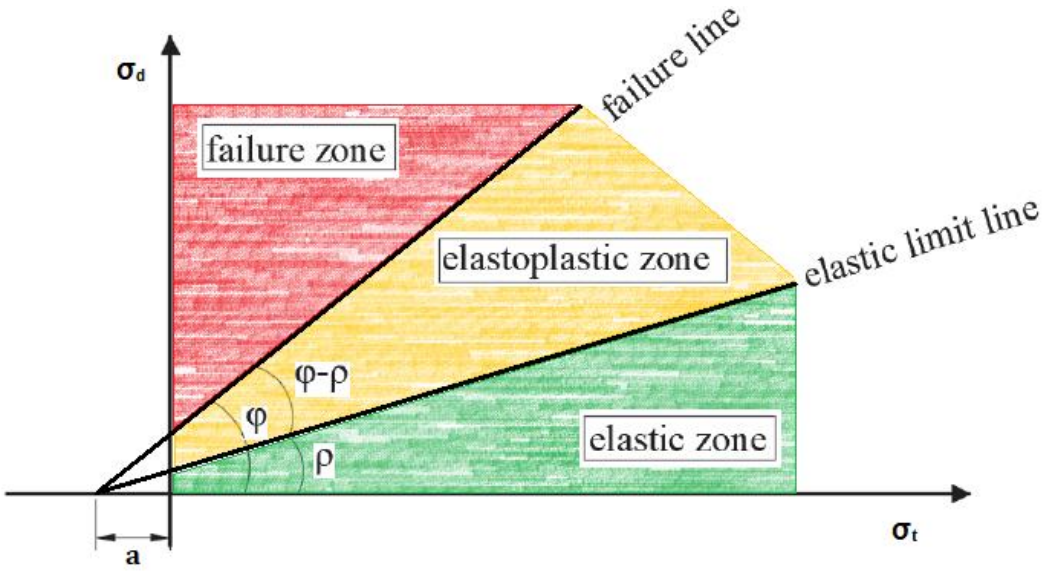

Figure 8: Angles of friction (ρ and φ) according to Coulomb approach (modified from Barbieri, 2019)

According to this approach and from (Barbieri, 2019), the mobilized angle of friction (Eq.5) is:

$$\sin \rho = \frac{\sigma_1 - \sigma_3}{\sigma_1 + \sigma_3 + 2a} \qquad \text{Eq. (5)}$$

and the equations for the elastic limit line (Eq. 6) and failure line (Eq.7) are:

$$\sigma_d = \frac{2 \sin \rho \ (\sigma_3 + a)}{1 - \sin \rho} \qquad \text{Eq. (6)}$$

$$\sigma_d = \frac{2 \sin \varphi \ (\sigma_3 + a)}{1 - \sin \varphi} \qquad \text{Eq. (7)}$$

3.4 Permafrost considerations

Permafrost is a soil (or rock) having a temperature below 0°C for at least two consecutive winters and the summer in between. The upper layer of ground with a temperature varying above and below 0°C is called the active layer. The natural depth of this layer is approximately 1m around Longyearbyen, but it goes deeper if the ground's thermal regime has been altered by human activities (e.g. it was measured at 2.3m under the airport's runway). The construction techniques applied in seasonal frost regions are not directly applicable in permafrost environment. Usually in a seasonal frost context, designers will try to prevent frost penetration to the soil underlying a structure in order to prevent issues such as frost-heave. Permafrost construction will try to avoid thawing the frozen ground since the ice formations in the soil matrix are already fully developed

(below the active layer). (Humlum, Instanes and Sollid, 2003; Andersland, Orlando B.; Ladanyi, 2004; Doré and Zubeck, 2009; Sinitsyn, Kotov and Aalberg, 2020)

Climate changes are modifying the thermal equilibrium that was established by the natural processes in polar regions. This phenomenon causes the warming and thawing of permafrost, a thicker active layer and a reduction in soil strength. From an engineering point of view, this results in a deterioration of mechanical properties, increased thaw settlements, accelerated creep rate and instability of slopes. The magnitude of these changes will vary greatly according to the permafrost and regional characteristics. Over the last few decades, engineers have been developing and adapting their design to minimize the impacts on built infrastructure. In general, the solutions are either to accept that the thermal regime will be warmer after the construction operations or to maintain the cold thermal regime (or even to bring the ground temperature down). (Humlum, Instanes and Sollid, 2003; Andersland, Orlando B.; Ladanyi, 2004; Doré and Zubeck, 2009; Canada, 2010)

4 State of the art

4.1 Scientific research

At the knowledge of the local stakeholders and the author, a specific research on the use of Svalbard rock as an unbound construction material has not been performed. A thorough study was realized by SINTEF to assess if the stones from Svalbard could be used as aggregates to produce concrete (Skjølsvold and Haugen, 2016). They tested samples collected from three different locations on the archipelago (Bolterelva, Longyearelva and Svea). SINTEF reported the following facts that are also relevant for this study:

- Crushing the material to a certain size should be done with only one crush. It maintained good grain shape. They tried to crush some material a second time, but it became more chipped and had to be discarded.
- Part of the rocks from Svea had an exterior crust that was heavily weathered and could be removed with the fingers (10% of sample).
- The aggregates tested all obtained an intermediate level of resistance to wear (Los Angeles test; LA_{30}-LA_{35}) and they were in the best frost resistance class (F1), according to NS-EN 12620.
- It was possible to crush the rocks down to a sand fraction. The grain shape was good, but the particle size distribution was not optimal. There was an excess of particle with a size close to 0.1 mm. This was explained by the size of the sand grains composing the sandstone.
- The result of the crushing is highly dependent on the equipment and procedures used (both for aggregate and sand).
- Concrete made with all three stone samples achieved a normal compressive strength for the designed mix, but they all fell outside the requirement for frost-resistant concrete.

4.2 Longyearbyen's common construction practices

A wide range of local stakeholders from Longyearbyen were interviewed to establish the current construction practices and what were the past experiences with local granular material. The interviewees were key persons in construction contractor companies, public organizations and engineering consultants. (Gunhildberget, 2020; Ingerø, 2020; Kanstad, 2020; Pedersen, 2020; Ringheim, 2020) A summary of the main findings is presented below:

- There are two granular material stockpiles that are currently being operated in Longyearbyen. The rock samples for this study were collected at Site 1 located near the junction of Bolterdalen and Adventdalen (coordinates are: 78°10'34.0"N; 15°58'11.2"E).

The granular material stored there are originating from riverbeds and riverbanks (mainly from the Longyearelva river). The granular material has a rounded shape and it is rare to find pieces bigger than 200mm. It is mechanically sorted (but not crushed) in three size fractions (0-30mm, 30-60mm and 60+ mm). The second site is located near the former coal mine 3 (Gruve 3). It is at the bottom of a cliff and the granular material is simply originating from rockfalls (coordinates: 78°14'01.0"N 15°26'50.8"E). The rocks are more angular (described as cubic) and have an average size of up to 400mm. Both sites are operated by a local construction contractor. Figure 9 shows the general location of both sites on a satellite photograph. The quantity of material in Site 1 is greater because it is easily reloaded due to the work being done around the rivers. The quantity in Site 2 is limited by the occurrence of rockfalls. Appendix 3 presents pictures of both sites.

- From past experiences, the granular material from Site 1 behaves in a satisfactory manner if it is not used for any load-bearing purpose or roads. It crushes under traffic load; it does not compact well, and the fine fraction transforms into mud rapidly. After being sorted by size, the material is mainly used as a ventilated cover for the district heating pipes (30-60mm), for levelling the ground where no traffic is intended (0-30mm) and as a general backfill material (0-60+mm, unless frost protection is specified). The largest sorted fraction (60mm+) is used in larger construction projects for the bottom part of granular pads and embankments.

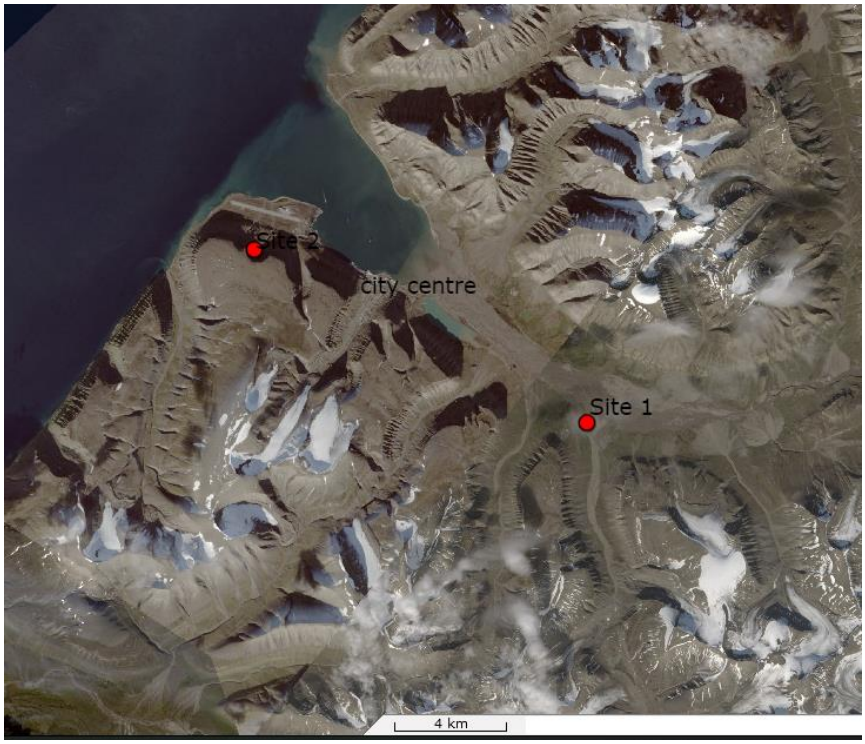

Figure 9: Location of the two granular stockpiles of Longyearbyen (satellite photograph from TopoSvalbard)

- The granular material from Site 2 has a suitable shape to be used in granular pads and under roads. Over time, it has been decided by the local stakeholders that this material would be used for the more critical work where some load bearing capacity is required.
- The rock imported from mainland is used for the following construction activities: concrete and asphalt production, riverbank and coastal erosion protection, road structure, structural embankments, gabion retaining walls, road repairs and winter road maintenance (sand).
- The local road designers follow the Norwegian pavement design manual N200 as much as practical and economical for Longyearbyen's context (thickness of layers and material specifications). In general, imported rocks are used for the pavement and base layer. Local rocks have been used for the subbase layer to reduce costs of most roads in town.
- The Norwegian Building Regulations for Longyearbyen § 4 (Byggeforskrift for Longyearbyen) does not specify any foundation type in permafrost area but refers to scientific literature from 1994-2000. (Justis- og beredskapsdepartementet, 2016)
- Each year approximately 20 000 tons of granular material is imported by the construction contractor that is in charge of this operation. Additionally, the company operating the local airport imports around 1700 tons of sand and fine gravel to use for the winter maintenance of the runway. This amount lasts for one or two years depending on the intensity of the winter.
- The Norwegian Water Resources and Energy Directorate (NVE) is executing two large projects in Longyearbyen that are increasing the average quantity of granular material imported from the mainland. The Longyearelva riverbanks protection required a significant amount of large boulders to be imported in the last two years. The avalanche protection wall's construction started in 2020 and it requires significant volumes of imported rocks for its completion (roughly 70 000 tons of different sizes).
- The granular material from Longyearelva is being mechanically sorted near Nybyen in order to use it in parts of the wall. The construction contractor has reported that a significant amount of fine is complicating the sieving task and lowering the expected granular production. The initial target of this project was to import around 70 000 tons of granular material (gravel, cobbles and large blocks) and to harvest almost 20 000 tons of riverbed gravel. The fraction of local material will possibly decrease since the production might be overestimated.
- Old fill material from mining operation (20 000m^3) might be re-used in the avalanche protection wall to supplement the granular material from Nybyen as it is only lightly contaminated and directly on the construction site. Otherwise, that material could not be used on Svalbard and would need to be shipped to mainland Norway for environmental remediation. For comparison, a past project had 800 m^3 of similar material brought back for disposition for a cost of 1.5 million NOK.

5 Methodology

This study aims at determining if the granular material available around Longyearbyen has the potential to be used as a road material, as foundation for buildings or as a general-purpose material for construction. Most laboratory equipment required for the testing is not available on Svalbard. Hence most tests were realized at the Department of Civil and Environmental Engineering of NTNU in Trondheim. The following tests were done at the NTNU's Road, Transport and Geomatics laboratory: abrasion tests (Los Angeles and Micro-Deval), determination of particle shape, specific density, thermal conductivity and cyclic triaxial. The freezing and thawing resistance test was done in the NTNU Concrete lab and in the Cold lab of the University Centre of Svalbard (UNIS). Some samples were sent to the Department of Geology at NTNU to have them perform an X-Ray Diffraction analysis.

The experiments were realized under the supervision of Inge Hoff and Arne Aalberg, Professors at NTNU. The lab work was executed over a seven-weeks period in September-October 2020.

5.1 Sampling & material preparation

A first bulk sample of granular material was collected from Site 1 in early February 2020. It was brought back for further analysis in the laboratory in Trondheim. The sample had a total mass of approximately 46 kg. It contained a mix of cobbles and pebbles that were covered by a dried mixture of finer material (sand, silt, clay). At the time, it was impossible to collect smaller material because it was frozen solid on the ground. As can be seen in Figure 10, the rocks were mostly sub-rounded to well-rounded with the presence of a few sub-angular pieces. The shapes varied between elongated to almost spherical and all the rocks were sedimentary.

Figure 10: Larger granular fraction of the sample with a 1-m ruler (left hand side) and smaller granular fraction with a 30cm ruler (right hand side)

A second bulk sample of granular material was collected from the same stockpile (Bolterelva) in late June 2020. It was shipped to the laboratory in Trondheim to conduct more analysis. The sample had a total mass of approximately 300 kg. It contained a similar mixture of cobbles and pebbles with a general size of 20 to 150mm. All the rocks were sedimentary, and they were covered by a dried mixture of finer material. As can be seen in Figure 11, the rocks were mostly sub-rounded to well-rounded with the presence of a few sub-angular pieces. The shapes varied between elongated to almost spherical.

Figure 11: Smaller fraction of the second bulk sample (30cm ruler)

The material preparation included crushing, washing and mechanical sieving in various size fractions. The crushing was realized with a jaw crusher (see Figure 12). It was possible to adjust the final opening of the crusher by removing or adding steel plates in order to produce different granular fractions.

Figure 12: Jaw crusher from the laboratory

5.2 Los Angeles and Micro-Deval abrasion tests

The abrasion tests are used to categorize material in road standards for various countries. The Los Angeles test indicates how the particle will resist to fragmentation (i.e. under heavy construction traffic) and the Micro-Deval test indicates the particle's long-term resistance to wear (i.e. during the road design life). In other words, the abrasion tests give information on the hardness of the material.

The Los Angeles (LA) test determine the mass of the sample that is crushed to a certain size in a rotating steel drum with steel balls. The Micro-Deval (MDE) test determines the mass proportion of a sample that is reduced after revolutions in a steel drum with smaller steel balls and water. The sketch of Figure 13 shows the difference between the two test methods (Doré and Zubeck, 2009).

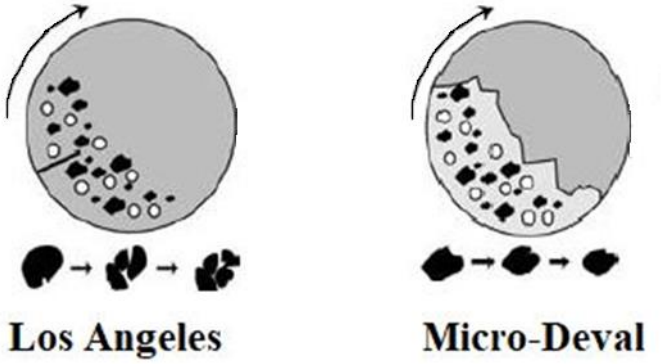

Figure 13: Los Angeles and Micro-Deval drums sketch (Doré and Zubeck, 2009)

The steps listed in the European Standards (DS-EN 1097-2 and DS-EN 1097-1) were followed. A total of 10 samples (5 LA and 5 MDE) were tested from the material brought from Longyearbyen. (European, 2010, 2011)

5.3 Determination of particle shape

Flat and elongated particles might break down under loading due to their weakness and this can become problematic for some construction applications. This test quantifies the mass proportion of particles with such shapes. The sieving operation occurs in two consecutive steps: one with square mesh sieves and the second one with bar sieves. The flakiness index (FI) is calculated as the total mass of particles passing the bar sieves as a percentage of the total dry mass of the particles tested. The procedure described in the European Standard (DS-EN 933-3) was followed for the three tests realized. (European, 2012)

5.4 Free-thaw resistance of particle

Material that cannot resist the annual freezing and thawing cycles should be identified prior to construction in cold regions. This test assesses if an aggregate of a certain size will change after 10 freeze-thaw cycles (crack formation, loss of mass, etc.). The test portions are soaked in water at atmospheric pressure before the beginning of those cycles. Since salts are not used in Longyearbyen as road de-icing agents, this test was realized in distilled water as per standard. The general steps listed in the European Standards (DS-EN 1367-1) were followed and one test was done. (European, 2007b) Due to logistical and equipment availability constraints, the listed deviations were made to the European Standards method:

- The sample was divided into six portions instead of three to better fit the containers.
- The containers were Nalgene plastic containers with a lid instead of metallic ones.
- Since no programmable freezer was available, the steps presented in Table 3 were followed to re-create a similar freeze-thaw cycle:

Table 3: In-house freezing-thawing sequence

Daily action time	Steps undertaken
09:00	From 21°C to around 0°C; in a -5°C storage room
13:00	From 0°C to -18°C; in a -18°C freezer room
18:00	From -18°C to 21°C; in a 21°C room with a lukewarm water bath
9:00 +1day	From 21°C to around 0°C; in a -5°C storage room

- The sieving after the 10-days test was done with a 4.75mm sieve instead of 4mm (unavailable).

5.5 Cyclic load triaxial test for unbound material

During the experiment, the specimen is subjected to predetermined dynamic stress cycles and a confining stress provided by a triaxial pressure chamber using water a confining medium. The total axial deformation recovered during the cycle is used to calculate the resilient modulus (Eq. 3). Figure 14 shows the upper and lower limit of a standard grading curve that was used for all four tests. (Barbieri, 2019) It is based directly on the requirements for a road base layer (0-31.5mm) from the Norwegian pavement design manual N200 (Statens vegvesen, 2018). The bulk and dry density of each samples is shown in Table 4. The multi-stage low stress level procedure described in the European Standard (DS-EN 13286-7) was followed for all tests. It consists of five loading sequences with a different confining pressure (σ_t = 20, 45, 70, 100 or 150 kPa). Additionally, six load steps (σ_d) are applied for each load sequence. (European, 2004) The low stress procedure was selected because the rocks from Longyearbyen are considered weak and it would provide enough

load steps for a thorough subsequent analysis. It is worth mentioning that a loading sequence is interrupted if the axial permanent deformation reaches 0.5%. The test would then be continued by starting the next sequence.

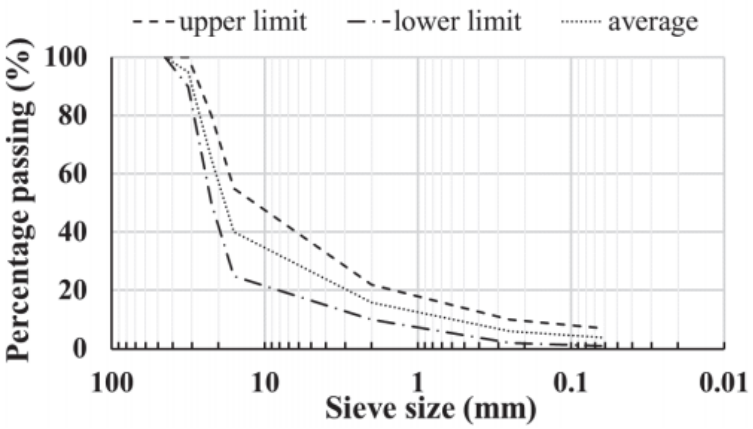

Figure 14: Grain size distribution limit curves for base layer (Barbieri,2019)

Table 4: RLTT specimen densities

Specimen #	Bulk density kg/m³	Dry density kg/m³
1	2013	1974
2	1992	1953
3	2050	1915
4	2051	1916

A total of four specimens were tested specimens. Each sample had a dry mass of 11kg. Specimens 1 and 2 had a water content of 2% and specimens 3 and 4 had a water content of 7%. The sample preparation steps are based on the expertise developed during a precedent study (Barbieri, 2019). In the beginning, the total granular mass was divided in five plastic bags and was mixed with the desired amount of water. The bags were left to rest overnight to ensure that the water was uniformly distributed. The granular material inside each plastic bag corresponded to the grading curve shown in Figure 14. Afterward, the content of the five plastic bags were compacted in five layers inside a steel mould to form the testing sample. A Milwaukee 2" SDS Max rotary hammer (hammer weight 12 kg, work per blow 27 N·m, tamping time 25 s) was used for the compaction, as seen in Figure 15. Once compacted, the sample was extracted from the mould with a customized ejection tool and covered by two latex membranes, four O-rings, two hose clamps and two metal end-platens. Finally, the specimen was placed into the RLTT device and two vertical Linear Variable Displacement Transformer (LVDTs) and three radial LVDTs were installed on the specimen (partially seen on Figure 15).

Figure 15: From left to right: Compaction apparatus and mould; compacted test specimen; triaxial cell being filled with water

5.6 Mineral identification using X-Ray Diffraction

X-Ray Diffraction (XRD) was used for the identification and quantification of mineral composition of four specimens from bulk sample 1 (see Figure 16). A fifth sample was sent for analysis after a rock core was extracted from a cobble of bulk sample 2. This rock core was used for the determination of thermal properties (Section 5.7). The XRD tests were performed by the Geology Department of NTNU. Basically, the studied sample is shot with an X-Ray beam and the diffracted beam is recorded as a peak on a pattern plot. Each material has a unique diffraction pattern (peak positions, intensities, widths and shapes). The composition of each samples is determined by computer with a database.

Figure 16: The five specimens sent for XRD analysis

5.7 Thermal conductivity

Thermal parameters are essential for accurate thermal modelling in cold regions. During this study, the unfrozen thermal conductivity was measured for two granular samples. The first one was made of crushed gravel (size from 2mm to 8mm) that was compacted in the PVC mold and saturated (see Figure 17). The second one was from a rock core drilled out of a cobble. The mineralogy of the rock core was determined by XRD analysis.

Figure 17: Saturated gravel sample

The experimental set up shown in Figure 18 was used for these measurements. It has been built in a similar way to the one described in details by (Côté and Konrad, 2005b). A thermal conductivity cell was put in an insulated refrigerator maintained at a constant temperature of about 5 °C for the unfrozen samples. The granular sample and the mold are placed between two Pyrex disks that have two thermistors embedded in the center, a few millimeters from the contact surface with the sample. The temperature boundary conditions are kept constant by two independent heat exchangers (top one at 9°C and bottom one at 1°C). This will result in a vertical heat flow through the thermal conductivity cell. The sample and the Pyrex disks are insulated with a 100 mm thick rigid insulation to avoid heat losses. The rock core's side had to be insulated with two layers of rock wool since it had a different height than the normal PVC mold. A thermal paste was used for the surfaces that were in contact (bottom of the mold, rock core, Pyrex disks). This substance allowed to have a more uniform contact and to avoid trapping some air between the surfaces. The temperatures of the top and bottom of each heat flux meter are recorded every minute and were subsequently plotted as a function of time. The steady-state heat flow condition was reached when the temperature profile became constant with time.

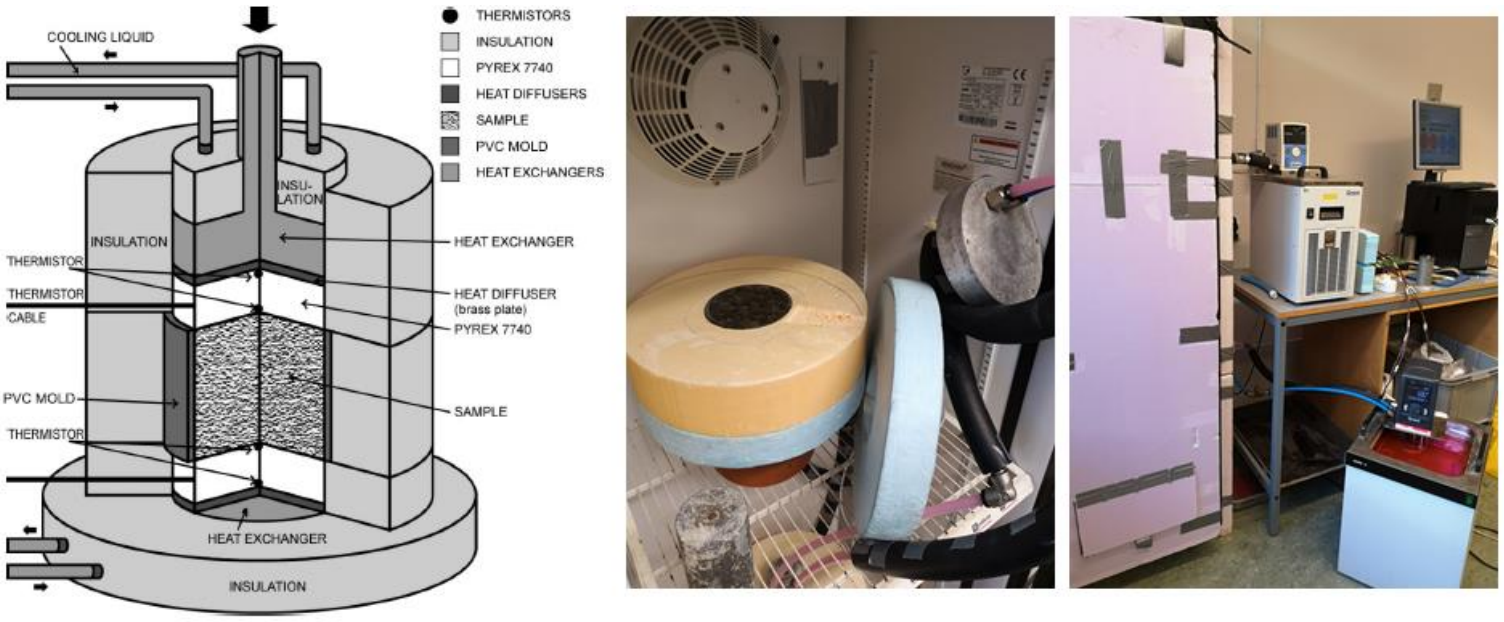

Figure 18: Schematic and pictures of the thermal conductivity cell (left from Côté and Konrad, 2005)

5.8 Specific density

The specific density of the material was measured for two size fractions: crushed gravel from 2mm to 8mm and cobbles (100-150mm). Two samples of gravel were tested with a pycnometer and a vacuum was applied to ensure that no air was entrapped. The procedure described in the European Standard (DS-EN 1097-6) was followed for the most part. (European, 2013) Another apparatus was used for the specific density of the two cobbles (shown in Figure 19). Firstly, the mass of the samples was measured in a dry condition in the air. Secondly, the mass was measured while suspended in a water basin. This experimental set up is based on the following two equations:

$$m_1 * g = m_2 * g + \rho_w * g * V \qquad \text{Eq. (8)}$$

$$\rho_{sample} = \frac{m_1}{V} \qquad \text{Eq. (9)}$$

Where:

m_1 is the sample mass in the air (in g)
m_2 is the sample mass in the water (in g)
g is the gravitational acceleration (m/s²)
ρ_w is the water density at the temperature during measurement (g/cm³)
ρ_{sample} is the sample's density (g/cm³)
V is the volume of the sample (cm³)

Figure 19: Specific density apparatus for cobbles

6 Results and discussion

The dataset includes results reported by SINTEF (Skjølsvold and Haugen, 2016) and additional tests aimed to fill-in knowledge gaps on the granular material from Longyearbyen. The results are detailed in this section and the raw data is in Appendix 4. The laboratory findings are discussed and compared to the standards thresholds. The sources of errors are also mentioned in the subsections, when relevant.

6.1 Crushing and sieving

Most of the tests required specific size fractions for their execution. All the material was passed twice into the crusher unlike what was done previously by SINTEF. The first gravel batches were meant to be used for the LA and MDE tests and were produced from natural gravel having an average size of 20-25mm. The targeted bulk production size was 8-14 mm by putting all the adjustment plates in the jaw crusher. It is represented by the sieving curve Type 1 in Figure 20. Once all the 20-25mm natural gravel was crushed, the author used 20-40mm natural rocks to produce more of the 8-14mm crushed gravel. Sieving occurred in-between the two passes in the crusher. Type 2 results from one crushing and Type 3 is after the second crushing of another portion from the same production batch.

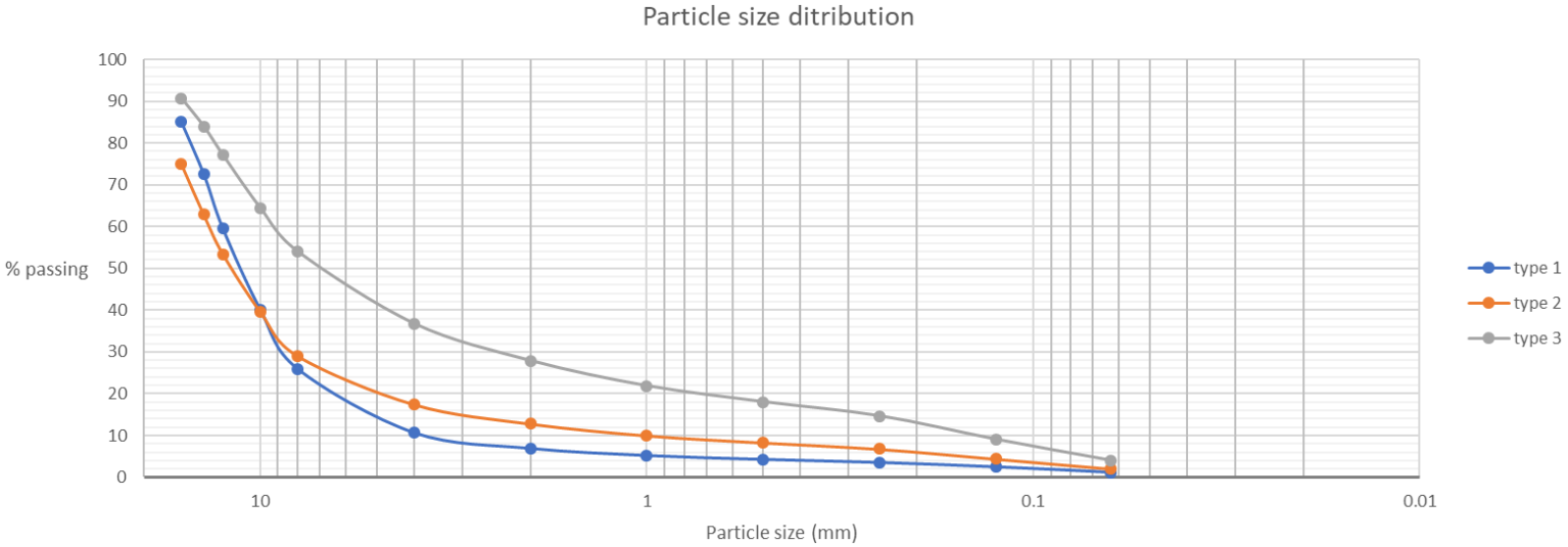

Figure 20: Particle size distribution after crushing operations

The fines content for each type of crushed product is presented in Table 5. The values obtained are in the lowest fines content categories for the «All-in» materials, according to (European, 2008).

Table 5: Fines content

	Mass fraction passing the 0.063 mm sieve (%)	Category
Type 1	1.2	f2
Type 2	2.0	f2
Type 3	4.0	f4

The C_u and C_c from the three Types were calculated and they were classified according to the USCS in Table 6.

Table 6: USCS classification

	C_u	C_c	USCS class	% passing 0.02 mm
Type 1	3.13	1.62	GP	< 1.16
Type 2	13.50	4.74	GP	< 2.04
Type 3	68.75	3.55	GP	< 3.98

The triaxial tests required larger particles and 50-150mm rocks were used to produce crushed material with a size from 0 to more than 31.5 mm. Most of the jaw crusher's adjustment plates were removed to make the coarser material. Figure 21 presents natural rocks versus the crushed material after 2 crushing cycles.

Figure 21: 50-150mm natural material to gravel (after 2 crushing cycles)

The moisture content (w) was measured at three locations for this study: during storage at NTNU and on the field on October 30, 2020 at both stockpiles. The sample from Bolterelva (Site 1) was picked up in an area that had just been reworked with an excavator and it did not have time to

refreeze. On the other hand, the sample from Gruve 3 (Site 2) was collected from a frozen pile. The results are presented in Table 7:

Table 7: Water content

Sample	w (%)
NTNU storage	0.57
Bolterelva stockpile	6.44
Gruve 3 stockpile	10.04

The natural rocks behaved well in the jaw-crusher (no projection outside of the machine) and it was possible to obtain various size fractions in sufficient quantities for the completion of the laboratory tests. The shape of the crushed granular material produced was ranging from sub-angular to angular with very few sub-rounded particles. By inspecting Table 6 and Figure 20, the produced material can be labelled as poorly graded within the sieves used (16-14-12.5-10-8-4-2-1-0.5-0.25-0.125-0.063mm). The Type 1 and Type 2 samples nearly show a gradation gap around the size 0.5mm to 2mm. It can be noticed from the percentage of passing particles between the 12.5mm and the 0.125mm sieves that there is a large increase of smaller particles between the first and second crushing (Type 2 and Type 3). This observation is consistent with what was mentioned in the SINTEF report.

During the manual sieving operations, some of the weakest crushed material was reduced to smaller size (particles of 1-4mm in size). Therefore, a small portion of the gravel sample can be considered as very brittle and it is likely that some wear also occurred during the mechanical sieving.

The three types of crushed rock that were sieved were classified according to the U.S. Army Corps of Engineers (USACE) Frost Design Soil Classification System (see Table 8). This classification system determines the frost susceptibility of various soils, base and subbase materials that could be used for linear infrastructures (roads, railway, airfields). Frost susceptibility can be defined as a soil that has a potential for frost-heaving and/or thaw-weakening that can affect an engineered structure. Two conditions must be present simultaneously before frost action becomes problematic: a source of water during the freezing period and a sufficient freezing period allowing temperature to penetrate the ground. Longyearbyen area satisfies both conditions because its thawed ground can act as a water source until the permafrost active layer is completely frozen back and it has a very cold climate. (Army, 2001; Andersland, Orlando B.; Ladanyi, 2004)

Table 8: USACE Frost Design Soil Classification System

TABLE 2-7 U.S. Army Corps of Engineers Frost Design Soil Classification System

Frost susceptibility[a]	Frost group	Kind of soil	Amount finer than 0.02 mm (wt %)	Typical soil type under USCS[b]
Negligible to low	NFS[c]	a. Gravels	0–1.5	GW, GP
		b. Sands	0–3	SW, SP
Possibly	PFS[d]	a. Gravels	1.5–3	GW, GP
		b. Sands	3–10	SW, SP
Low to medium	S1	Gravels	3–6	GW, GP, GW-GM, GP-GM
Very low to high	S2	Sands	3–6	SW, SP, SW-SM, SP-SM
Very low to high	F1	Gravels	6–10	GM, GW-GM, GP-GM
Medium to high	F2	a. Gravels	10–20	GM, GM-GC, GW-GM, GP-GM
Very low to very high		b. Sands	6–15	SM, SW-SM, SP-SM
Medium to high	F3	a. Gravels	>20	GM, GC
Low to high		b. Sands except very fine silty sands	>15	SM, SC
Very low to very high		c. Clays, $I_p > 12$	—	CL, CH
Low to very high	F4	a. All silts	—	ML, MH
Very low to high		b. Very fine silty sands	>15	SM
Low to very high		c. Clays, $I_p > 12$	—	CL, CL-ML
Very low to very high		d. Varved clays and other fine-grained banded sediments	—	CL and ML; CL, ML, and SM; CL, CH, and ML; CL, CH, ML, and SM

[a] Based on laboratory frost-heave tests.
[b] G, gravel; S, sand; M, silt; C, clay; W, well graded; H, high plasticity; L, low plasticity.
[c] Non-frost susceptible
[d] Requires laboratory frost-heave test to determine frost susceptibility.

Table 9 presents the classification of the three sieved material in relation with Table 6 (USCS classification).

Table 9: Classification under the USACE Frost Design Soil Classification System

	Frost susceptibility	Frost group	% passing 0.02 mm
Type 1	Negligible to low	Non-frost susceptible	< 1.16
Type 2	Possibly	Possibly frost susceptible	< 2.04
Type 3	Low to medium	S1	< 3.98

The main factor influencing the ranking of the three samples was the amount of fine material (passing the 0.02mm) that they contained. As can be seen from Table 8, a maximum of 1.5% fine content is necessary for a non-frost susceptible (NFS) gravel. The sample from Type 2 would require a frost-heave test to ensure that it can be considered as a NFS material. Type 3 could be improved by removing the finer fraction before considering using it for linear infrastructures.

6.2 Los Angeles and Micro-Deval abrasion tests

The results from the abrasion tests are presented in Table 10 and Table 11. A procedural error was made for the two first Micro-Deval tests and they were discarded.

Table 10: Los Angeles results

Test #	LA value
1	33
2	34
3	34
4	34
5	33
Average	34

Table 11: Micro-Deval results

Test #	MDE value
3	50
4	47
5	45
6	46
7	48
Average	47

The LA values obtained are at an intermediate level (approximately Class LA_{30}-LA_{35}) and the MDE results are at the highest level ($M_{DE}45$-$M_{DE}50$), according to (European, 2008). The LA values are in the same class as what SINTEF reported in their work for concrete aggregates.

The abrasion tests result from Table 10 and Table 11 indicate that the local material is more sensitive to wear during its service life than to fragmentation during construction. From a critical point of view, the LA test is useful to identify brittle materials which degrade under impact, but it does not adequately measure the interparticle friction that would happen during cyclic loading. The MDE test was deemed more effective at identifying good granular material since it correlates with field performance. In Canada and in the USA, numerous transport agencies decided to include the MDE test to replace older tests and to supplement the results given by the LA test. (Richard and Scarlett, 1997; Lang *et al.*, 2007)

The results obtained are compared below to the Norwegian pavement design manual N200 and to other foreign cold regions standards to assess its possible use in a pavement structure.

6.2.1 Norwegian Public Roads Administration (Statens vegvesen)

The Norwegian Public Roads Administration is relying on the Norwegian pavement design manual N200 for all the specifications regarding roads. (Statens vegvesen, 2018) The requirements for the subbase and baselayer are presented in Table 12 and Table 13. Many factors are presented but only the LA and MDE will be discussed. In Table 12, the relevant material type for this study are the two uppermost (*knuste steinmaterialer* and *knust og uknust grus*).

Table 12: N200 material requirements for subbase

Krav til mekaniske egenskaper (knuste steinmaterialer)	**Trafikkgruppe**	
	A[1]	**B, C, D, E og F**
Los Angeles-verdi, LA	≤40	≤35
Micro-Deval-koeffisient, M_{DE}	≤25	≤20
Krav til mekaniske egenskaper (knust og uknust grus)	**Trafikkgruppe**	
	A[1]	**B og C**
Los Angeles-verdi, LA	≤40	≤35
Micro-Deval-koeffisient, M_{DE}	≤25	≤20
Krav til mekaniske egenskaper (resirkulerte materialer)	**Trafikkgruppe**	
	A[1]	**B, C og D**
Los Angeles-verdi, LA	≤40	≤35
Micro-Deval-koeffisient, M_{DE}	≤25	≤20
Krav til humusinnhold og knusningsgrad (samfengte grusmaterialer)	**Trafikkgruppe**	
	A[1]	**B og C**
Humusinnhold	< 1 %	< 1 %
Knusningsgrad C	-	$C_{50/30}$

[1] Gjelder også gang- og sykkelveger og parkeringsplasser for lette kjøretøy.

Table 13: N200 material requirements for base layer

Parameter	**Krav**	**Kontrollomfang, 1 prøve pr. påbegynt**	**Andel avvikende prøver**	**Maks. avvik**
Los Angeles-verdi [1]	≤ 35 [1]	5000/1500 m³ [2]	1 av 5	+2
Micro-Deval-koeffisient [1]	≤ 15 [1]	5000/1500 m³ [2]	1 av 5	+1
Flisighetsindeks	≤ 25	5000/1500 m³ [2]	1 av 5	+2
Humusinnhold for Gk, % [3]	≤ 1	5000 m³	1 av 5	+0,2
Masseprosent av knuste korn [4] Masseprosent av fullstendig rundete korn [4]	≥ 50 ≤ 30	2500 m³	1 av 5	-4 +2
Korngradering	Tabell 641.2	500 m³	Kun innenfor toleranse, se tabell 641.2	Se tabell 641.2 (toleranse)
Overstørrelser Maksimal kornstørrelse	Tabell 641.2	500 m³	Kun innenfor toleranse, se tabell 641.2	Se tabell 641.2 (toleranse)
Maksimum finstoffinnhold : (< 63 µm av total prøve): Sortering 0/22 (kun Gk), 0/32 [5] Sortering 0/45 Sortering 0/63 (kun Fk og Gjb)	 ≤ 7 % ≤ 5 % ≤ 3 %	500 m³	0	0

[1] For veger i trafikkgruppe A er kravet Los Angeles-verdi ≤ 40 og micro-Deval-koeffisient ≤ 20. Det aksepteres verdier fra materialprodusent for disse to egenskapene.
[2] Kontrollomfang er 1 prøve pr. påbegynt 5000 m³ for Gk og Fk, og 1 prøve pr. påbegynt 1500 m³ for Gjb.
[3] Kravet til kontroll av humus gjelder ikke for Fk siden det antas at humus i svært liten grad er til stede i materialet.
[4] For knust berg (Fk) og knust gjenbruksbetong (Gjb) kan kravet ansees oppfylt uten ytterligere dokumentasjon.
[5] Fk 0/22 kan benyttes til forkiling av forsterkningslag og som bærelag i veger med grusdekke. Krav til korngradering er da som for Gk.

The relevant traffic groups for this study are A and B with an Average Annual Daily Traffic (AADT; abbreviated ÅDT in Norwegian) of roughly 200 to 400 cars. For the main roads, the Traffic Groups are C and D. The assumptions made by the author are presented in Appendix 5. The LA value of the local crushed material meets the criteria for both the subbase and the baselayer. At the same time, the MDE value is too high to meet any requirements for those layers.

There are a few different road surfaces described in the Norwegian pavement design manual N200: gravel, asphalt mixes and gravel surface treatment. A gravel pavement surface requires a LA value of 35 and an MDE of 15. In order for a granular material to be used in an asphalt mix or in a gravel surface treatment, it must have a maximum LA value that depends on the AADT. Most of the mixes listed (Agb, Ab, Ma, Da, Egt, Asg, Eo, Do, Eog, Dog) require a LA value of 35 or 40 for an AADT of 301-1500 and less than 300, respectively. Therefore, the produced gravel could be used in some asphalt mixes and in the gravel surface treatment for low-volume roads.

6.2.2 Longyearbyen Lokalstyre Technical Standard

The local council of Longyearbyen standardized some typical municipal work in a local technical standard. (Longyearbyen Lokalstyre, 2018) A section of this document is dedicated to road design for the town. The geometry and layer thicknesses of the local road classes are defined in detail with some typical drawings. On the contrary, there are no specifications for the constituents of the base and subbase layers. The technical standard refers to the Norwegian Public Roads Administration's handbooks (explicitly the N100 for geometrical design). (Vegvesen, 2019) Hence, it is fair to assume that the Handbook N200 is used for material requirements for imported rocks masses. The Traffic Group assumptions made in 6.2.1 are partly based on facts from the local technical standard.

6.2.3 Quebec Ministry of Transportation

The Quebec Ministry of Transportation (MTQ) is responsible for the transport and related infrastructure in the province of Quebec in Canada. The province's climate is cold with regional variations and it is generally comparable to Norway with seasonal frost and snow accumulation. The BNQ 2560-114 manual is defining the properties of granular material to be used for civil engineering purposes. (Québec, 2014) The MTQ's approach is based on two types of criteria: intrinsic properties (LA, MDE) and manufacturing properties (flakiness, percentage of crushed particles, elongated particles). This study can only be compared with the first type as not all the second type of tests were run. As seen on Table 14, the materials are classified in six groups according to their LA, MDE and LA + MDE values. The BNQ manual states that to belong in a category, it must satisfy each of the three criteria.

Table 14: Intrinsic properties for coarse aggregates, translated from BNQ 2560-114

Intrinsic properties	MTQ test method	Coarse aggregate category					
		1	2	3	4	5	6
Micro-Deval (MD), in %	LC 21-070	≤ 15	≤ 20	≤ 25	≤ 30	≤ 35	≤ 40
Los Angeles (LA), in %	LC 21-400	≤ 35	≤ 45	≤ 50	≤ 50	≤ 50	≤ 50
Micro-Deval Los Angeles (MD + LA), in %	LC 21-070 et LC 21-400	≤ 40	≤ 55	≤ 70	≤ 75	≤ 80	≤ 85

Longyearbyen's material would not fit in any category for the MDE, but it would belong in category 1 for the LA test. The MD + LA combined value (equal to 81) puts it in category 6. However, the material cannot be categorized due to its poor MDE result.

Granular material belonging to category 1 to 5 can be considered for the following items in a pavement system (see Figure 5): surfacing layer, shoulder, base layer and subbase. The subbase layer can be built with material from category 1 to 6.

6.2.4 Danish Road Directorate (DRD)

In Denmark, most manufacturers of sand and gravel for the road sector have had their products certified by a third party over the last decades. Since then, the unbound road materials are well known and uniform across the country. It is generally assumed that the particle strength is not an issue from those certified products. The abrasion tests are not usually run, but the road designers can specify a supplementary material requirement for an LA or MDE value, if deemed necessary. At the moment, it is only done for aggregates coming from regions with significant porous flint content (i.e. Northwest Jutland). The base course should have a maximum LA value of 30. (Vejregler, 2016a) The base and subbase layer also have specifications regarding the amount of crushed particles and sieving fractions. (Vejregler, 2003b, 2003a, 2003c, 2016b)

In terms of pavement surface, there are specifications regarding abrasion tests for two types of surface treatments (AAB and SAB-P) and for gravel surface. The AAB requires granular material with an MDE value of 15 and less. The SAB-P calls for granular material having an LA value of 30 and less. A road with a gravel surface layer should use gravel with a LA value of 30 and less (40 for trails). (Vejregler, 2017, 2019b, 2019a) Thus, the material from Longyearbyen could only be used for trails where no MDE is specified.

6.2.5 Greenland

The main focus of the Greenlandic road construction guidelines is the geometric design of the roads in regard to the natural ground underneath (i.e. permafrost). There is an abundance of competent rock outcrops in Greenland, but it is rare to have deposited material near a construction site. Therefore, the use of blast rock with subsequent crushing is common. The Danish Road Directorate publications are referred to in the guidelines in relation to the laboratory tests that could be specified. The only material characteristics that are mentioned in the guidelines relate to the size fractions and thicknesses of each road layers. Thorough granular material investigations occurred for large-scale projects (e.g. new airports), but they are not usually performed for local road construction. (Organization, 1984; Ramboll, 2008)

6.3 Determination of particle shape

The results from the three particle shape tests are presented in Table 15.

Table 15: Particle shape results (Flakiness index)

Test #	FI value
1	16
2	14
3	11
average	14

The FI values obtained are in the best category (FI_{20}) according to (European, 2008). As was mentioned in Section 6.1, a portion of the material is brittle, and a fine dust was created during the bar sieving of this test. That dust was weighted, and the maximal value was 0.5g (less than 2%) for some size fractions.

The FI results indicate that the crushing produces a portion of flaky particles (FI=14%, from Table 15). The Norwegian pavement design manual N200 prescribes a FI ≤ 25% for the base layer and there is no parameter specified for the subbase. The FI for the pavement layer (asphalt of surface treatment) varies with the selected type and the traffic. In all cases, it varies between 20% and 25%. The Quebec standard states that a granular material with a FI ≤ 25% belongs to category «a». It can be used for the surfacing layer, shoulder, base layer and subbase of a road structure. The Danish guidelines call for a FI ≤ 20% for the SAB-P surface treatment, but there is no explicit threshold for the other layers. The crushed material studied meets all the criteria above regarding the flakiness index. This gives an indication that it might be feasible to crush the rocks from the local stockpiles into a granular product that has a satisfactory shape for construction.

6.4 Freeze-thaw resistance of particles

The loss of mass in percentage (F) after the freeze-thaw cycles is presented in Table 16.

Table 16: Result for the freeze-thaw test

Test #	F (%)
1	0.50

The six granular material portions individually achieved the same resistance to freezing and thawing, F <1%, which corresponds to the best frost resistance class (F1) according to DS-EN-1367-1 (European, 2008). The freezing and thawing resistance values are similar to what SINTEF reported in their work for concrete aggregates.

In arctic regions, many freeze-thaw cycles occur each year during the transition seasons. It is essential that granular materials used in construction can withstand those cycles with little or no effect. From Table 16, it can be stated that the crushing operations did not affect the freezing-thawing resistance of the local rock.

The effect of the deviations from the standard test are estimated to be minimal. The in-house temperature cycle was created to be similar to the one presented in the standard (DS-EN-1367-1). Both temperature curves have a gradual cooling (21°C to 0°C) before completely freezing the sample (0°C to -18°C) and then slowly thawing it (-18°C to 21 °C). The most concerning error source was from the different aperture size during the final sieving. During that step, the residues passing through the sieve were examined to ensure that they would not be retained on a 4mm sieve. As seen on Figure 22, it was mainly composed of sand-like particles with a few larger pieces. It is deemed unlikely that any 4mm particle slipped through unnoticed.

Figure 22: Residue from a test portion

6.5 Cyclic triaxial

The data from the triaxial were processed through a MATLAB program developed by the main researcher using the triaxial apparatus at NTNU. This program has been used for hundreds of tests and it is considered very efficient, if the test runs properly. The four triaxial tests ran according to the standard (DS-EN-13286-7) and no manipulation errors occurred.

The values of M_R for all sequences of the RLTT for each specimen are presented in Figure 23 (larger plots in Appendix 6).

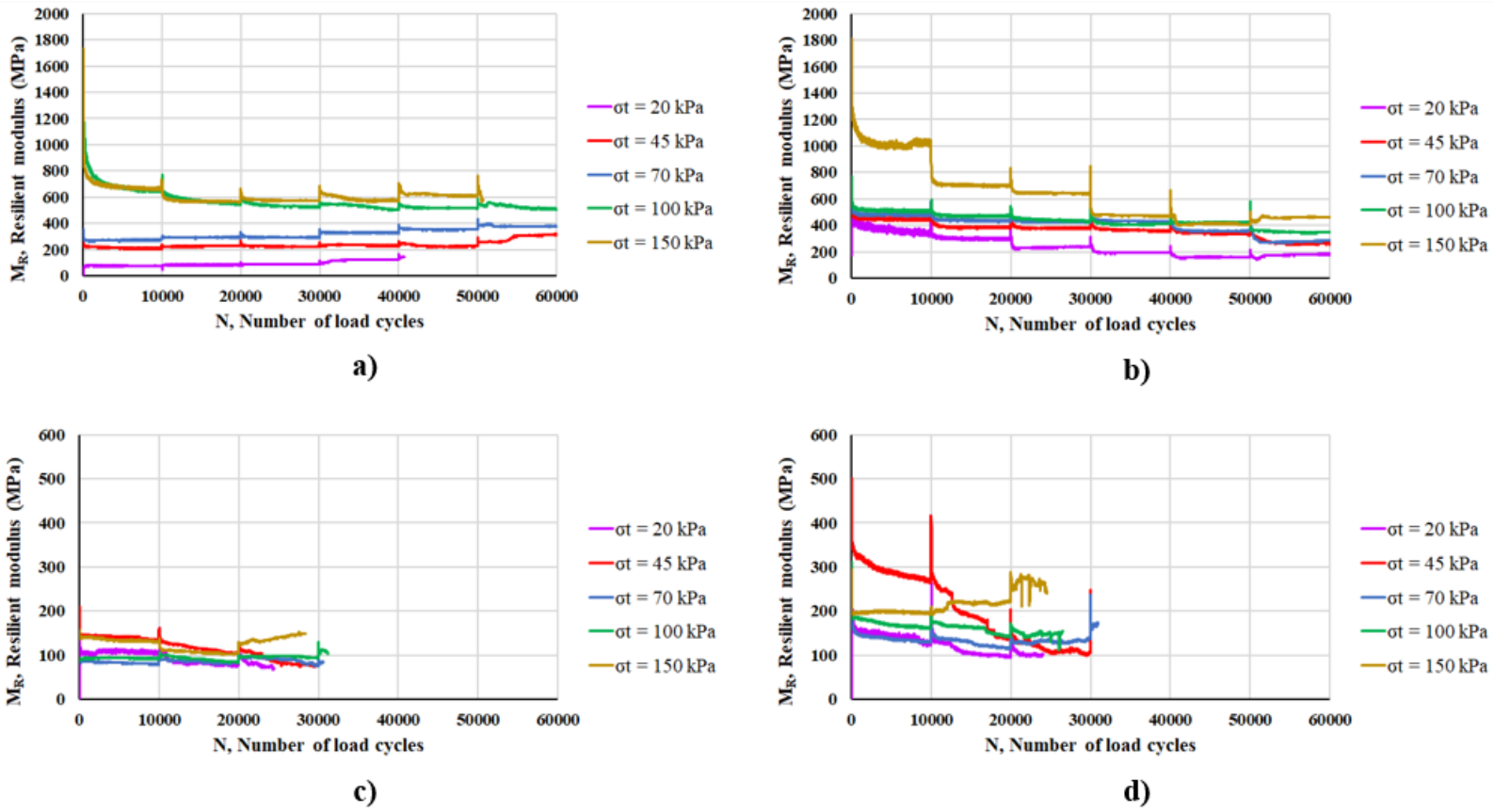

Figure 23: Resilient modulus with the number of load cycles (Specimen 1 to 4 are a) to d), respectively)

After processing the data with the Hicks & Monismith regression model, Figure 24 was obtained. It shows the M_R as a function of the bulk stress for both water content.

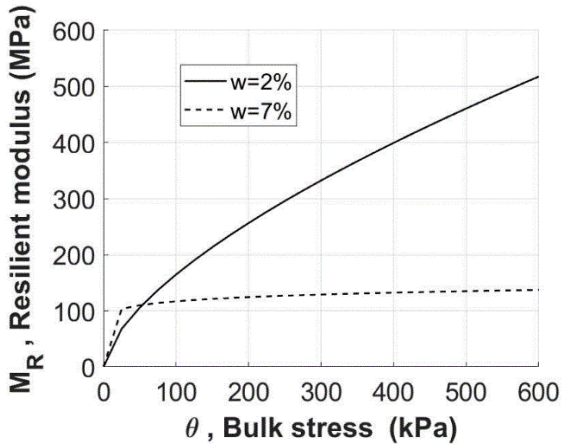

Figure 24: Resilient modulus and bulk stress according to the Hicks & Monismith model

Table 17 shows the regression parameters (k_1 and k_2) as presented in Eq. 4.

Table 17: Regression parameters

	k_1	k_2
w = 2%	1646.2	0.64
w = 7%	1169.7	0.09

It is important to point out that there is a different y-axis scale between specimens 1-2 and 3-4 on Figure 23. The M_R values for the two tests with w=7% are below 600 MPa whereas the ones with w=2% goes up to almost 1800 MPa. One can observe that all the lines for specimens 3-4 do not go further than approximately 30 000 load cycles. Since the 0.5% axial permanent deformation criterion was reached for those load sequences, they were considered completed and the next one would begin. Additionally, Specimen 1 shows a similar behavior for σ_t = 20 kPa and 150 kPa. The water content of an unbound granular material has a strong impact on its M_R: if the water content is high, the M_R is lower.(Werkmeister, 2003) The Hicks & Monismith θ-M_R plot outlines (Figure 24) clearly this relationship. The specimens with w=7% have a M_R that is almost 2 to 4 times smaller than the specimens with w=2% at equivalent θ.

Figure 25 shows the axial plastic deformation and the number of load cycles for all four specimens (larger plots are in Appendix 6).

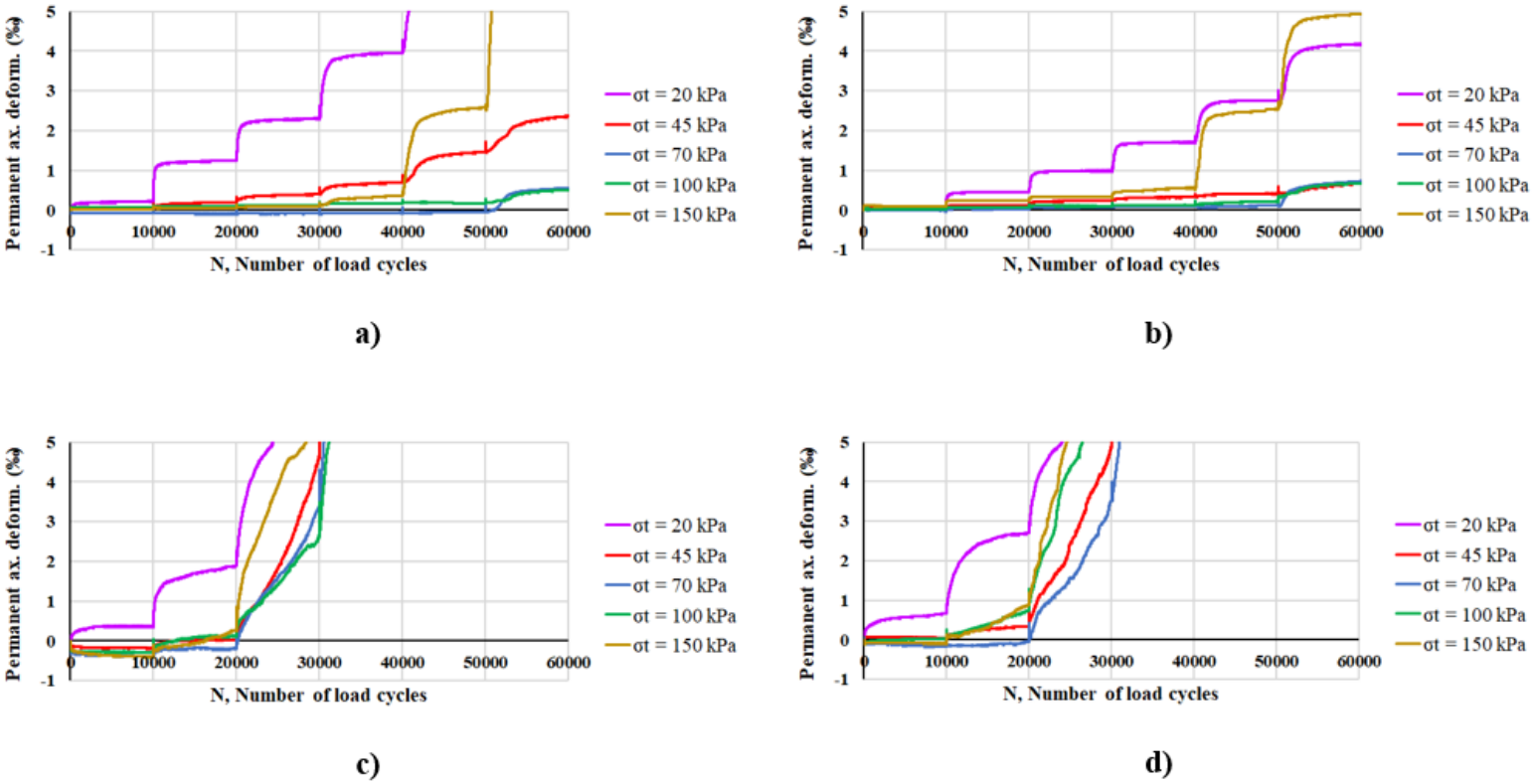

Figure 25: Axial plastic deformation as a function of the number of load cycles (Specimen 1 to 4 are a) to d), respectively)

Figure 25 concur with the observations mentioned for the M_R plots. Specimen 1-3-4 had at least a few load sequences that reached the maximum deformation allowed (5‰). For all cases, the load sequence with the lowest and the highest confining pressure σ_t = 20 kPa and σ_t = 150 kPa) were the ones with the largest deformation or that met the limit value first. The sequence σ_t = 20 kPa can be seen as a conditioning sequence as it compacts or rearranges slightly the granular material for the following parts of the test. The deformation for intermediate stress levels (σ_t = 45, 70 and 100 kPa) of the specimens with the highest moisture content reached the 0.5% limit at around 30 000 load cycles. On the contrary, the specimens with the low water content completed the 60 000 load cycles with 0.23% and 0.08% deformation, for the same stress level.

By comparing the axial plastic deformations to Table 2, each load step's stage was determined by the Coulomb approach and color-coded on Figure 26. The green, yellow and red symbols represents the elastic, elastoplastic and failure range, in such order.

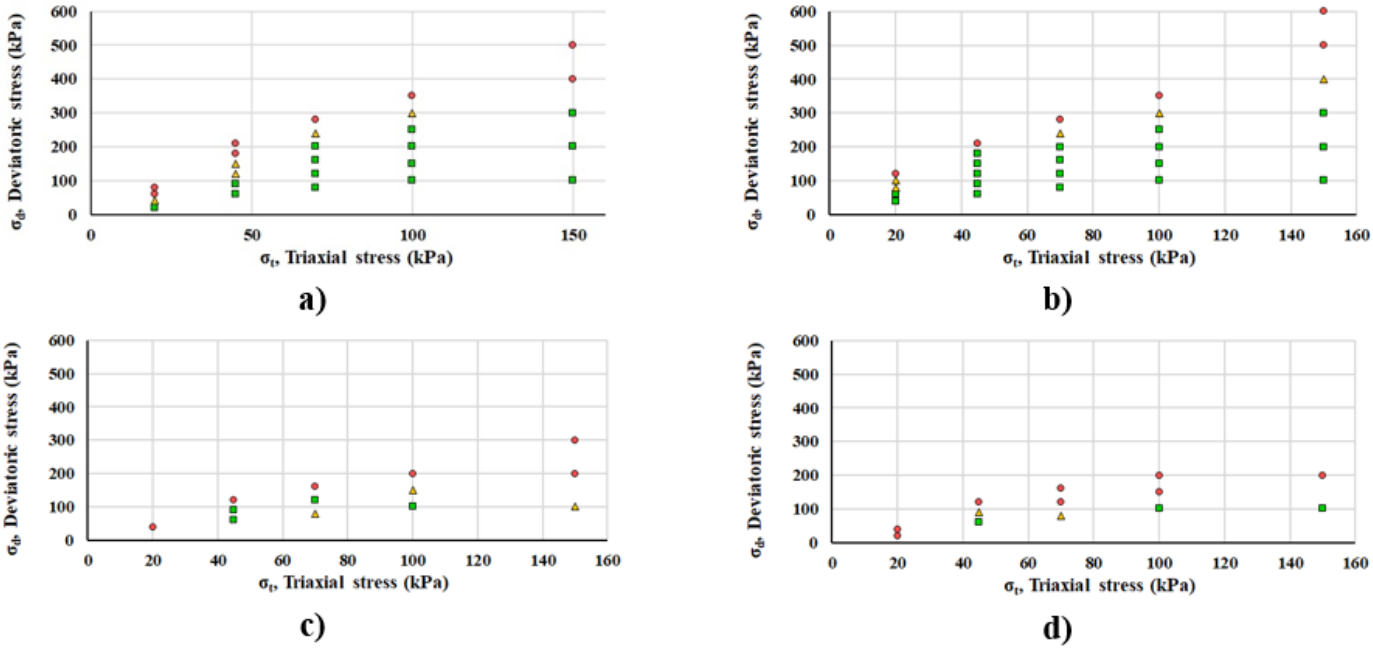

Figure 26: Classification of each RLTT loading step according to the Coulomb approach (Specimen 1 to 4 are a) to d), respectively)

Every load step was categorized into the different material behavior stage according to Table 2. As seen on Figure 26, a material that completed all the load steps of a sequence would have six individual color-coded points (e.g. specimen 2). The stress state of the specimen is an important factor in its behavior, as can be seen on the plots. The allowable stress (σ_d under the failure line) increases with a larger confining stress (σ_t). This highlights the importance of considering the combination of σ_d and σ_t when assessing the range of operation of a geomaterial. The specimens with a low water content can withstand a wider range of stresses before reaching incremental failure. In other words, the area between the elastic and failure ranges is increased with a lower moisture content.

Figure 27 presents the mobilized angle of friction (ρ) and the angle of friction at incremental failure (φ) for the two water contents. Table 18 compiles the average values for those angles.

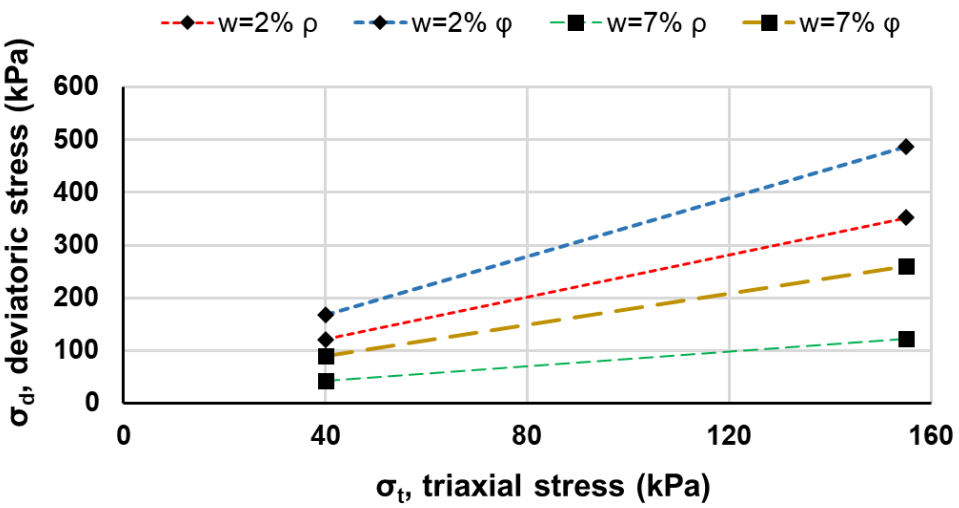

Figure 27: Mobilized angle of friction and angle of friction at failure

Table 18: Average friction angle values

	ρ (°)	ϕ (°)
w = 2%	63.6	70.3
w = 7%	35.1	56.1

Figure 27 is an easy representation of where the material stands at a certain (σ_t, σ_d) combination. Below the «ρ» line is the elastic zone, above the «ϕ» line is the failure zone and in-between is the elastoplastic area. In Table 18, the average angles of those line are shown. The specimens with the high water content have angle values that are more than 20% lower than the ones with low moisture content.

The development of permanent deformation is the result of compaction, particle crushing or material migration under repeated load (i.e. traffic). In a long-term road context (high number of load cycles), the plastic deformation increases the risk of rutting. If the material operates in the failure range, there will be rutting or cracking on the pavement surface. This situation would only worsen as the permanent deformations will only increase with any load cycle. (Werkmeister, 2003) That behavior is clearly observable in Figure 25 c-d) as the permanent axial strain is steeply increasing after N = 20 000 cycles.

6.6 Mineral identification using X-Ray Diffraction

The results from the five XRD analysis are shown in Table 19.

Table 19: XRD analysis

	Composition of sample in %				
Mineral	**Sandstone 1**	**Sandstone 2**	**Silt/Mudstone 3**	**Silt/Mudstone 4**	**LYR 1**
Quartz	54	81	4	58	79
Mica	7	7	6	4	6
Plagioclase	19	7	1	25	9
K-feldspar	15	<1	0	4	1
Chlorite	5	3	<1	6	3
Kaolinite	0	2	0	4	1
Siderite	0	0	88	0	0

For most samples the quartz mineral content is high, and it originates from the degradation of clastic rocks that then transformed into sedimentary rocks. This parameter is interesting since quartz content has a strong influence on the thermal conductivity (see Section 6.7). The plagioclase and K-feldspar (potassium feldspar) both belong to felspar mineral family. They originate from crystallizing magma and are strong minerals (granite has a high percentage of feldspar). Sandstone 1 and Silt/Mudstone 4 would both be classified as arkose, a type of sandstone that has more than 25% felsdpar in its composition. All the samples showed only little amount of clay minerals (kaolinite) and the compositions showed no expansive clay (montmorillonite).(Bell, 2004) The chemical weathering of the feldspar is a source of clay mineral such as kaolinite. It has a more stable structure than other clays. All sample presented a similar amount of mica and chlorite. The mica content can affect the sensitivity of a granular material to water. (Uthus, 2007) However, it is unlikely that it would have a noticeable effect at a low level. The Sandstone 2 and LYR 1 samples might be siltstone due to their high quartz content, since this element does not break down smaller than silt size. The Silt/Mudstone 3 sample has a different composition than all other samples. It is almost completely composed of siderite (iron carbonate). Usually, this is encountered in a concretion which is the result of the precipitation of a mineral in sedimentary. Siderite is considered relatively weak and would not be suitable as a construction material. This sample is an outlier and its mineralogy is not representative of a gravel stockpile (concretions are a very small fraction of the total volume). For this reason, it is excluded from further analysis and conclusions.

Considering the mineral composition of this study's samples, there appears to be no issue in using this granular material for civil engineering purposes (earthworks, road structure, etc.). A more thorough mineral investigation could be made in the case of a specialized construction project involving aggressive environment (e.g. maritime structure or coastal protection).

6.7 Thermal parameters

Upon achieving steady-state heat flow, the average value for a 30 minutes period was taken to calculate the thermal conductivity. The saturated gravel sample measurements were giving values for a water-soil sample. Afterward, the geometric mean method described in (Côté and Konrad, 2005a) allowed to isolate the thermal conductivity of the soil fraction. The rock core only had a solid fraction since it was oven-dried before the test. Those results are shown in Table 20 and Table 21.

Table 20: Saturated thermal conductivity of the samples

Saturated thermal conductivity			
Sample	Unfrozen ($\lambda_{sat,u}$)	Frozen ($\lambda_{sat,f}$)	
Saturated gravel	1.57	3.07	W/m °C
Rock core	3.45	3.45	W/m °C

Table 21: Thermal conductivity of solid

Sample	Thermal conductivity of solid (λ_s)	
Saturated gravel	4.47	W/m °C
Rock core	3.45	W/m °C

Using the mineralogy of the samples, it was possible to estimate the thermal conductivity of each samples analyzed by XRD. Each component had its own thermal conductivity which was combined by the geometric mean method. (Andersland, Orlando B.; Ladanyi, 2004; Côté and Konrad, 2005a) Table 22 presents the result of a quick estimation based only on quartz content versus the result by including all the minerals.

Table 22: Estimation of the thermal conductivity of solids

Thermal conductivity of solid			
Sample	Quartz content only	Complete mineralogy	
Sandstone 1	4.14	4.35	W/m °C
Sandstone 2	5.96	6.20	W/m °C
Silt/Mudstone 3	3.12	3.05	W/m °C
Silt/Mudstone 4	4.37	4.66	W/m °C
Rock core LYR1	5.80	5.91	W/m °C

Heat capacity is the other parameter usually required to define a material in a thermal analysis software. It was calculated for the 2-8mm gravel that was used for the specific density test in the pycnometer. A specific density of 2.639 g/cm³ with a water content of 6% (corresponding to the field condition at Boltervelva stockpile (Site 1) in early November) was used for the calculation.

The general formulas from the Frozen Ground Engineering book were used. (Andersland, Orlando B.; Ladanyi, 2004) The numerical values are presented in Table 23.

Table 23: Heat capacity

	Heat capacity		
	Unfrozen	Frozen	
Gravel 2-8mm	2.54	2.21	MJ/m³

It is generally accepted within the thermal parameter research community that the best way to measure the thermal conductivity of a solid are as follow, in decreasing precision order:

1. Direct measurements on parent rocks cores
2. Indirect measurements on saturated samples
3. Estimation from global or partial mineral content
4. Estimation from index properties

This study made level 1 and 2 measurements (Table 20 and Table 21) and these are compared to level 3 estimations (Table 22). The NTNU experimental set up has an accuracy of ±10% with its current calibration, according to the responsible researcher who ran several thermal tests with it.

The comparison between the measured thermal conductivity of the rock core LYR1 and the estimation through the theoretical approach (complete mineral composition) shows a large difference (3.45 W/m°C vs 5.91 W/m°C). The measured value is close to the average sandstone value presented in (Côté and Konrad, 2005b) of 3.40 W/m°C. The theoretical model result is strongly influenced by the quartz content of the sample and it could be overestimating our result since we have a high quartz content. Sandstone 2 has a high theoretical thermal conductivity and it also presents a high quartz content. Unfortunately, no thermal measurements were taken for that sample (not enough material for a core).

The thermal conductivity of solid derived from the saturated gravel sample measurement seems to be well in line with the calculated values from Sandstone 1, Silt/Mudstone 4 and Silt/Mudstone 3 (to a limited extent). Since the saturated gravel sample was comprising various mineral composition, this value seems to be a good average thermal conductivity for our granular material. If more measurements were taken on different crushed gravel samples from Longyearbyen, it would increase the accuracy of this value and be more representative.

The heat capacity values are deemed to be representative since they used measurements from actual samples. For a more specific construction project, the accuracy could be improved by using the specific density of the manufactured material and its targeted moisture content.

6.8 Specific density

The specific densities of the samples are presented in Table 24. The volume of the rock core used for the thermal properties was known, and therefore its density was added to the other measurements.

Table 24: Results for the specific density

Specific density (ρ_s)		
Gravel with pycnometer	2.639	g/cm³
Cobble 1 with water displacement	2.444	g/cm³
Cobble 2 with water displacement	2.542	g/cm³
Rock core LYR1	2.499	g/cm³
SINTEF 2016 report	2.460	g/cm³

The specific density measurements for the gravel are reasonably close to each other (9% difference between this study and SINTEF). Since the crushed granular material was not produced from the same sampling campaign, it is possible that there were some differences in the sample composition. The specific densities of the cobbles/rock core are of similar magnitude and could be used for larger sized gravel in its natural state.

It would be recommended to measure the specific density of the gravel again to reduce the margin of error, if a larger production was to be made.

7 Recommendations

Following the testing campaign, the local rocks can be recommended for various uses in order to reduce the dependency to imported material for construction projects around Longyearbyen. These options are discussed in detail below: road material, granular pad material, air convection embankment, gabion retaining walls and winter maintenance.

7.1 Road material

Following a review of selected road standards (section 6.2), the abrasion tests results from the studied crushed material met some material criteria. The LA value is sufficient to be used in base course or subbase of a road according to the Norwegian and Quebec standards. Additionally, this parameter classifies for some of the Norwegian asphalt mixes, for the Norwegian gravel surface treatments and for the gravel surface of trails in Denmark. The MDE value is too high for all standards which indicates that the local granular material would wear faster than imported aggregates from mainland. This correlates with past construction experiences from Longyearbyen. The combination of LA and MDE, a criterion of the Quebec standard, would categorize the local gravel as a suitable subbase material. From the result of section 6.4, the crushing operations did not affect the freezing-thawing resistance of the local rock which makes them suitable as a road material. The RLTT results presented the mechanical properties and resistance against permanent deformation of the crushed material in details (Section 6.5). These results can be helpful for designers to classify to which stage the material belongs for a certain loading scenario (elastic, elastoplastic or failure). Optimized design involving local material would prevent the road material to reach the failure stage which would translate by permanent deformations (rutting, cracking, etc.) and more serious issues (loss of material, structural failure).

In Longyearbyen, the local material is already used as a subbase material in its uncrushed state for a cost-saving purpose. According to standards, it could be used more broadly if it was crushed and sorted/sieved to regular size distributions, as any aggregate from the mainland. The behavior of the road structure could be improved by using materials that have known mechanical properties in each layer. This study confirms that the material could be used for the subbase layer and opens up the possibility of using it for surface treatment (Norwegian mixes: Eo Do Eog Dog). This could be an interesting alternative for low volume roads as it is already being used extensively in northern regions of America (Yukon and Alaska). Surface treatments help controlling dust emission as well as improving the drainage and driving surface. The benefits come with a lower price than a conventional hot-mix asphalt and the surface can be rehabilitated more often if the profile changes over the years (for instance, in a disturbed permafrost context). (Doré and Zubeck, 2009) Another use for the local crushed gravel is the pedestrian and bicycle path. Typically, these structures are subjected to significant loads during their construction, but not during their operation.

Once the laboratory part of the study was completed, the typical road profiles for Longyearbyen (Longyearbyen Lokalstyre, 2018) was analyzed with the i3c-me software. The results were compared to different design variations implying more local materials in the layers. This road design software was developed by the i3c research chair of Laval University in Canada. It uses the mechanistic-empirical approach to design a pavement structure with a two-steps process. Firstly, i3c-me calculates the stresses, strains and displacements using a mechanistic model. Secondly, the performance of the road is assessed using empirical damage functions.

Since the software has a built-in database of aggregates, the typical road profiles from Longyearbyen were slightly modified to fit the available material and make it possible to compare alternate designs. Figure 28 and Table 25 present the cross-section and the material properties used for the i3c-me calculations.

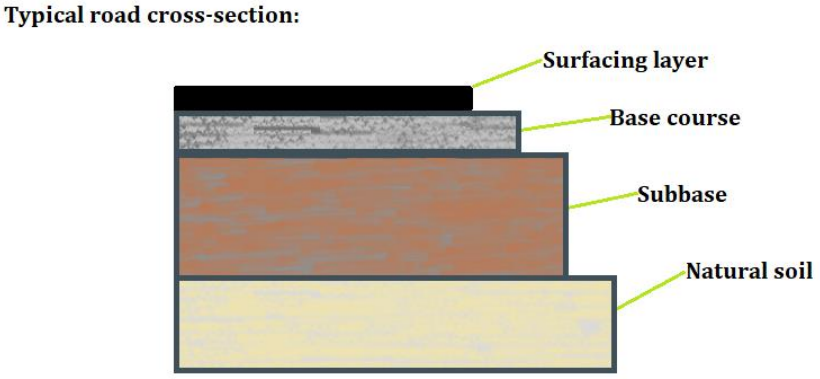

Figure 28: Sketch of the simplified road section used in i3c-me

Table 25: Material comparison for i3c-me

Layer	Longyearbyen Lokal Norm	i3c-me
Surfacing layer	AB16 asphalt layer	GB-20 asphalt layer (same thickness as in the Lokal Norm); bitumen for -34°C
Base course	Fk/Gk; gravel size 0-32 mm	MG 20 (or MG56 in a few iterations); gravel size 0-20mm (or 0-56mm)
Subbase	Local material; cobbles 0-400mm	MG112; gravel size 0-112mm
Natural soil	Considered a gravel-sand-silt or clay mixture (GM-GC according to USCS)	

The main and secondary roads were studied according to the design criterion derived from the traffic group assumptions made in 6.2. The local standard layers (1) were compared to the following alternate designs: 50% of local rock in the base course (2), 100% of local rocks in the base course (3), 100% of local rocks in the base course in two sublayers (4) and 100% of local rocks in the base course in two sublayers on a weakened natural soil (5). The i3c-me gives the results as a comparison to the design criterion in equivalent single-axle load (ESAL). The default load studied for all cases was a 40kN force applied on a 150mm circular plate (representing the footprint of a truck tire) moving at a 40 km/h speed. The mechanistic-empirical software calculates

the number of ESALs before the road section reaches a fatigue or a permanent deformation threshold. Those limit values vary according to which model used by the software. In this study, the Norwegian Fatigue criteria and the MnPave permanent deformation were used for all cases. The climate of Longyearbyen was mimicked by a temperature function that reached an air-freezing index of 2430 °C days corresponding to a mean annual air temperature of -7.22 °C. This temperature function is loosely based on the climate data from (Instanes and Mjureke, 2003). Table 26 presents the five different road scenarios and their results. The temperature function and material properties are displayed in Appendix 7 .

Table 26: i3c-me results

Main roads							
Scenario	**Surfacing layer**	**Base course**		**Subbase**	**Allowable ESAL during design life (in millions)**		**Remarks:**
		Sublayer 1	Sublayer 2		Fatigue	Permanent deformation	
1	100	200	0	600	23.907	129.409	
2	100	100	100	600	18.796	119.441	Base course 2 is made of local material (MG20)
3	100	200	0	700	11.742	152.091	Base course 1 is made of local material (MG20)
4	100	200	300	300	16.054	115.64	Base course 1 and 2 are made of local material (MG20 and MG 56)
5	100	200	300	300	15.328	49.032	Same as scenario 4 but with a weak natural soil
Design criteria (in million ESAL):					1.985837		based on the assumptions for the Traffic group

Secondary roads							
Scenario	**Surfacing layer**	**Base course**		**Subbase**	**Allowable ESAL during design life (in millions)**		**Remarks:**
		Sublayer 1	Sublayer 2		Fatigue	Permanent deformation	
1	60	150	0	600	1.313	57.915	
2	60	75	75	600	0.952	53.272	Base course 2 is made of local material (MG20)
3	60	150	0	600	0.591	48.016	Base course 1 is made of local material (MG20)
4	60	150	150	450	0.763	52.801	Base course 1 and 2 are made of local material (MG20 and MG 56)
5	60	150	150	450	0.752	21.837	Same as scenario 4 but with a weak natural soil
Design criteria (in million ESAL):					0.250843		based on the assumptions for the Traffic group

The i3c-me analysis shows that the local material can be used as a subbase with no noticeable issues. Both types of road are structurally overdesigned in relation to the ESALs. Although it is important to keep in mind that these results do not account for frost protection criterion or any thermal performance which might be determinant in permafrost area. The studied granular material could be used for up to 50% of the main road's base layer without much effect on the fatigue or permanent deformations. The other scenarios are all successfully passing the i3c-me verification with a large margin of ESALs. The secondary road results show the same general trends. The scenario 4 shows that using three size fractions for the aggregates in the road structure might be considered to maximize the use of local material.

The results of the i3c-me are encouraging, but they remain preliminary. The accuracy of the calculations can be improved by entering manually the surfacing layer (Ab16) parameters into the software (requires determining them in a lab). The assessment of the M_R or the CBR value (California Bearing Ratio) of the natural soil underneath the road would increase the accuracy even further. In a permafrost area, the thermal design of a road is usually determining the thickness of the road layers. The outcome is a structurally overdesigned road with a large number of ESAL compared to the design criterion. In the end, the production of locally crushed granular material and its specification for the road construction in Longyearbyen will be a balance between production cost, allowable deformations and maintenance of the future roads.

7.2 Granular pad material

There are many fills around Longyearbyen (storage areas, snowmobile parking, etc.) that are made from local material. A preliminary evaluation of the crushed aggregate to build a granular pad was conducted for a three meters thick embankment. The properties from the RLTT samples were used to define the material. Three load scenarios were verified: a 400mm-thick concrete slab used for a building floor, a fully loaded maritime container and a double stack of loaded maritime containers (each at 75% capacity). These added loads are vertically and horizontally distributed in the pad. The magnitude of the stress decreases with depth as the affected area increases. At every meter in depth, a calculation node was positioned. The pad is considered normally consolidated, unsaturated (well-drained) and sitting on permafrost. Figure 29 shows the cross-section of the middle portion of the granular pad. The effective stress, lateral earth pressure at rest and uniformly loaded rectangle foundation calculations were derived from the equations presented in the Chapter 7 of (Budhu, 2010). The sum of those stresses, at a given depth, is considered as the bulk stress. The formulas and the detailed assumptions for the calculations are shown in Appendix 8. The assumptions are based on the results from this study, (Budhu, 2010) and (European, 2007a).

The resistance of the natural gravel around Longyearbyen has been the subject of many discussion in the past. A side experiment was made in February 2020 to assess the load-bearing capacity of the local material to support a concrete slab. During that experiment, stresses higher than those

calculated in this study were applied to natural gravel in order to verify the amount of stone that would be crushed. The pertinent parts of this report are attached in Appendix 9.

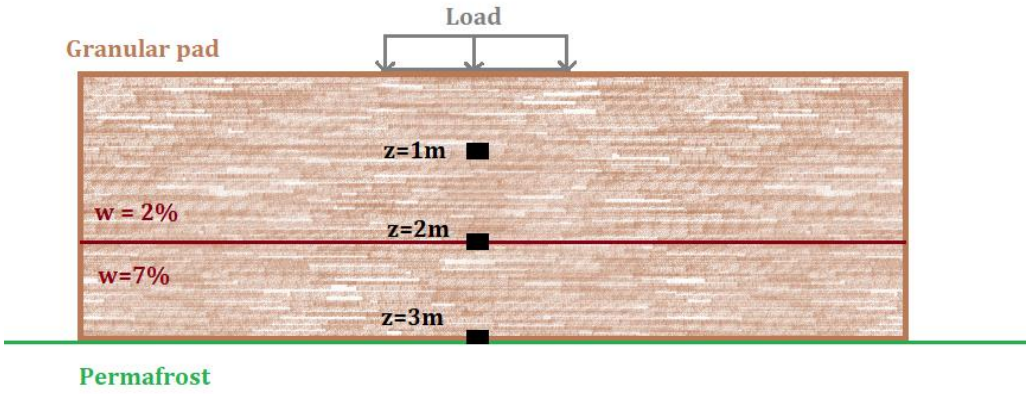

Figure 29: Sketch of the granular pad

At each calculation node, an element of material (similar to Figure 6) was imagined to make a link between the scenarios and the M_R obtained from the cyclic triaxial. The bulk stresses resulting from the forces acting on the element were estimated and are shown on Table 27.

Table 27: Bulk stress for each scenario

Bulk stress (θ)				
z (m)	Concrete slab	Container 20'	Double stack container 20'	
1	36.33	47.40	56.54	kPa
2	62.53	73.79	80.13	kPa
3	92.44	100.44	104.84	kPa

Afterward, Figure 24 was used to determine an average modulus for the granular pad at this stress level. The value of 80 MPa was selected using a water content of 7%, a θ of 100kPa and a safety factor of roughly 20%. The vertical elastic settlement at the ground surface (Δz) was calculated for two locations per scenario and is presented in Table 28.

Table 28: Vertical elastic settlement at the ground surface

	Concrete slab	Container 20'	Double stack container 20'	
Δz, under the center	0.0002	0.0009	0.0014	mm
Δz, under a corner	0.0001	0.0005	0.0007	mm

This preliminary verification showed that the elastic settlements are very small for the three load scenarios. The M_R has a strong impact on the calculation of the settlement, and it should be ascertained before any detailed design. The load scenarios aimed to reproduce the situation in which the local rock masses are used. If properly laid down and compacted, the local crushed

material could be used for the construction of granular pads for storage purpose. It might be possible to recommend it as supporting layer for a concrete slab floor (e.g.: garage, warehouse, etc.) with further structural verifications.

7.3 Air convection embankment (ACE)

The possibility of using local granular material to build air convection embankment has been shortly investigated after the determination of the thermal parameters (Section 6.7). ACE are using large poorly graded granular material to construct the main portion of the embankment. As a result, natural convective cells will be created from the temperature difference between the surface and base of the embankment. During cold periods, the air present in voids is cooled at the top of the embankment. Once it is cold enough, it will move downward and push warmer air upward (as shown in Figure 30). Convective cells are increasing the cooling rate under the embankment. In summer, the system becomes dormant because the warm air is at the top of the embankment. The heat exchange is greater in the wintertime than over the summer period which effectively contribute to maintaining permafrost. (Doré and Zubeck, 2009; McHattie and Goering, 2009; Canada, 2010)

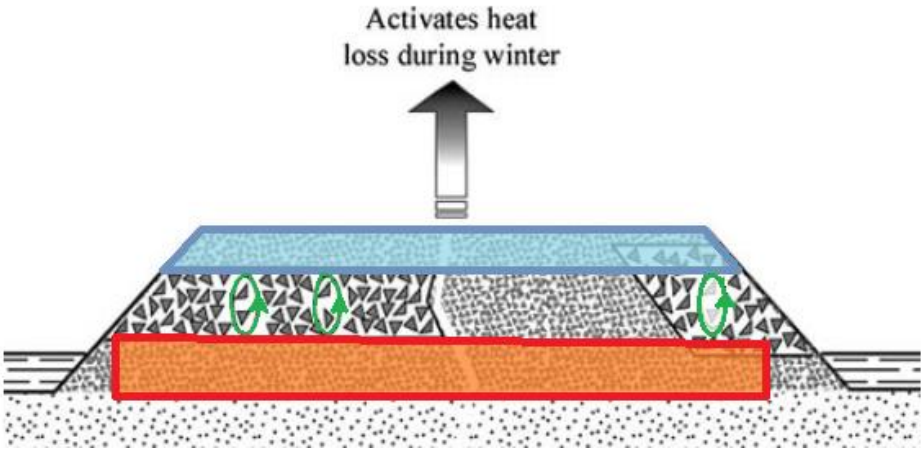

Figure 30: ACE embankment during winter (modified from Doré & Zubeck, 2009)

The critical temperature difference (ΔT_c) between the top and bottom of an embankment is mathematically defined in (Goering, 2002; McHattie and Goering, 2009). ΔT_c was calculated for three average particle sizes (5, 7.5 and 10 cm) based on available material from the Site 1 stockpile. Some parameters obtained from the laboratory results were used to fine-tune the analysis. The results are summarized on Figure 31.

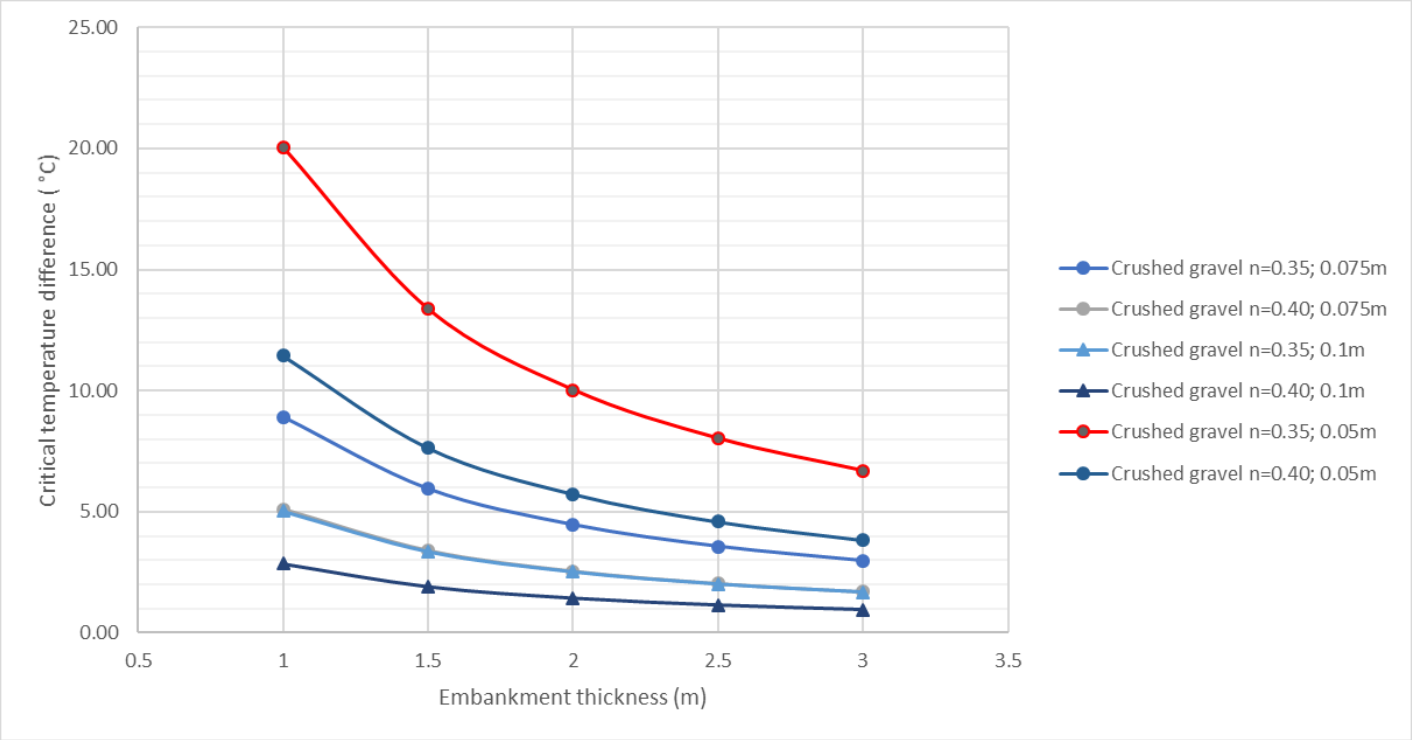

Figure 31: Critical temperature difference for different thickness

The granular material is assumed to be crushed and sieved to remove finer particle that could lower the porosity (n). A high porosity of 0.35 and 0.4 was used for the calculations with the different embankment thickness. From this theoretical verification, a 2m-thick embankment could initiate a convective cell with a ΔT_c that is between 5 and 10°C (depending on porosity and particle size). The ACE technique could be used for some road portion that are experiencing thaw settlement issues or for any new structures requiring the permafrost to be maintained. Since there are many different design possibilities, the local rock masses could be appropriate to increase the cooling rate of mainland granular material used for load-bearing tasks (i.e. the core of a road embankment).

7.4 Gabion basket

In Longyearbyen, gabion retaining walls are used as a structural component or as an architectural feature (see Figure 32). Generally, gabion baskets are filled with strong rocks (igneous or metamorphic). Sedimentary rocks can be used if they are not too elongated or stratified to avoid the risk of having weak planes. The results from the Los Angeles test indicate that the local granular material can resist fragmentation to some extent. It is likely that the initial placement in the gabion basket may break a few rocks. Since gabion fill material is not mechanically compacted afterward, local rock would behave as any other material after being put in place. The freezing-thawing resistance of the rock is important in cold climate since it would be detrimental to the

structure if the rock disintegrated over time and lost mass through the basket mesh openings. The test result does not indicate any undesired behavior that would prohibit the use of the local rock masses.

Figure 32: Use of gabions in Longyearbyen (structural with imported rocks on the left and architectural with local rocks on the right)

Depending on the project, gabion baskets could be filled with local rock (crushed or natural) instead of importing rock from the mainland. In order to maximize the efficiency of those retaining walls, special care should be made during the installation to avoid crushing the rocks or deforming the wire mesh baskets. Sorted rocks should be used to minimize material losses through the gabion.

7.5 Winter maintenance

Longyearbyen is not using salt for de-icing its road network during winter, but rather sand to increase the friction between the tires and the surface. The MDE test results are showing that the local material wears down under at a fairly easily under traffic load. The same phenomenon was also reported by local stakeholders when they used the small fraction on roads and mentioned it was easily crushed down. The preliminary recommendation for winter maintenance would be to avoid using a locally crushed sand unless specific investigation is made for such purpose.

8 Conclusion

The sedimentary rocks from one of the stockpiles in Longyearbyen were tested to verify the possibility of using them in the local construction industry. The crushing and sieving of the sample produced different size fraction (from 0 to more than 31.5mm). It was observed that a second pass through the crusher increased the fine content noticeably. The abrasion tests (five Los Angeles and five Micro-Deval) showed that the aggregates resist well to fragmentation but are greatly sensitive to wear. The latter result limited the possible usage for this crushed material in a road structure. The crushing operation resulted in a reasonable amount of flaky particles for the three sample tested. According to various standards, the obtained value is not problematic. The sample was resistant to freezing and thawing cycles and fitted in the best category. The cyclic triaxial provided useful parameters under various loading steps for a typical grain size distribution. The four tests were realized at two different water content which outlined the effect of the moisture for this particular unbound granular material. The information gathered allowed to classify the behavior into three categories: elastic, elastoplastic and failure. The samples sent out for XRD analysis showed a generally high quartz content and no potential issues for construction. The thermal parameters were measured and showed a thermal conductivity lower than what would have been estimated from theoretical models using only the mineralogy. In the light of the laboratory results and with the calculations done, the local gravel could be crushed and used for different aspects of construction in Longyearbyen. The parameters obtained can help designer to improve their use of local resources compared to imported rock masses.

The objectives of this study were satisfactorily met. The gaps in the engineering knowledge were identified and an evaluation of the use of granular material was completed during the interviews and in the literature review. The evaluation of the properties of the local material was done during the laboratory portion of the study. Following the data processing, it was possible to classify the material according to different standards and to give recommendations for the possible use of crushed local material.

This study opens the way for other research projects to fill some knowledge gaps. An investigation of the mechanical properties of the material from Gruve 3 (Site 2) would result in having design parameters from the two stockpiles of Longyearbyen. A full-size test section could be made to ascertain the load-bearing capacity of locally produced crushed aggregates (e.g. a road embankment section or a granular pad). If a thermal design was being considered, a more thorough assessment of the thermal parameters of the gravel should be made.

9 References

Andersland, Orlando B.; Ladanyi, B. (2004) *Frozen Ground Engineering, 2nd edition*. Second Edi. John Wiley & Sons.

Army, U. (2001) *Field Manual 5-472 Materials Testing*. Washington D.C.

Barbieri, D. M. (2019) *Doctoral thesis: Use of local materials for road construction*. Trondheim: NTNU.

Bell, F. G. (2004) *Engineering Geology and Construction*. New York: Taylor & Francis.

Benn, Douglas I.; Evans, D. J. A. (2010) *Glaciers & Glaciation*. 2nd editio. Hodder Education.

Budhu, M. (2010) *Soil mechanics and foundations*. 3rd edn. John Wiley & Sons.

Cable, S., Elberling, B. O. and Kroon, A. (2018) 'Holocene permafrost history and cryostratigraphy in the High-Arctic Adventdalen Valley , central Svalbard', *BOREAS*, 47, pp. 423–442. doi: 10.1111/bor.12286.

Canada, T. A. of (2010) *Guidelines for Development and Management of Transportation in Permafrost regions.pdf*. Ottawa: Transport Association of Canada.

Côté, J. and Konrad, J.-M. (2005a) 'A generalized thermal conductivity model for soils and construction materials', 458, pp. 443–458. doi: 10.1139/T04-106.

Côté, J. and Konrad, J.-M. (2005b) 'Thermal conductivity of base-course materials', 78, pp. 61–78. doi: 10.1139/T04-081.

Dallmann, W; Kjaenet, T; Nottvedt, A. (2001) *Geomorphological and Quaternary geological map of Svalbard 1:100,000*. C9G/C9Q Ad. Tromso: Norwegian Polar Institute.

Dallmann, W. (2009) *Svalbard's geological development, Cruise Handbook - Norwegian Polar Institute*. Available at: http://cruise-handbook.npolar.no/en/svalbard/geological-development.html (Accessed: 20 April 2020).

Dawson, A. R. (1999) *Implications of Granular Material Charactheristics on the Response of Different Pavement Construction*. A A BALKEMA.

Doré, G. and Zubeck, H. K. (2009) *Cold Regions Pavement Engineering*. 1st edn. USA: ASCE Press. Available at: http://trid.trb.org/view.aspx?id=903094.

Elvevold, S., Dallmann, W. and Blomeier, D. (2007) *Geology of Svalbard*. Tromso: Norwegian Polar Institute.

European, C. for S. (2004) 'Unbound and hydraulically bound mixtures - Part 7: Cyclic load triaxial test for unbound mixtures', *European Standard*, DS-EN 1328, p. 39.

European, C. for S. (2007a) 'Eurocode 1: Actions on structures Part 1-1', *European Standard*, DS-EN-1991, p. 48.

European, C. for S. (2007b) 'Tests for thermal and weathering properties of aggregates - Part 1: Determination of resistance to freezing and thawing', *European Standard*, DS-EN 1367, p. 12.

European, C. for S. (2008) 'Aggregates for unbound and hydraulically bound material for use in civil engineering work and road construction', *European Standard*, DS-EN-1324, p. 58.

European, C. for S. (2010) 'Tests for mechanical and physical properties of aggregates - Part 2: Determination of the resistance to fragmentation', *European Standard*, DS-EN 1097, p. 38.

European, C. for S. (2011) 'Tests for mechanical and physical properties of aggregates - Part 1: Determination of the resistance to wear (Micro-Deval)', *European Standard*, DS-EN 1097, p. 18.

European, C. for S. (2012) 'Tests for geometrical properties of aggregates - Part 3: Determination of particle shape - Flakiness index', *European Standard*, DS-EN 933-, p. 26.

European, C. for S. (2013) 'Tests for mechanical and physical properties of aggregates - Part 6: Determination of particle density and water absorption', *European Standard*, DS-EN-1097, p.

54.
Goering, D. J. (2002) ‘Convective Cooling in Open Rock Embankments’, *Cold Regions Engineering*, pp. 629–644.
Gunhildberget, A. (2020) *Interview LNS Spitsbergen by J-G Dorval on Oct 21, 2020*.
Hjelle, A. (1993) *Geology of Svalbard*. Issue 7 of. Tromso: Norwegian Polar Institute.
Hoff, I. (2008) *Properties of unbound granular materials - Required reading material for Pavement Technology course*. Trondheim.
Hoff, I., Bakklok, L. J. and Aurstad, J. (2003) ‘Influence of laboratory compaction method on unbound granular materials’, *6th international symposium on Pavements unbound*, (7465), pp. 1–11.
Humlum, O., Instanes, A. and Sollid, J. L. (2003) ‘Permafrost in Svalbard: a review of research history , climatic background and engineering challenges’, pp. 191–215.
Ingerø, K. O. (2020) *Interview Lokalstyre by J-G Dorval on Oct 22, 2020*. Longyearbyen.
Ingólfsson, Ó. (2008) *Outline of the Physical Geography and Geology of Svalbard, Svalbard Geology*. Available at: https://notendur.hi.is/oi/svalbard_geology.htm (Accessed: 20 April 2020).
Instanes, A. and Mjureke, D. (2003) *Svalbard airport runway. Performance during a climate-warming scenario.*
Institute, N. P. (2020) *TopoSvalbard*. Available at: https://toposvalbard.npolar.no/.
Justis- og beredskapsdepartementet (2016) *Byggeforskrift for Longyearbyen*. Available at: https://lovdata.no/dokument/SF/forskrift/2016-11-15-1329?q=byggeforskrift for longyearbyen (Accessed: 26 October 2020).
Kanstad, S. B. (2020) *Interview Norwegian Water Resources and Energy Directorate by J-G Dorval on Nov 4*. Longyearbyen.
Lang, A. P. *et al.* (2007) ‘Prediction of Coarse Aggregate Performance by Micro-Deval and Other Soundness , Strength , and Intrinsic Particle Property Tests’, *Journal of the Transportation Research Board*, (no 2026), pp. 3–8. doi: 10.3141/2026-01.
Longyearbyen Lokalstyre (2018) *Lokal Norm - Tekniske anlegg, Longyearbyen*. Longyearbyen.
McHattie, R. L. and Goering, D. J. (2009) *Air Convecting Embankment (ACE) design guide*. Alaska Department of Transportation.
Organization, G. T. (1984) *Bygdeveje i Grønland*.
Pedersen, M. B. (2020) *Email correspondance with Ramboll Svalbard by J-G Dorval in November 2020*.
Piepjohn, K. *et al.* (2012) *The Geology of Longyearbyen*. Longyearbyen: Longyearbyen feltbiologiske forening.
Prestvold, K. (2015) *Svalbard’s history - The Cruise Handbook for Svalbard*. Edited by O. Overrein. Norwegian Polar Institute.
Québec, B. de normalisation du (2014) *BNQ 2560-114 - Travaux de génie civil - Granulats*. Québec.
Ramboll (2008) *Veje i Grønland*.
Reymert, P. K. (2013) *Longyearbyen*. Edited by I. S. Sandodden and S. Haukalid. Governor of Svalbard, Environmental Protection Department.
Richard, J. A. and Scarlett, J. R. (1997) *Airport Engineering - A review and evaluation of the Micro-Deval test*. Ottawa.
Ringheim, A. (2020) *Interview Store Norsk by J-G Dorval on Oct 27, 2020*. Longyearbyen.
Sinitsyn, A. O., Kotov, P. I. and Aalberg, A. (2020) ‘The MonArc Project: Monitoring Programme for Foundation Settlements and Initial Results’, *Proceedings of TRANSOILCOLD*

2019, 1, p. 537.
Skjølsvold, O. and Haugen, M. (2016) *Kortreist betong på Svalbard*. Trondheim.
Statens vegvesen (2018) *Vegbygging – Håndbok N200, SVV Håndbok - Normal*.
Statistics Norway (2020) *Svalbard population*. Available at: https://www.ssb.no/en/befsvalbard/ (Accessed: 20 September 2020).
Uthus, L. (2007) *Doctoral thesis: Deformation Properties of Unbound Granular Aggregates*. Trondheim: NTNU.
Vegvesen, S. (2019) *Veg- og gateutforming - Håndbok N100*.
Vejregler (2003a) *BASE COURSE OF GRAVEL – General Work Specification*.
Vejregler (2003b) *SUBBASE OF SAND AND GRAVEL – General Work Specification*.
Vejregler (2003c) *Tender and construction specifications Subbase of Sand and Gravel*.
Vejregler (2016a) *Almindelig arbejdsbeskrivelse (AAB) for Stabilt grus*.
Vejregler (2016b) *VEJLEDNING - Stabilt grus - vejl.*
Vejregler (2017) *SLIDLAGSGRUS – SAB-P*.
Vejregler (2019a) *ALMINDELIG ARBEJDSBESKRIVELSE OVERFLADEBEHANDLING - AAB.*
Vejregler (2019b) 'OVERFLADEBEHANDLING - SAB-P', p. 10.
Werkmeister, S. (2003) *Permanent Deformation Behaviour of Unbound Granular Materials in Pavement Constructions*. Dresden: Technical University of Dresden.

Appendix 1

Health, safety and environmental risk assessment

RISK ASSESSMENT (RiskManager alternative)

Unit/Institute:	NTNU Road building	**Date:**	2020-02-13
Responsible line manager (name):	Jean-Gabriel Dorval	**Revised:**	
Responsible for activities being risk assessed (name):	Inge Hoff, Arne Aalberg		
Participants in the risk assement (names):	Jean-Gabriel Dorval		

Description of the activity, process, area, etc.:

This risk assessment is for the laboratory portion of the student's Master thesis

Activity / process	**Unwanted incident**	**Existing risk reducing measures**	**Probability (P)**	**Consequence (C)** Evaluate the categories individualley. *Health should always be evaluated.*				**Risk value (P x C)**	**Risk reducing measures - suggestions** Measures reducing the probability of the unwanted incident happening should be prioritized.	**Residual risk after measures being implemented**
			(1-5)	Health (1-5)	Material values (1-5)	Environment	Reputation (1-5)			
General work in the road lab (basement)	Any accident	General HSE rules	1	3				3	Always follow the HSE rules and do not work alone	1
	Equipment/tools falling on the ground	Protective equipment is available	2	1				2	Wear basic PPE (safety shoes, gloves, glasses)	2
Crushing granular material (sample prepar	Eye injury due to particle projection	Safety goggles are available	3	3				9	Wear safety glasses and face shield	3
	Other injuries due to particle projection	Protective equipment is available	3	2				6	Wear gloves and work clothing	3
	Heavy noise	Protective equipment is available	3	3				9	Wear ear protection	3
	Small wounds due to handling of rocks	Protective equipment is available	2	1				2	Wear basic PPE (safety shoes, gloves, glasses)	2
	Incompetent use of the crushing machin	Training available by lab tech	2	3				6	Attend relevant training for that machine	2
Los Angeles and Micro Deval tests	Heavy noise	Protective equipment is available	3	3				9	Wear ear protection	3
	Small wounds due to handling of rocks d	Protective equipment is available	2	1				2	Wear basic PPE (safety shoes, gloves, glasses)	2
	Incompetent use of the testing machine	Training available by lab tech	2	2				4	Attend relevant training for that machine	2
	Getting burned after removing samples	Protective equipment is available	1	2				2	Wear basic PPE and use oven mitt	1
Flakiness index test	Small wounds due to handling of rocks d	Protective equipment is available	2	1				2	Wear basic PPE (safety shoes, gloves, glasses)	2
	Getting burned after removing samples	Protective equipment is available	1	2				2	Wear basic PPE and use oven mitt	1
Confined compression test	Eye injury due to particle projection	Safety goggles are available	3	3				9	Wear safety glasses and face shield	3
	Other injuries due to particle projection	Protective equipment is available	3	2				6	Wear gloves and work clothing	3
	Small wounds due to handling of rocks	Protective equipment is available	2	1				2	Wear basic PPE (safety shoes, gloves, glasses)	2
	Incompetent use of the crushing machin	Training available by lab tech	1	3				3	The hydraulic press will be operated by the lab technici	1
Cyclic triaxial test	Small wounds due to handling of rocks	Protective equipment is available	2	1				2	Wear basic PPE (safety shoes, gloves, glasses)	2
	Incompetent use of the testing machine	Training available by lab tech	2	2				4	Attend relevant training for that machine	2

Appendix 2

Geological map Svalbard C9G; Temakart 31/32; 1:100,000

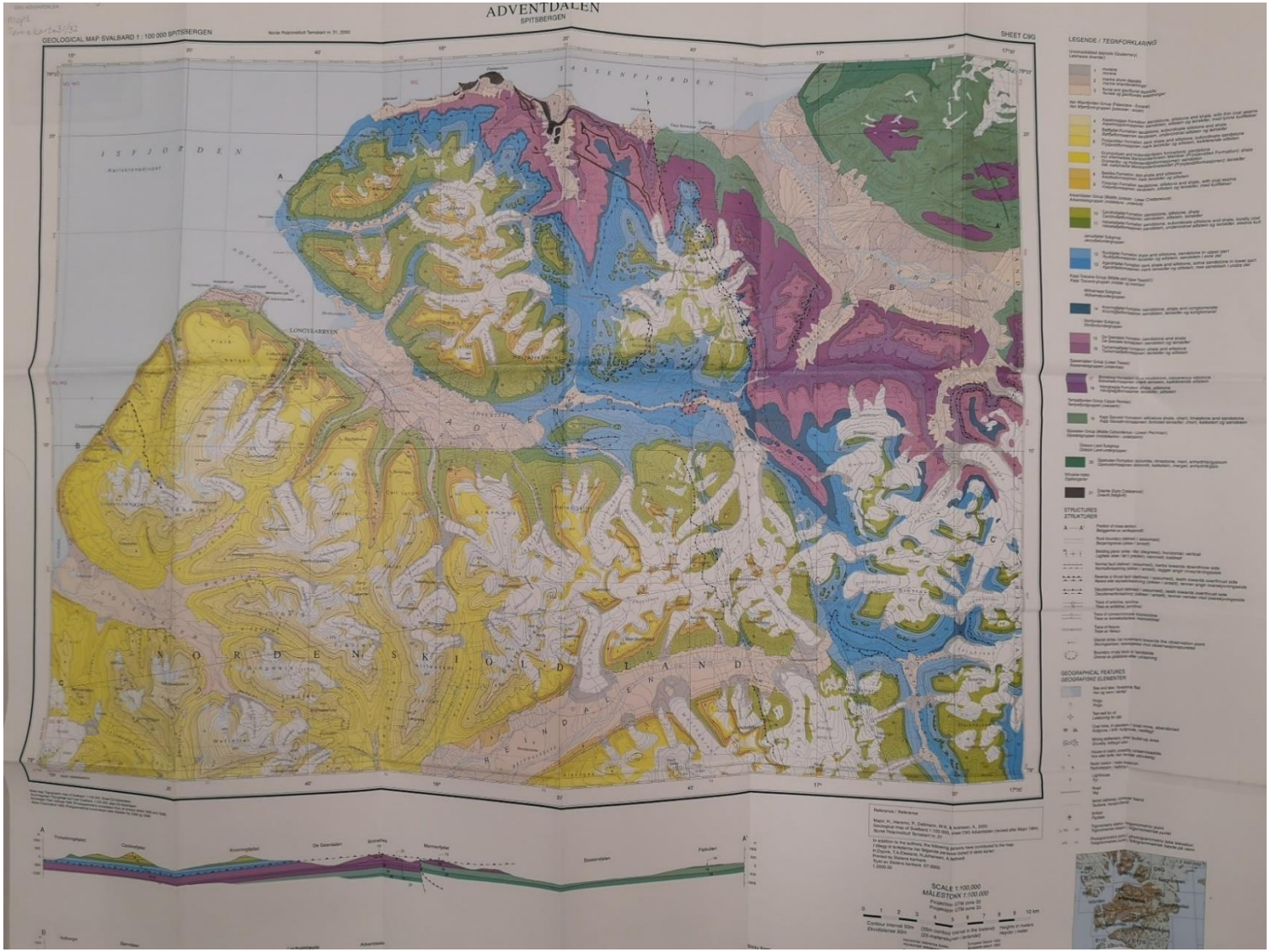

Appendix 3

Pictures of Longyearbyen gravel stockpiles

Site 1: Bolterelva



Site 2: Gruve 3



Appendix 4

Lab data

Sieving data

Sieving curve									
	Type 1			Type 2			Type 3		
	Mass retained (kg)	% retained	% passing	Mass retained (kg)	% retained	% passing	Mass retained (kg)	% retained	% passing
Sieve (mm)	2 crushings of 20-25mm rocks			1st crushing of 20-40mm rocks			2nd crushing of 20-40mm rocks		
16	0.633	15.0	85.046	1.092	25.052	74.9	0.467	9.344	90.7
14	0.529	12.5	72.549	0.528	12.113	62.8	0.337	6.743	83.9
12.5	0.551	13.0	59.532	0.41	9.406	53.4	0.341	6.823	77.1
10	0.824	19.5	40.066	0.602	13.811	39.6	0.635	12.705	64.4
8	0.599	14.2	25.915	0.461	10.576	29.0	0.52	10.404	54.0
4	0.647	15.3	10.631	0.505	11.585	17.5	0.862	17.247	36.7
2	0.159	3.8	6.875	0.202	4.634	12.8	0.443	8.864	27.9
1	0.072	1.7	5.174	0.123	2.822	10.0	0.301	6.022	21.8
0.5	0.039	0.9	4.252	0.074	1.698	8.3	0.191	3.822	18.0
0.25	0.031	0.7	3.520	0.067	1.537	6.8	0.169	3.381	14.6
0.125	0.044	1.0	2.481	0.103	2.363	4.4	0.281	5.622	9.0
0.063	0.056	1.3	1.158	0.103	2.363	2.0	0.252	5.042	4.0
below	0.049	1.2	0.000	0.089	2.042	0.0	0.199	3.982	0.0
total	4.233			4.359			4.998		

Los Angeles and Micro-Deval data

Determination of the resistance to fragmentation - Los Angeles			
Los Angeles DS-EN 1097-2		**Laboratory:**	NTNU
		Operator:	J-G Dorval
Identification of the sample:	LA#1	**Date:**	24-09-2020
Initial mass (g)	5002	Size fraction: 65% passing sieve 12.5mm	
Mass retained on the 1.6mm sieve (g)	3364		
Los Angeles coefficient (LA)	32.76		
Identification of the sample:	LA#2	**Date:**	24-09-2020
Initial mass (g)	5002	Size fraction: 65% passing sieve 12.5mm	
Mass retained on the 1.6mm sieve (g)	3304		
Los Angeles coefficient (LA)	33.96		
Identification of the sample:	LA#3	**Date:**	24-09-2020
Initial mass (g)	4999	Size fraction: 65% passing sieve 12.5mm	
Mass retained on the 1.6mm sieve (g)	3286		
Los Angeles coefficient (LA)	34.26		
Identification of the sample:	LA#4	**Date:**	25-09-2020
Initial mass (g)	5001	Size fraction: 65% passing sieve 12.5mm	
Mass retained on the 1.6mm sieve (g)	3309		
Los Angeles coefficient (LA)	33.84		
Identification of the sample:	LA#5	**Date:**	25-09-2020
Initial mass (g)	5001	Size fraction: 65% passing sieve 12.5mm	
Mass retained on the 1.6mm sieve (g)	3343		
Los Angeles coefficient (LA)	33.16		

Determination of the resistance to wear - Micro-Deval

Micro-Deval DS-EN 1097-1			Laboratory:	NTNU
			Operator:	J-G Dorval
Identification of the sample:	MD#3		**Date:**	26-09-2020
Variation of the test (wet conditions or dry):			wet	
	Test portion 1	Test portion 2		
Initial mass (g)	501	501	Grading class: 65% passing the 12.5mm sieve	
Mass retained on the 1.6mm sieve (g)	257	250	Mean value of MDE:	49.5
Micro-Deval coefficient (MDE)	48.8	50.2		
Identification of the sample:	MD#4		**Date:**	26-09-2020
Variation of the test (wet conditions or dry):			wet	
	Test portion 1	Test portion 2		
Initial mass (g)	502	499	Grading class: 65% passing the 12.5mm sieve	
Mass retained on the 1.6mm sieve (g)	259	269	Mean value of MDE:	47.3
Micro-Deval coefficient (MDE)	48.6	46		
Identification of the sample:	MD#5		**Date:**	26-09-2020
Variation of the test (wet conditions or dry):			wet	
	Test portion 1	Test portion 2		
Initial mass (g)	501	500	Grading class: 65% passing the 12.5mm sieve	
Mass retained on the 1.6mm sieve (g)	279	269	Mean value of MDE:	45.3
Micro-Deval coefficient (MDE)	44.4	46.2		
Identification of the sample:	MD#6		**Date:**	26-09-2020
Variation of the test (wet conditions or dry):			wet	
	Test portion 1	Test portion 2		
Initial mass (g)	499	500	Grading class: 65% passing the 12.5mm sieve	
Mass retained on the 1.6mm sieve (g)	264	276	Mean value of MDE:	45.9
Micro-Deval coefficient (MDE)	47	44.8		
Identification of the sample:	MD#7		**Date:**	27-09-2020
Variation of the test (wet conditions or dry):			wet	
	Test portion 1	Test portion 2		
Initial mass (g)	501	501	Grading class: 65% passing the 12.5mm sieve	
Mass retained on the 1.6mm sieve (g)	258	260	Mean value of MDE:	48.4
Micro-Deval coefficient (MDE)	48.6	48.2		

Particle shape data

Determination of particle shape - Flakiness Index					
Flakiness Index DS-EN 933-3	**Date:**	2020-10-05	**Laboratory:**	NTNU	
Identification of the sample:	Flakiness 3		Operator:	J-G Dorval	
Test portion mass (M0) in g:	2973		Mass retained on the 100 mm sieve in g:		0
			Mass retained on the 4 mm sieve in g:		52
			Sum of the discarded masses in g:		2
Sieving on test sieves			**Sieving on bar sieves**		
Particle size fraction di/Di (mm)	Mass of particle size fraction di/Di (Ri) in g		Nominal width of slot in bar sieve (mm)	Mass (mi) passing bar sieve in g	FIi = (mi/Ri) x 100
80/100	0		50	0	-
63/80	0		40	0	-
50/63	0		31.5	0	-
40/50	0		25	0	-
31.5/40	0		20	0	-
25/31.5	0		16	0	-
20/25	0		12.5	0	-
16/20	320		10	24.9	7.78
12.5/16	747		8	39.6	5.30
10/12.5	666		6.3	47.9	7.19
8/10	468		5	52	11.11
6.3/8	316		4	60.3	19.08
5/6.3	235		3.15	54.3	23.11
4/5	169		2.5	42.5	25.15
M1 = ∑Ri =	2921		M2 = ∑mi =	321.5	-
FI = (M2/M1) x 100 =	11				

Freeze-thaw resistance

Determination of the resistance to freezing and thawing							
DS-EN 1367-1						**Laboratory:**	UNIS
						Operator:	J-G Dorval
Variation of the test (distilled or demineralized water):						Distilled water	
	Test portion 1	Test portion 2	Test portion 3	Test portion 4	Test portion 5	Test portion 6	Size fraction: 8-16mm
Initial dry mass (g)	341.8	323.2	323.3	330.9	338.6	331.2	
Mass retained on the 1.6mm sieve (g)	339.8	321.5	321.8	329.9	336.3	329.8	
Freeze-thaw result (F)							
Initial total dry mass (M1) in g:	1989.0						
Final total dry mass retained on the 4.75 mm sieve (M2) in g:	1979.1						
F (%) = M1-M2 / M1 x 100 =	0.498						

Cyclic triaxial

See attached Excel spreadsheets

Mineralogy using XRD

See attached pdf reports

Thermal conductivity data

Rock core:

			Glass	Glass	Glass	Glass
			plate	plate	plate	plate
	Flux	Flux	1	1	2	2
	3	4	Temp	Temp	Temp	Temp
Time	[W/m2]	[W/m2]	F	B	F	B
---------- -	-------	-------	-------	-------	-------	-------
2020.10.12 19:54:12.699	6.44448	6.52309	3.28981	0.894022	8.04546	5.62045
2020.10.12 19:55:12.726	6.43346	6.5241	3.29172	0.90003	8.04688	5.62149
2020.10.12 19:56:12.756	6.44633	6.53926	3.29348	0.897006	8.05267	5.62164
2020.10.12 19:57:12.780	6.45215	6.53318	3.29295	0.894312	8.04964	5.62088
2020.10.12 19:58:12.803	6.44772	6.52866	3.29456	0.89756	8.05198	5.62489
2020.10.12 19:59:12.832	6.44631	6.51986	3.29151	0.895039	8.0444	5.62059
2020.10.12 20:00:12.866	6.44547	6.52036	3.29467	0.898506	8.04586	5.62185
2020.10.12 20:01:12.892	6.45344	6.52161	3.29072	0.891601	8.04565	5.62118
2020.10.12 20:02:12.918	6.44952	6.52142	3.29468	0.897017	8.04707	5.62268
2020.10.12 20:03:12.958	6.43419	6.53065	3.29168	0.899714	8.05031	5.62248
2020.10.12 20:04:12.992	6.44852	6.52473	3.29072	0.893426	8.04434	5.61871
2020.10.12 20:05:13.024	6.44811	6.53451	3.29516	0.89802	8.05184	5.62258
2020.10.12 20:06:13.054	6.45291	6.53062	3.29134	0.892411	8.04983	5.62201
2020.10.12 20:07:13.079	6.44247	6.5348	3.2937	0.898659	8.05212	5.62275

2020.10.12 20:08:13.101	6.45223	6.52593	3.29118	0.89251	8.04661	5.62054
2020.10.12 20:09:13.126	6.45212	6.54088	3.29504	0.896414	8.05447	5.62284
2020.10.12 20:10:13.153	6.45427	6.53336	3.29642	0.89699	8.05158	5.62275
2020.10.12 20:11:13.180	6.43127	6.52449	3.2908	0.899924	8.04694	5.62141
2020.10.12 20:12:13.208	6.45072	6.52667	3.29365	0.895537	8.04882	5.62247
2020.10.12 20:13:13.240	6.44568	6.53405	3.29247	0.896233	8.04788	5.61879
2020.10.12 20:14:13.270	6.4432	6.52766	3.29454	0.899225	8.05024	5.62352
2020.10.12 20:15:13.288	6.43692	6.53591	3.29128	0.898297	8.05052	5.62074
2020.10.12 20:16:13.315	6.44769	6.54125	3.29128	0.894294	8.05241	5.62065
2020.10.12 20:17:13.335	6.44776	6.53233	3.29518	0.898168	8.05247	5.62402
2020.10.12 20:18:13.347	6.43625	6.52895	3.28857	0.895836	8.04834	5.62114
2020.10.12 20:19:13.366	6.45549	6.51851	3.29661	0.896724	8.04442	5.62111
2020.10.12 20:20:13.388	6.45357	6.51663	3.2922	0.893033	8.04277	5.62016
2020.10.12 20:21:13.419	6.45601	6.52159	3.29558	0.895502	8.04829	5.62383
2020.10.12 20:22:13.452	6.4362	6.52607	3.29296	0.900242	8.04722	5.6211
2020.10.12 20:23:13.470	6.45469	6.53092	3.29533	0.895742	8.04975	5.62183
2020.10.12 20:24:13.503	6.44919	6.53156	3.28995	0.892411	8.04849	5.62033
AVERAGE	**6.44672065**	**6.52850355**	**3.29289484**	**0.89627113**	**8.04868613**	**5.62165839**

Gravel sample:

			Glass	Glass	Glass	Glass
			plate	plate	plate	plate
	Flux	Flux	1	1	2	2
	3	4	Temp	Temp	Temp	Temp
Time	[W/m2]	[W/m2]	F	B	F	B
----------------	-------	-------	-------	-------	-------	-------
2020.10.06 22	4.65542	4.3018	2.69057	0.959877	8.26981	6.67058
2020.10.06 22	4.65542	4.3018	2.69057	0.959877	8.26981	6.67058
2020.10.06 22	4.65542	4.3018	2.69057	0.959877	8.26981	6.67058
2020.10.06 22	4.65542	4.3018	2.69057	0.959877	8.26981	6.67058
2020.10.06 22	4.65542	4.3018	2.69057	0.959877	8.26981	6.67058
2020.10.06 22	4.65542	4.3018	2.69057	0.959877	8.26981	6.67058
2020.10.06 22	4.65542	4.3018	2.69057	0.959877	8.26981	6.67058
2020.10.06 22	4.65542	4.3018	2.69057	0.959877	8.26981	6.67058
2020.10.06 22	4.65542	4.3018	2.69057	0.959877	8.26981	6.67058
2020.10.06 22	4.65542	4.3018	2.69057	0.959877	8.26981	6.67058
2020.10.06 22	4.65542	4.3018	2.69057	0.959877	8.26981	6.67058
2020.10.06 22	4.65542	4.3018	2.69057	0.959877	8.26981	6.67058
2020.10.06 22	4.65542	4.3018	2.69057	0.959877	8.26981	6.67058
2020.10.06 22	4.65542	4.3018	2.69057	0.959877	8.26981	6.67058
2020.10.06 22	4.65542	4.3018	2.69057	0.959877	8.26981	6.67058
2020.10.06 22	4.65542	4.3018	2.69057	0.959877	8.26981	6.67058
2020.10.06 22	4.65542	4.3018	2.69057	0.959877	8.26981	6.67058
2020.10.06 22	4.65542	4.3018	2.69057	0.959877	8.26981	6.67058
2020.10.06 22	4.65542	4.3018	2.69057	0.959877	8.26981	6.67058
2020.10.06 22	4.65542	4.3018	2.69057	0.959877	8.26981	6.67058
2020.10.06 22	4.65542	4.3018	2.69057	0.959877	8.26981	6.67058
2020.10.06 22	4.65542	4.3018	2.69057	0.959877	8.26981	6.67058
2020.10.06 22	4.65542	4.3018	2.69057	0.959877	8.26981	6.67058
2020.10.06 22	4.65542	4.3018	2.69057	0.959877	8.26981	6.67058
2020.10.06 22	4.65542	4.3018	2.69057	0.959877	8.26981	6.67058
2020.10.06 23	4.65542	4.3018	2.69057	0.959877	8.26981	6.67058
2020.10.06 23	4.65542	4.3018	2.69057	0.959877	8.26981	6.67058
2020.10.06 23	4.65542	4.3018	2.69057	0.959877	8.26981	6.67058
2020.10.06 23	4.65542	4.3018	2.69057	0.959877	8.26981	6.67058
2020.10.06 23	4.65542	4.3018	2.69057	0.959877	8.26981	6.67058
2020.10.06 23	4.65542	4.3018	2.69057	0.959877	8.26981	6.67058
AVERAGE	**4.65542**	**4.3018**	**2.69057**	**0.959877**	**8.26981**	**6.67058**

Specific density

SPECIFIC DENSITY

Standard: Statens vegvesen - håndbok 014-271

NTNU
BAT
Veg, transport og geomatikk

Trondheim — JG Dorval

Date measured — 2020-10-07

Material: Svalbard gravel

Description: crushed gravel passing 8mm sieve but retained on 2mm

	Sample 1	Sample 2
Pycnometer number	19	15
Weight of sample + pycnometer	966.1 g	919.8 g
Weight of pycnometer	301.5 g	313.3 g
Weight of sample	664.6 g	606.5 g
Weight of sample + pycnometer + water	1833.9 g	1776.0 g
Weight of sample + pycnometer	966.1 g	919.8 g
Weight of water = volume of water	867.8 g	856.2 g
Volume of pycnometer	1091.0 ml	1119.9 ml
Volume of water	867.8 ml	856.2 ml
Volume of sample	223.2 ml	263.7 ml
Specific density	2.978 g/cm3	2.300 g/cm3
Average specific density	2.639 g/cm3	

Datakatalog: I:\labskjem\EXCEL\ Skjema: densitet

Density using water displacement			
	1	2	
m1 (cleaned and dried)	596.3	751.1	g
m2 (in water)	352.8	456.2	g
V in water	243.989932	295.493351	cm^3
rho sample	2.4439533	2.54185077	g/cm^3
rho water at 21°C	0.997992	0.997992	g/cm^3

Appendix 5

Norwegian pavement design manual N200 – Traffic group Longyearbyen

Main roads

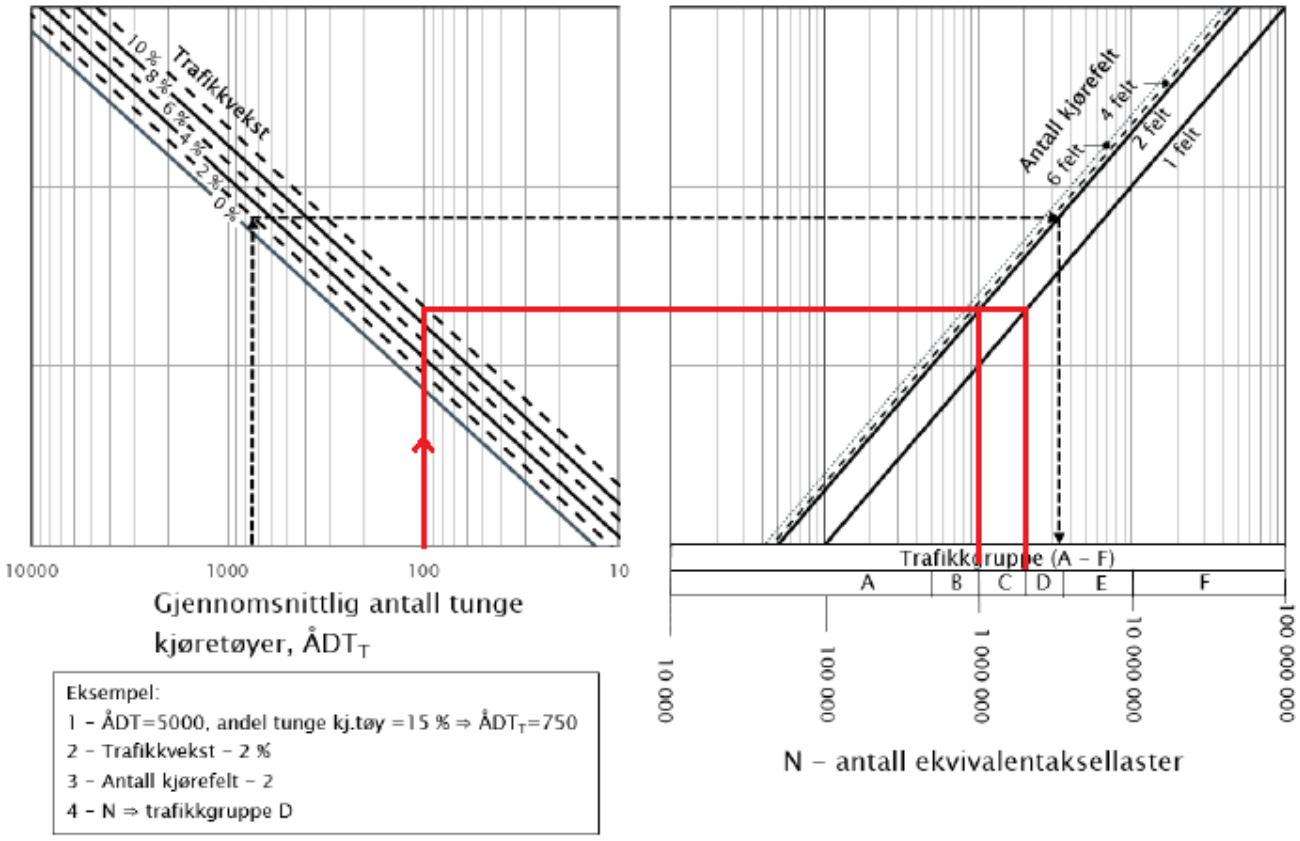

Assumptions for the main road in Longyearbyen:

500 cars per hour as AADT (about 25% of the total car in the city) with a 20% heavy traffic. This gives an AADTT of 100 trucks.

Then, an annual growth of 10% with one or two lanes results in Traffic Group C or D for the main roads.

Secondary roads

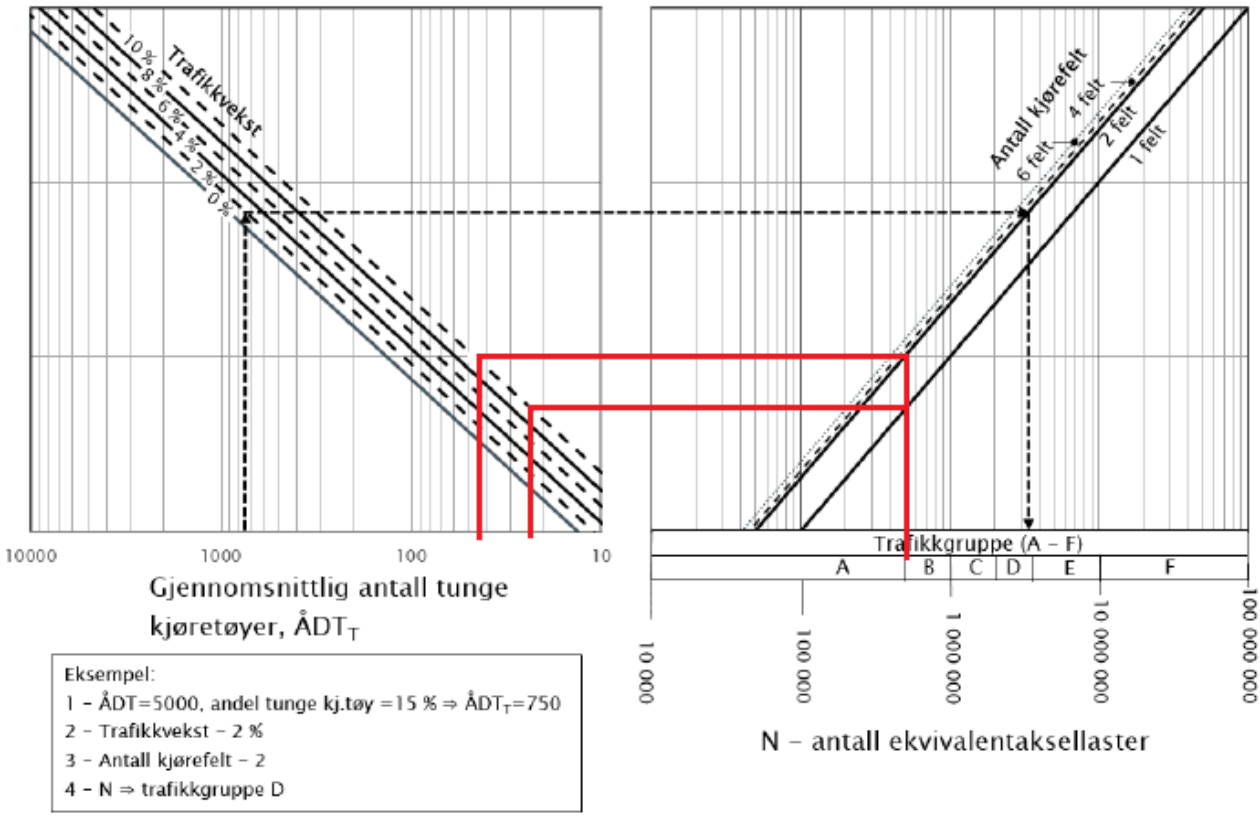

Assumptions for the Longyearbyen case:

From the borderline between Traffic Group A and B --> roads with one or two lanes --> traffic growth of 10% per year

Result is 22 to 41 heavy trucks per day on a specific road segment. Assuming this corresponds to 10% of the total circulation, this gives 220 to 410 cars per day on the same road segment.

It is realistic to assume that most roads in Longyearbyen belongs to Traffic Group A and B.

Appendix 6

Triaxial figures

Larger version of the triaxial figures – Resilient modulus

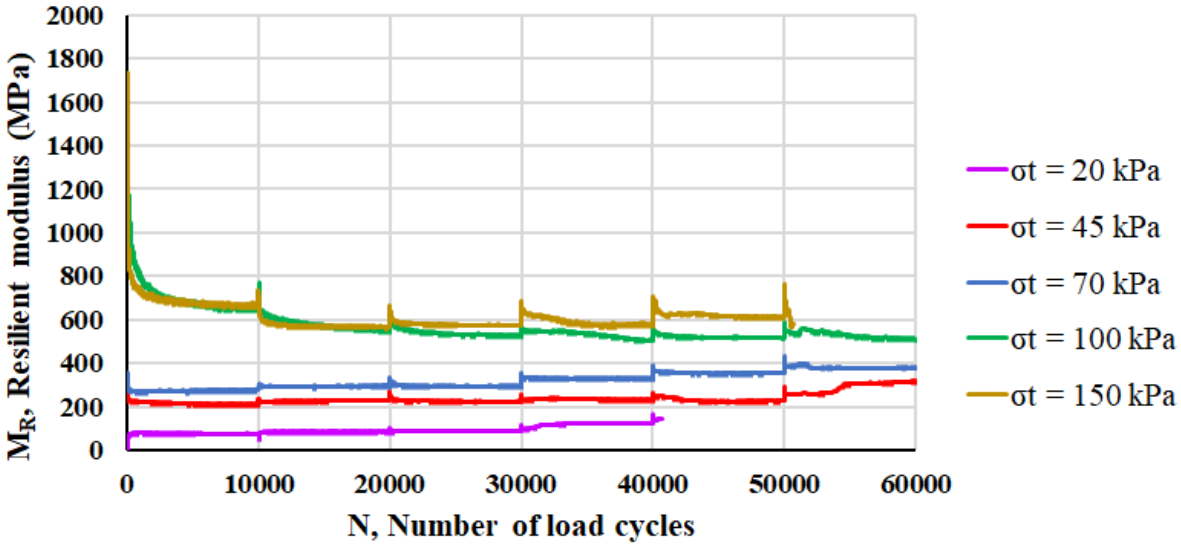

Specimen 1

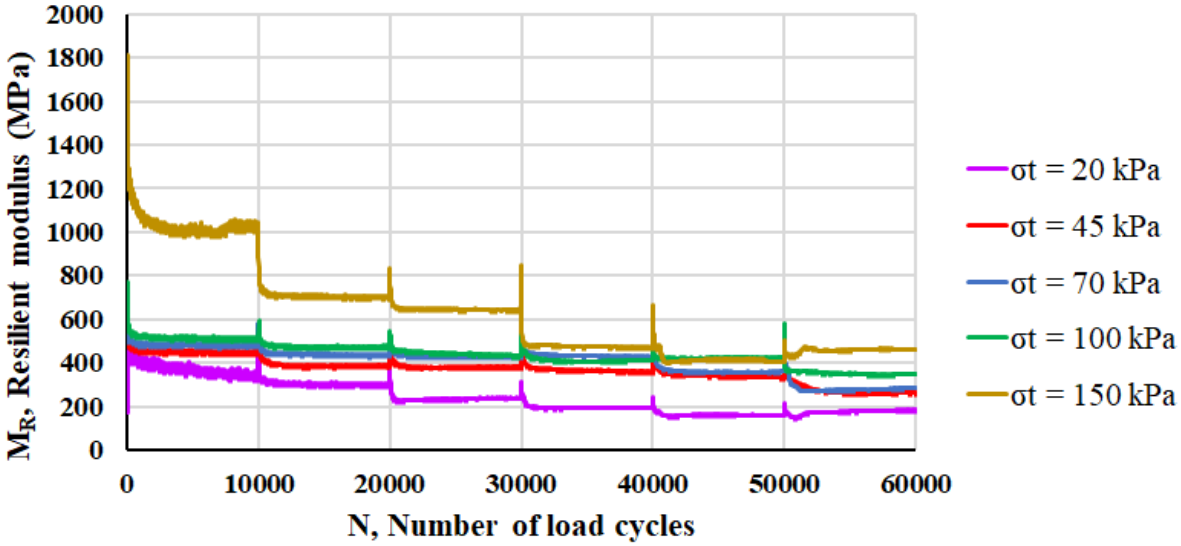

Specimen 2

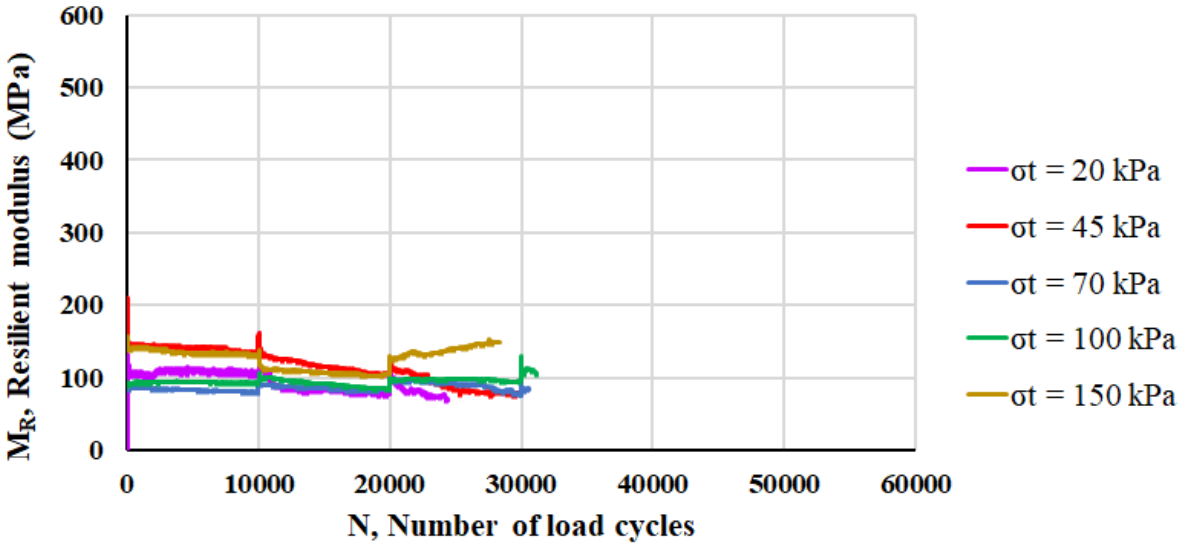

Specimen 3

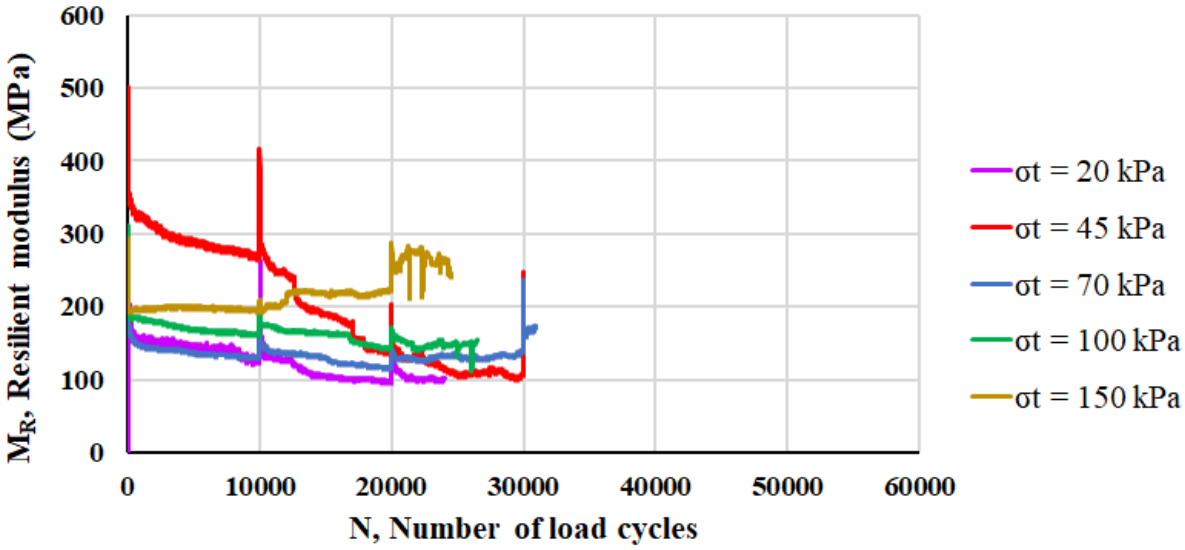

Specimen 4

Larger version of the triaxial figures – Permanent axial deformation

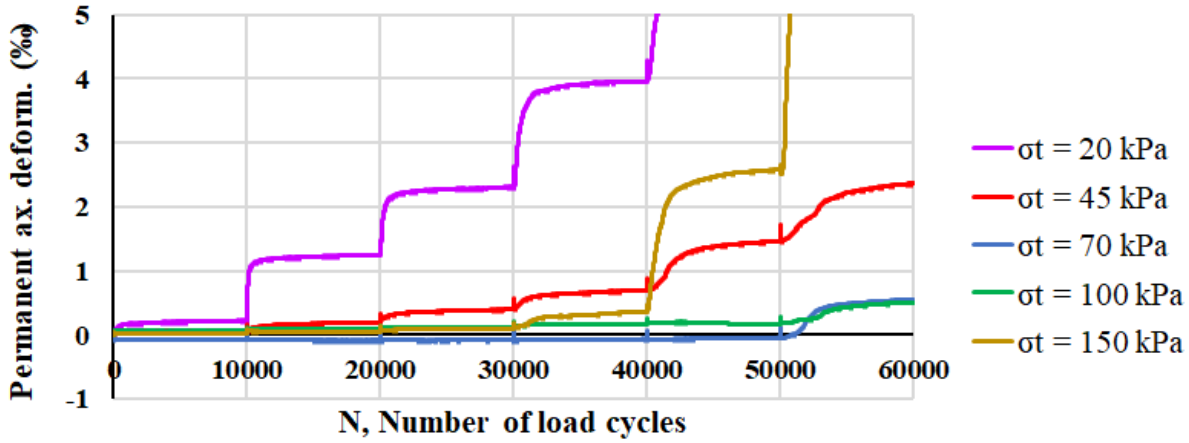

Specimen 1

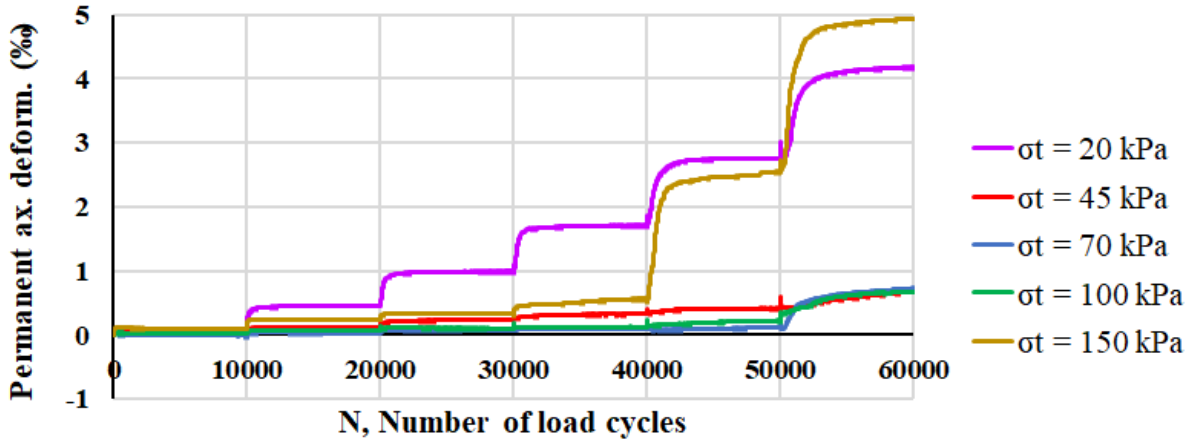

Specimen 2

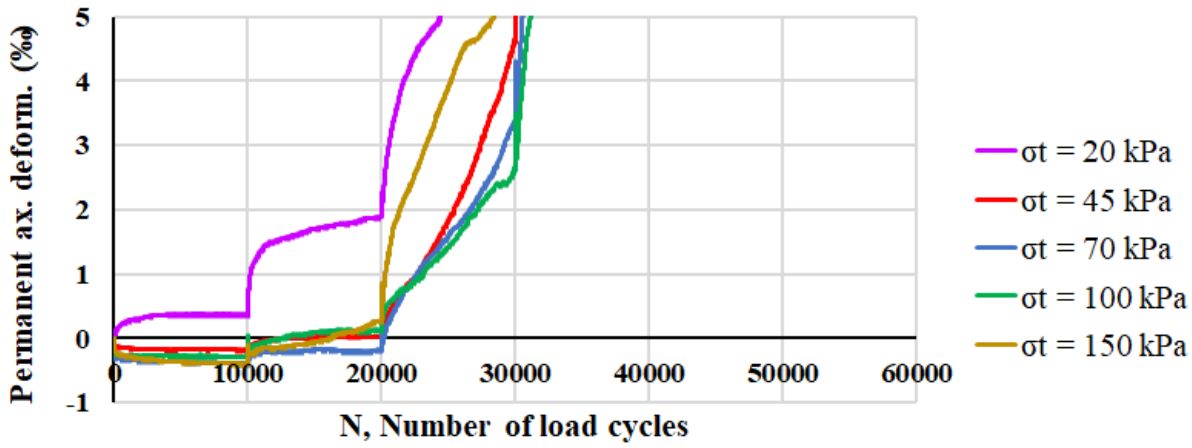

Specimen 3

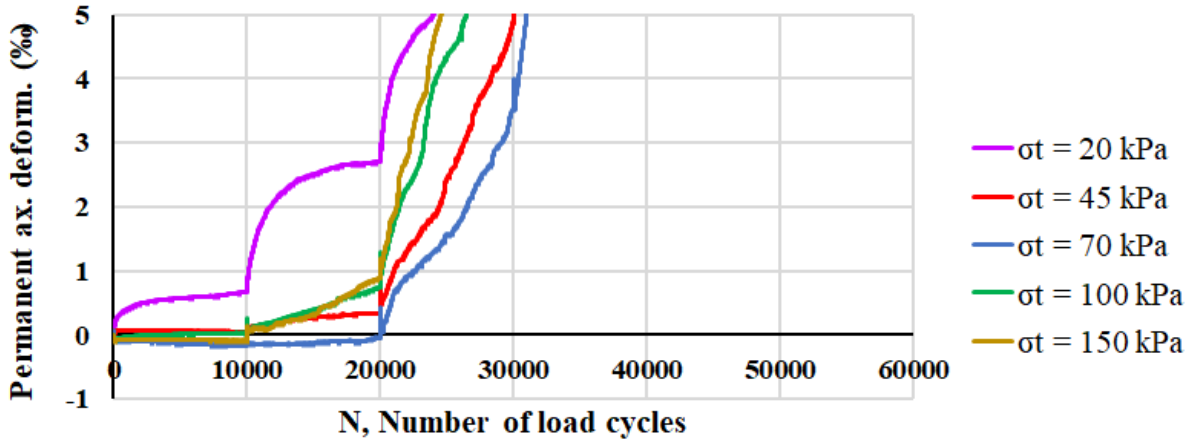

Specimen 4

Larger version of the triaxial figures – Deformation stages

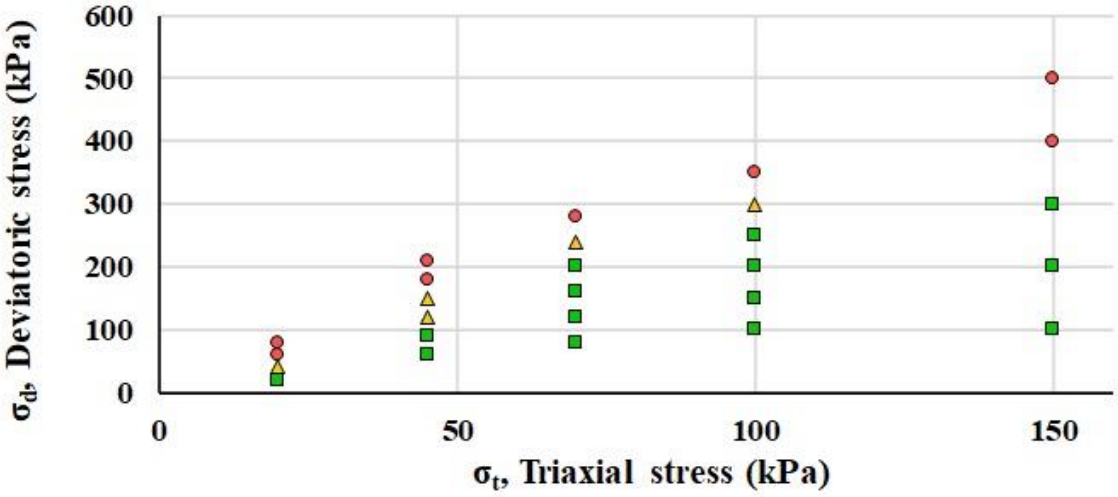

Specimen 1

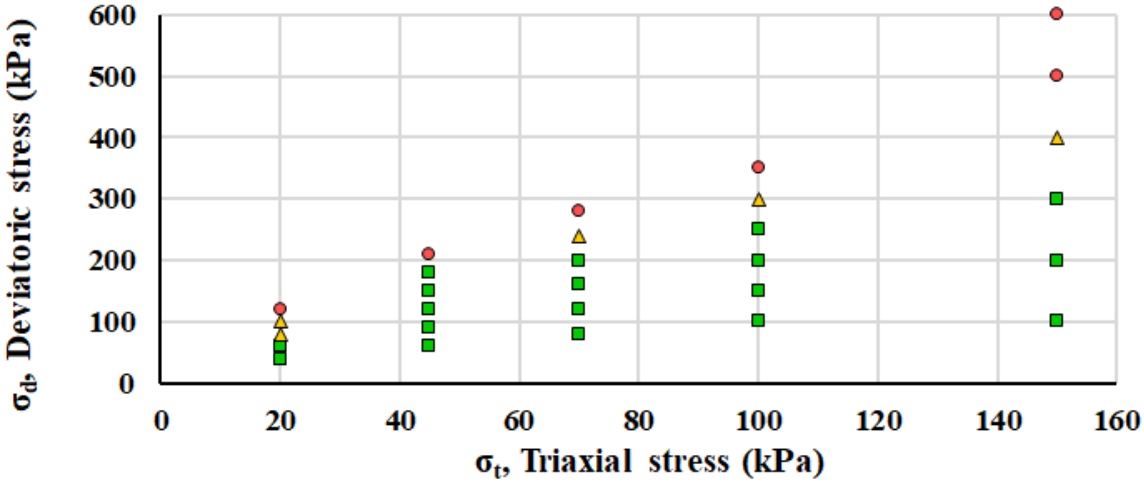

Specimen 2

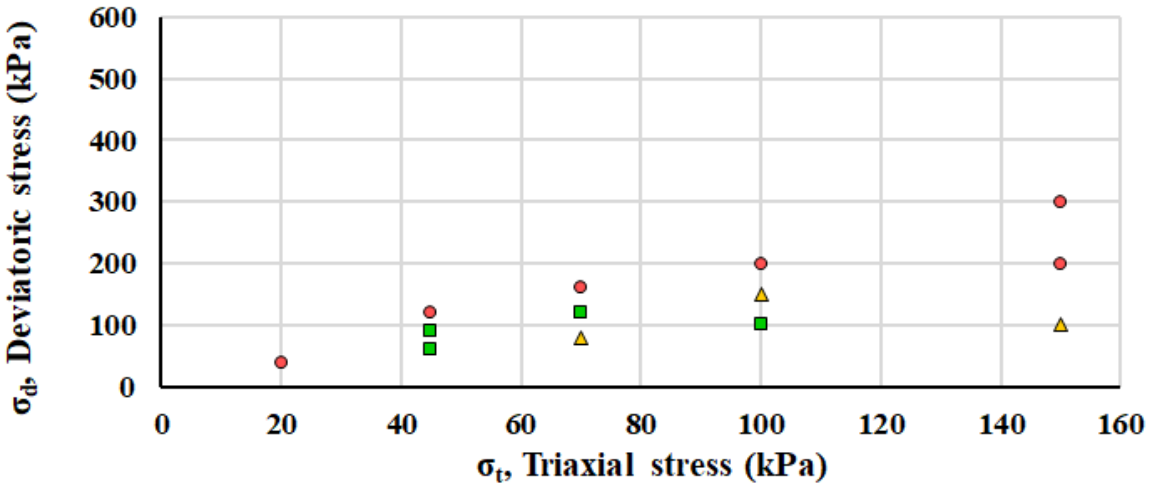

Specimen 3

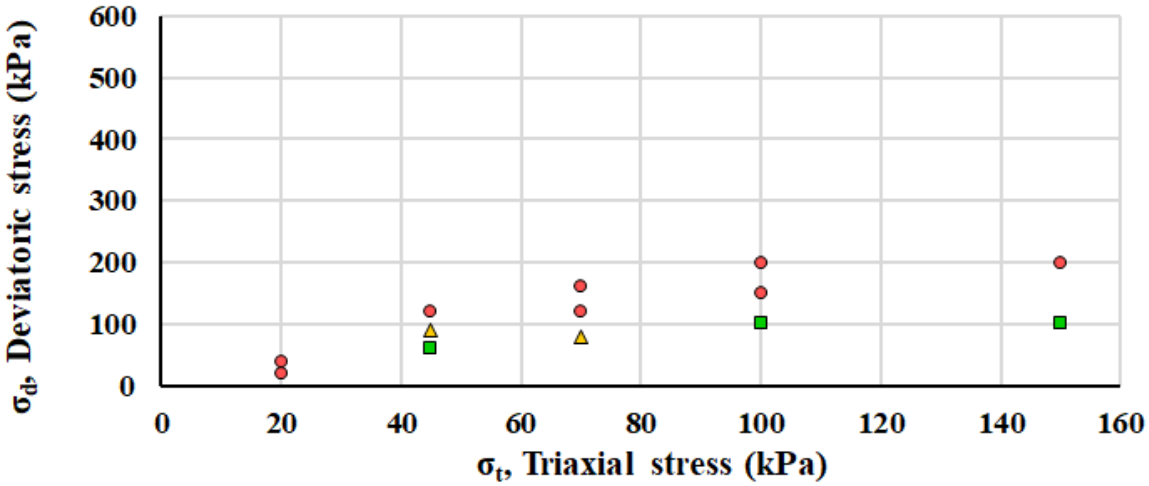

Specimen 4

Appendix 7

Parameters for i3c-me:

Material properties					
Scenario	**Layer**	**Poisson coefficient**	**Type**	**Model**	**Remark**
1	Surfacing layer	0.35	GB-20, PG58-34	Level 2 Witczak, using it by default from the software	
	Granular material	0.35	MG20, imported	M_R = 450 MPa with w=5%	from (Barbieri, 2019)
	Granular material	0.35	MG112, local	M_R = 120 MPa at w=7% and bulk stress 300 kpa	according to the present study
	Natural soil	0.35	GC, GM soil	M_R= 95MPa by default from software	
2	Surfacing layer	0.35	GB-20, PG58-34	Level 2 Witczak, using it by default from the software	
	Granular material	0.35	MG20, imported	M_R = 450 MPa with w=5%	from (Barbieri, 2019)
	Granular material	0.35	MG20, local	M_R= 250 Mpa at w=3% and bulk stress 300 kPa	according to the present study
	Granular material	0.35	MG112, local	M_R = 120 MPa at w=7% and bulk stress 300 kpa	according to the present study
	Natural soil	0.35	GC, GM soil	M_R= 95MPa by default from software	
3	Surfacing layer	0.35	GB-20, PG58-34	Level 2 Witczak, using it by default from the software	
	Granular material	0.35	MG20, local	M_R= 250 Mpa at w=3% and bulk stress 300 kPa	according to the present study
	Granular material	0.35	MG112, local	M_R = 120 MPa at w=7% and bulk stress 300 kpa	according to the present study
	Natural soil	0.35	GC, GM soil	M_R= 95MPa by default from software	
4,5	Surfacing layer	0.35	GB-20, PG58-34	Level 2 Witczak, using it by default from the software	
	Granular material	0.35	MG20, local	M_R= 250 Mpa at w=3% and bulk stress 300 kPa	according to the present study
	Granular material	0.35	MG56, local	M_R = 200 MPa at w=5% and bulk stress 300 kPa	according to the present study
	Granular material	0.35	MG112, local	M_R = 120 MPa at w=7% and bulk stress 300 kpa	according to the present study
	Natural soil	0.35	GC, GM soil	M_R= 95MPa or M_R= 50 MPa (scenario 5)	

Soil densities:

	ρ_d	ρ_s
	kg/m³	kg/m³
Local material	2050	2640
Imported material	2200	2650

Temperature function:

	Duration (days)	Average air temperature (°C)
Autumn	68	-7
Winter	162	-15
Early Spring	30	-4
Late Spring	30	3
Summer	75	4

Appendix 8

Granular pad assumptions, material properties and load scenarios:

Local fill material properties			Remark
ρ_s	2.64	ton/m³	from this study
ρ_{bulk}	2.05	ton/m³	from this study (RLTT gradation)
ρ_{dry}	1.94	ton/m³	from this study (RLTT gradation)
γ_{dry}	19.03	kN/m³	
γ @w=2%	19.41	kN/m³	
γ @w=7%	20.36	kN/m³	
G_s	2.64	-	
ϕ'_{cs}	30	°	from Table 10.3 Budhu
K_o	0.5	-	assuming that a man-made embankment of gravel is not overconsolidated
E	80	Mpa	from this study (RLTT)
ν	0.35	-	assumption from i3c-me and (Diego, 2019)

Load scenario			
Maritime container			capacity from: https://www.lantenne.com/Les-dimensions-du-conteneur-maritime_a32692.html
Single stack			
q_s	21157	Pa	
Double stack			
q_s	31736	Pa	75% capacity per container
Concrete slab			
Dead load	9418	Pa	concrete: 2400 kg/m³; 400 mm-thick and 1m² of the slab
Floor load	5000	Pa	to fit most categories of Table 6.2 and 6.8 of Eurocode 1 Part 1-1
qs	14418	Pa	sum of dead and live load

Equations ((Budhu, 2010):

Unit weight above groundwater level

$$\gamma = \left(\frac{G_s + Se}{1 + e}\right)\gamma_w = \frac{G_s(1 + w)}{1 + e}\gamma_w$$

Total stress (above the groundwater level)

$$\sigma = \sigma' + u$$

Where u is equal to 0 since it is above the groundwater level

Lateral earth pressure coefficient at rest

$$K_o^{nc} \approx 1 - \sin \phi'_{cs}$$

Vertical stress increase below the corner of a uniformly loaded rectangle (dimensions: B by L):

$$\Delta\sigma_z = q_s I_z$$

$$I_z = \frac{1}{4\pi}\left[\frac{2mn\sqrt{m^2 + n^2 + 1}}{m^2 + n^2 + m^2n^2 + 1}\left(\frac{m^2 + n^2 + 2}{m^2 + n^2 + 1}\right) + \tan^{-1}\left(\frac{2mn\sqrt{m^2 + n^2 + 1}}{m^2 + n^2 - m^2n^2 + 1}\right)\right]$$

Where m=B/z and n=L/z

Vertical elastic settlement under a uniformly loaded rectangle (dimensions B by L):

$$\Delta z = \frac{q_s B(1 - \nu^2)}{E} I_s$$

At center of a rectangle (Giroud, 1968):

$$I_s = \frac{2}{\pi}\left[\ln\left(\xi_s + \sqrt{1 + \xi_s^2}\right) + \xi_s \ln\frac{1 + \sqrt{1 + \xi_s^2}}{\xi_s}\right]$$

At corner of a rectangle (Giroud, 1968):

$$I_s = \frac{1}{\pi}\left[\ln\left(\xi_s + \sqrt{1 + \xi_s^2}\right) + \xi_s \ln\frac{1 + \sqrt{1 + \xi_s^2}}{\xi_s}\right]$$

Where ξs = L/B

Appendix 9

Confined compression test of Svalbard rocks

Extracted from a short report written by Jean-Gabriel Dorval in February 2020. This was part of a Specialization project to prepare for this study.

Introduction

In the light of the construction of a new waste sorting facility in Longyearbyen, there was some uncertainties regarding the mechanical behavior of locally sourced granular material for such a large building footprint (50mX50m). The new facility's foundation would be a floating concrete slab lying on a gravel pad. In order to meet the specifications and for economical reason, the use of local gravel is considered.

Confined compression tests were realized to better understand how those rocks would behave in an embankment with a distributed load from the top part

Sample description

The sample contained a mix of cobbles and pebbles that were covered by a dried mixture of finer material (sand, silt, clay). It was impossible to collect material that was a bit smaller because it was frozen solid on the ground. The rocks were mostly sub-rounded to well-rounded with the presence of a few sub-angular pieces (see Figure 1). The shapes varied between elongated to almost spherical. All the rocks were sedimentary and upon completion of the tests, a very large portion revealed to be sandstone or siltstone.

Figure 1: Larger fraction of the sample with a 1m ruler

The bulk density of the larger fraction was approximated by using a large plastic bucket and vibrating it long enough so that the rocks stood in place. The average value was 1534 kg/m³.

Methodology

The experimental set up consisted of a steel cylinder/outer casing, two steel load caps, two thin aluminum caps and a hydraulic press. The diameters of the outer casing and the caps differed slightly (±1mm). This was meant to prevent finer particle or rock shards from getting stuck and restraining the movement of the caps. The inner diameter of the outer casing was 150mm. Figure 2 shows the experimental set up before a compression.

Figure 2: Experimental set up

The following steps were made for the four compression tests:

1. Install the lower part of the set-up on a concrete vibration table (outer casing, lower load cap and lower aluminum cap). The lower part was laid a thin steel sheet for transport to the hydraulic press.
2. Use small shims (wood or metal, as seen on Figure 3) to ensure that the outer casing is approximately 1cm above the bottom of the load cap and levelled.
3. Handpick the right size of cobbles and place them inside the cylinder. It was necessary to use smaller pieces at both extremities to ensure a maximum contact area.
4. Vibrate the cylinder without, and then with the top part. Ensure that the top load cap is stable enough to sustain the beginning of the compression test. If this was not achieved, the procedure was restarted.
5. Carefully install the cylinder in the hydraulic press, remove the metal sheet and shims.
6. Execute the test with a few load increments. Measure the set-up height at the front and the back for each load increment.
7. Remove the specimen and visually segregate the different damage category.

8. Weight each damage category.

The first test damaged most of the specimen (force too high) but the others did not. The rocks considered intact were used in the subsequent test because there was not a lot of material suitable for testing (i.e. having the optimal size). The damaged rocks were replaced by new ones. Ideally, completely new rocks would have been used for each test.

Figure 3: Placement of rocks in the cylinder

Results and discussion

The results from the compression tests are presented in Table 1. The hydraulic press had a large dial showing the mass applied (in tons) and its precision was 0.1ton.

Table 1: Compressive strength results

Test#	m applied	h front	h back	h average	Δh	Force applied	Stress applied	
	kg	mm	mm	mm	mm	N	MPa	**Remarks**
1	4000	314	-		-	39240	2.221	Lots of pop sounds starting before 4t
	5000	-	323	318.5	-	49050	2.776	
	7500	307	314	310.5	-	73575	4.163	
	8900	307	316	311.5	-	87309	4.941	
2	0	348	352	350.0	-	0	0.000	A single pop sound occured at 0.4ton
	700	346	351	348.5	1.5	6867	0.389	
	1000	346	350	348.0	0.5	9810	0.555	
	1300	345	349	347.0	1.0	12753	0.722	
	1500	344	349	346.5	0.5	14715	0.833	
3	0	327	331	329.0	-	0	0.000	
	700	327	331	329.0	0.0	6867	0.389	
	1600	327	330	328.5	0.5	15696	0.888	Pop at 1t, 1.4t and 2.0t
	2400	325	329	327.0	1.5	23544	1.332	Lots of pop sound at 3.0t
	3100	324	327	325.5	1.5	30411	1.721	
	3500	324	326	325.0	0.5	34335	1.943	
4	0	347	351	349.0	-	0	0.000	This test was made with larger rocks than 1-2-3
	2000	342	345	343.5	5.5	19620	1.110	Single popping sound at 0.4t and 0.6t
	2400	341	344	342.5	1.0	23544	1.332	Multiples sounds at 0.8t-1t
	2700	341	344	342.5	0.0	26487	1.499	

During the execution of the test, it was possible to clearly hear the cracking sound of a rock within the specimen when the applied mass was slowly increased. The first sound noticed by the lab workers was noted and defined as the «first cracking of rock».

The first compression test started with a too high stress and was discarded. For the second and fourth test, there were a cobble piece that was partly sticking out from the specimen on the top load plate. It is most likely why it broke at a lower stress than tests 3. Tests 3 and 4 were made using a slightly larger material than Tests 1 and 2, due to the lack of smaller sized cobbles. Table 2 shows the results for the three last compression tests.

Table 2: First cracking of rock

Test#	m applied	Force applied	Stress applied	
	kg	N	Pa	kPa
2	400	3924	222053	222.05
3	1000	9810	555132	555.13
4	800	7848	444106	444.11

After the completion of each test, the content of the cylinder was weighted. Each pieces of the specimen were visually examined for damages. It was observed that some pieces had a weak outer layer (0-2mm thick) and a solid core. The first test was quite destructive hence the definitions that follow are based on tests 2-3-4:

- Highly damaged/crushed: The piece is either missing large portion of its outer layer, broken in half, crushed, punctured or cracked through. In most cases, it could be broken down by hand. Figure 5 shows this damage class for Test 4.

Figure 5 : Example of highly damaged/crushed material

- Minimum damage: The piece is still complete. It can present some outer layer removal to a small extent. A crack can be visible but is not going through the rock. No pieces could be taken apart by hand. Figure 6 shows this damage class for Test 3.

Figure 6 : Example of minimum damage

- Intact: The piece is in its original state. It was considered that a single small outer layer loss (0.5cmX0.5cm) was belonging to this category. No cracks are visible. It cannot be broken down by hand. Figure 7 shows this category for Test 2.

Figure 7: Example of intact material

Table 3 shows the damages that resulted from the four compression tests, by mass.

Table 3: Mass fractions by damage category

Test #	m total g	Highly damaged/crushed g	Minimum damage g	Intact g	Remarks
1	4633.4	1650.3	1987.5	995.6	The minimum damage has been re-assessed after first compression and is more consistent for test 2-3-4
2	5222	660.3	699.6	3862.1	
3	4885.2	1980	933.9	1971.3	
4	5317.5	755.7	1625.2	2936.6	

The percentage of mass for each damage category was then put together with the maximum stress applied for each test. This is shown in Table 4.

Table 4: Damage related to stress

Test #	Stress MPa	Highly damaged/crushed	Minimum damage	Intact
1	4.94	36%	43%	21%
2	0.83	13%	13%	74%
3	1.94	41%	19%	40%
4	1.5	14%	31%	55%

As expected, the fraction of highly damaged rocks is higher at higher stress. The second compression test left almost 75% of the specimen intact. It is interesting since it highlights the capacity of this material to resist to a larger stress than what would be transferred from a typical building slab. From those data, a very preliminary curve was established to link the percentage of intact rock in the sample in relation to the stress applied. It is shown as Figure 8.

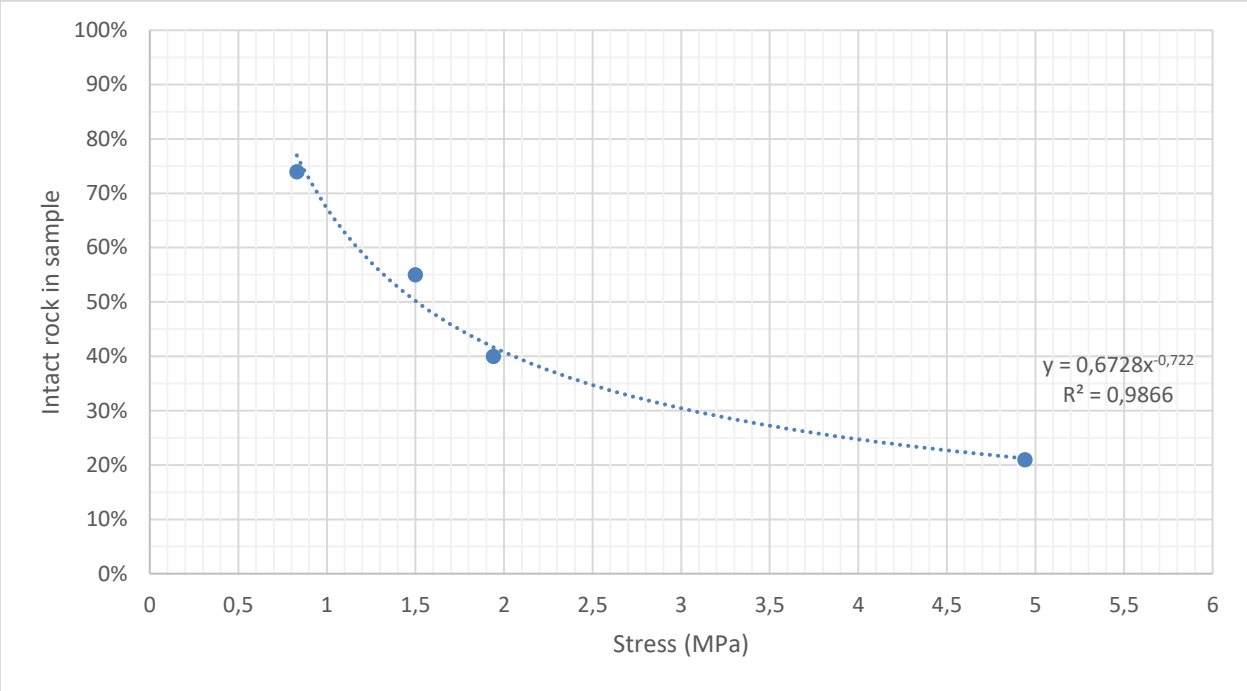

Figure 8: Intact fraction in relation to stress applied

Conclusion and recommendations

The granular material tested behaved more positively than what was expected for sedimentary rocks. This was particularly true at lower stress range. The next step would be to test rocks from mainland Norway with the same apparatus to have a clear comparison between the two materials. It is recommended that further tests are conducted with stresses ranging from 100 kPa to 1 MPa. It would be more centered toward the expected stress from the new waste sorting facility. The effect of smaller pebbles within the specimen should be evaluated, it is expected that it might help in distributing the load and act to interlock the larger cobbles together. It would be interesting to see the impact of trapping slightly larger particles between two layers of smaller particles.

The size of the experimental apparatus doesn't allow it to be representative of what would happen within an embankment made out of larger cobbles. It would be of interest to evaluate the behavior under compression in a larger experimental set up (1mX1mX0.4m) that might better represent an embankment under construction traffic.

Jean-Gabriel Dorval

Using local Svalbard rocks as a construction material

NTNU
Kunnskap for ei betre verd

UNIS
The University Centre in Svalbard

DTU